

Multiscale modeling of elastic wave propagation in heterogeneous materials

by

Chen Wang

A thesis submitted in partial fulfillment of the requirements for the degree of

Doctor of Philosophy

Department of Mechanical Engineering
University of Alberta

© Chen Wang, 2019

Abstract

Heterogeneous materials have been used extensively due to their desirable properties achieved by combining various constituents and tailored local structures. More recently, the metamaterials have attracted extensive attention because of their exotic dynamic properties, which are caused by either or both of the periodic and resonant local structures. Since the separation of scales exists between the fine-scale features and the macroscopic structures, the multiscale modeling and simulation of the elastodynamic behavior of the heterogeneous materials are essential for their design, optimization and application. This thesis aims to develop computational methods for the multiscale modeling of elastic wave propagation in heterogeneous materials.

Firstly, an analytical-numerical method is developed for the multiple scattering problem of elastic media with interacting inhomogeneities under time-harmonic antiplane incident waves. The main focus is on the detailed evaluation of the effectiveness and accuracy of the method in the determination of the local dynamic behavior of such heterogeneous media with significant numbers of inhomogeneities. The method is based on the eigenfunction expansion and the use of a pseudo-incident wave technique. Then, by introducing the Helmholtz decomposition, the method is extended to in-plane problems. The accuracy and effectiveness of the method for dealing with multiple interaction problems are discussed in detail.

Then, for the periodic materials, an analytical-numerical method is developed for determining the eigenstate of the unit cell under designated frequency and propagation direction. Based on the eigenfunction expansion and Floquet-Bloch theory, the nonlinear eigenvalue problem is established. The Newton's method is employed for computing the expansion coefficients as the

eigenvector by which the eigenstate of the unit cell can be determined. The method is validated by the comparison with the finite element method.

Based on the explicitly solved multiple scattering wave fields and the eigenstates of periodic unit cell, two kinds of computational homogenization methods are developed. The first kind is based on the domain averaging, and two methods are developed. The first method is based on the volume averages of the field variables with considering the effective wave form, which is iteratively adjusted using the self-consistent scheme. The second method is developed for periodic materials based on the kinetic energy equivalence. The homogenization results are verified by comparing the direct numerical simulations of the original heterogeneous material and the homogeneous substitution with the obtained effective properties.

Another computational homogenization method is developed based on the boundary matching technique. The effective material properties are obtained by being adjusted so that the boundary response of the representative volume element has the minimum mismatch with that of a congruent piece of homogeneous material. According to different frequency ranges and materials, different RVE models are established. The validity of the homogenization is also verified by the comparison of direct numerical simulations. The homogenization results obtained by using boundary matching method and the domain averaging method are in a good consistency.

At last, the multiscale modeling method is summarized by combining the developed methods. The method for recovering the local response from the homogenized model is developed. The effectiveness and accuracy of the method are shown by general examples of elastic wave propagation in heterogeneous materials with fine-scale local structures.

Preface

The main body of this thesis is composed of three journal papers, which are published or in preparation. See below for details.

Chapter 2 and the first section of Chapter 4 are based on the published journal paper: Chen Wang and Xiaodong Wang, “Modeling and simulation of wave scattering of multiple inhomogeneities in composite media” *Composites Part B: Engineering*, vol. 90, pp. 341-350, January 2016. The thesis author conducted this research under the supervision by Dr. Xiaodong Wang.

Chapter 3 and Chapter 5 are based on a journal paper in preparation: Chen Wang and Xiaodong Wang, “Computational homogenization for antiplane wave propagation in heterogeneous materials”. The thesis author conducted this research under the supervision by Dr. Xiaodong Wang.

The second section of Chapter 4 is based on a journal paper in preparation: Chen Wang and Xiaodong Wang, “A computational homogenization method based on the energy equivalence”. The thesis author conducted this research under the supervision by Dr. Xiaodong Wang.

Acknowledgements

I would like to express my deepest gratitude to my supervisor Dr. Xiaodong Wang for his patient guidance, enthusiastic encouragement and unwavering support. His insightful and valuable advices helped me a lot throughout my study.

I would like to extend my sincere thanks to my Ph.D. supervisory committee members, Dr. Tian Tang and Dr. Peter Schiavone, for their constructive advices on my research. I would also like to give my appreciation to my candidacy exam committee members, Dr. Ben Jar and Dr. Mustafa Gul, for their helpful suggestions on my research proposal.

I am also grateful to China Scholarship Council and National Sciences and Engineering Research Council for the financial supports.

Special thanks to the ASML members, Dr. Zhengwei Li, Dr. Huangchao Yu, Dr. Mohammad Molavi Nojumi, Dr. Shadi Abdel-Gawad and Huan Hu. It was a great pleasure and honor to work with them.

Last but not least, I am deeply indebted to my parents, my parents-in-law and my wife. Without their endless supports and encouragement, I could never achieve this goal.

Contents

Abstract	ii
Preface	iv
Acknowledgements	v
1 Introduction	1
1.1 Background	1
1.2 Motivation	2
1.3 Literature Review	4
1.3.1 Multiple scattering of elastic waves	4
1.3.2 Elastodynamic homogenization	5
1.3.3 Multiscale modeling of elastodynamic problem	7
1.4 Research objectives and outline	8
2 Multiple scattering of elastic waves	10
2.1 Introduction	10
2.2 Formulation of the problem	12
2.2.1 The single scattering problem	14

2.2.2	Interaction of multiple inhomogeneities	20
2.3	Verification of the method	23
2.3.1	Evaluation of numerical integration	23
2.3.2	Convergence of the series	26
2.3.3	Comparison with existing results	28
2.3.4	Limiting cases	30
2.4	Application examples	33
2.4.1	General case example	33
2.4.2	Interactions among the inhomogeneities	37
2.4.3	Stop band	38
2.5	In-plane problem	42
2.5.1	Formulation of the problem	42
2.5.2	General example	46
2.6	Conclusion	50
3	Elastic waves in periodic materials	52
3.1	Introduction	52
3.2	Formulation of the problem	54
3.3	Verification of the method	60
3.4	Conclusion	63

4	Homogenization based on domain averaging	64
4.1	Volume average	64
4.1.1	Basic concepts of the elastostatic homogenization	64
4.1.2	Basic concepts of the elastodynamic homogenization	68
4.1.3	Formulations and results	72
4.2	Energy equivalence	77
4.2.1	Formulations	78
4.2.2	Verification of the method	80
4.2.3	Effective properties	86
4.3	Conclusion	87
5	Homogenization based on boundary matching	89
5.1	Introduction	89
5.2	Methodology	90
5.3	RVE modeling	94
5.3.1	Random material	94
5.3.2	Periodic material	95
5.4	Verification of the method	96
5.4.1	Random materials	96
5.4.2	Periodic materials	101

5.5	Effective material properties of periodic material	109
5.6	Multiscale modeling	113
5.6.1	Multiple scattering in large scale	113
5.6.2	Recovery of the local response	115
5.7	Conclusion	121
6	Contributions and future work	123
6.1	Main contributions	123
6.1.1	Efficient method for solving the multiple scattering problem	123
6.1.2	Efficient method for eigenstate determination	124
6.1.3	Homogenization methods based on domain averaging	124
6.1.4	Homogenization method based on boundary matching	125
6.2	Future works	125
6.2.1	Extension to in-plane wave problem	125
6.2.2	Different shapes of inhomogeneity	126
6.2.3	Viscoelastic materials	127
6.2.4	Experimental verifications	127
	Bibliography	128

List of Figures

2.1	Schematic sketch of the model.	13
2.2	Deviation of the computed coefficients compared with the analytical ones.	25
2.3	Comparison of the computed stresses from numerical and analytical results.	26
2.4	Convergence of the series	27
2.5	Normalized stress τ_{rz} around the left inhomogeneity, compared with the analytical solution.	29
2.6	Normalized stress $\tau_{\phi z}$ around the left inhomogeneity, compared with the analytical solution.	29
2.7	Normalized stress $\tau_{\phi z}$ around the smaller cavity, compared with the BEM results.	30
2.8	The mismatch of normalized displacement under limiting condition.	32
2.9	The mismatch of normalized τ_{rz} under limiting condition.	32
2.10	Computational model of the general case.	34
2.11	Displacement amplitude of the general case.	35
2.12	τ_{xz} amplitude of the general case.	35
2.13	τ_{yz} amplitude of the general case.	36
2.14	Stress amplitudes along L1 and L2.	36
2.15	Stress amplitudes along each interface in the model with 6 inhomogeneities.	37

2.16	Stress amplitudes along each interface in the model with 8 inhomogeneities.	38
2.17	Computational model for showing stop band.	39
2.18	Displacement amplitude of the points right behind the arrangement.	39
2.19	Displacement amplitude decays for the specific frequency.	40
2.20	Distribution of displacement amplitude when $k_m R = 0.2$	41
2.21	Distribution of displacement amplitude when $k_m R = 0.8$	41
2.22	Distribution of displacement amplitude when $k_m R = 1.2$	42
2.23	Amplitude of displacement in x direction (m).	47
2.24	Amplitude of displacement in y direction (m).	47
2.25	Amplitude of stress σ_{xx} (Pa).	48
2.26	Amplitude of stress σ_{yy} (Pa).	49
2.27	Amplitude of stress σ_{xy} (Pa).	49
2.28	The mismatch of normalized displacement and traction.	50
3.1	Model of unit cell under periodic boundary condition	54
3.2	Eigenstate of the unit cell.	59
3.3	Dispersion relation comparison.	60
3.4	Normalized displacement amplitude $ w $ along L1.	61
3.5	Normalized stress amplitude $ \tau_{xz} $ along L1.	62
3.6	Normalized stress amplitude $ \tau_{yz} $ along L1.	62

4.1	RVE for elastostatic homogenization.	65
4.2	RVE for elastodynamic homogenization.	69
4.3	Computational model of homogenization.	73
4.4	Effective phase velocity for the square and hexagonal arrangement	76
4.5	Attenuation of the square and hexagonal arrangement	77
4.6	Comparison with existing results	81
4.7	Direct numerical simulation models for comparison	82
4.8	Comparison between the displacement fields of the periodic model and homogenized model	83
4.9	Normalized displacement amplitude $ w $ along the lines	84
4.10	Normalized stress amplitude $ \tau_{xz} $ along the lines	85
4.11	Effective mass density.	86
4.12	Effective shear modulus.	87
5.1	Schematic sketch of the model	91
5.2	Direct numerical simulation models for comparison	96
5.3	Coefficients of variation obtained by RVEs with different radii	97
5.4	Averages of effective properties obtained by RVEs with different radii	98
5.5	Comparison between the displacement fields of the random model and homogenized model	99

5.6	Normalized displacement amplitude $ w $ along the lines in the random model and homogenized model	100
5.7	Normalized stress amplitude $ \tau_{xz} $ along the lines in the random model and homogenized model	101
5.8	Direct numerical simulation models for comparison	102
5.9	Normalized displacement distributions of the two models	102
5.10	Normalized displacement amplitude $ w $ along the lines in the pass-band	103
5.11	Normalized stress amplitude $ \tau_{xz} $ along the lines in the pass-band	104
5.12	Homogenization model for frequencies in the stop-band	105
5.13	Comparison between the effective properties obtained by the RVEs with multiple scattering and PBC	106
5.14	Normalized displacement distributions of the two models in stop-band	107
5.15	Normalized displacement amplitude $ w $ along the lines in the stop-band	108
5.16	Normalized stress amplitude $ \tau_{xz} $ along the lines in the stop-band	109
5.17	Effective material properties in the first pass-band	110
5.18	Comparison of the effective mass density obtained by different methods	111
5.19	Comparison of the effective shear modulus obtained by different methods	111
5.20	Effective material properties in the first stop-band	112
5.21	Direct numerical simulation models for multiple scattering	113
5.22	Normalized displacement distributions of the two models of multiple scattering	114

5.23	Normalized displacement amplitude $ w $ along the circles	115
5.24	Normalized stress amplitude $ \tau_{rz} $ along the circles	115
5.25	Comparison of the recovered local response with the direct numerical simulation.	117
5.26	Normalized displacement amplitude $ w $ along the center line.	118
5.27	Normalized stress amplitude $ \tau_{xz} $ along the center line.	118
5.28	Normalized stress amplitude $ \tau_{yz} $ along the center line.	119
5.29	Normalized displacement amplitude $ w $ along the interface.	120
5.30	Normalized stress amplitude $ \tau_{rz} $ along the interface.	120
5.31	Normalized stress amplitude $ \tau_{\theta z} $ along the interface.	121

Chapter 1: Introduction

1.1 Background

Heterogeneous materials have been extensively used due to their desirable properties achieved by combining various constituents and tailored local structures. For example, reinforced concretes are the most widely used artificial materials in civil engineering because the steel reinforcing bar can compensate the relatively low tensile strength of the concrete. Carbon fiber reinforced polymer has high strength-to-weight ratio and is ideal for the structure of aircraft (Hashin, 1972). Since most of the working conditions involve dynamic loads, the evaluation of their elastodynamic behavior is essential for the damage tolerance design against dynamic failure. The ultrasonic non-destructive evaluation of the structure composed of heterogeneous materials also relies on the understanding of the elastic wave propagation in such materials.

More recently, metamaterials, which are the artificial materials with unusual properties caused by the well-designed local structures, have attracted extensive attention (Kadic et al., 2019). By on the effects of Bragg scattering or the use of local resonant structures, the wave propagation in the metamaterials can be manipulated. Based on the different types of wave on which the metamaterials work, the metamaterials can be generally categorized into electromagnetic metamaterials and mechanical metamaterials, which can be further classified by the existence of shear stress, into elastic metamaterials or acoustic metamaterials. Since the primary waves are coupled with the shear waves in elastic metamaterials, the modeling and simulation of their elastodynamic response plays a significant role in the design and optimization of the

microstructures of these materials.

1.2 Motivation

A major difficulty in the simulation of the elastic wave propagation in such heterogeneous media is the interaction among the multiple inhomogeneities involved, which form complicated boundary/interface conditions. It is usually very difficult, if not impossible, to develop analytical solutions to this type of problems. As a result, dynamic modeling of such materials is either based on pure numerical simulation or focused on the effective properties of homogenized models.

The pure numerical simulation faces significant challenges when both the local and global responses are important. The direct numerical modeling is inefficient to describe all the fine-scale features as well as the macroscopic structures simultaneously. For example, with finite element method (FEM), the local structures need to be discretized with fine elements which has smaller lengthscale, then the element number will be too large to handle if the macroscopic structure is discretized with the same meshing scheme. So the pure numerical simulations becomes prohibitive due to the substantial separation of scales.

Accordingly, for the systems with complex structures in various scales, the multiscale models are usually necessary. The local structures are replaced by homogeneous materials with effective properties in which the local response is incorporated approximately. Then the macroscopic structures can be modeled and simulated with well developed techniques.

Like the polymorphism in crystallography, the macroscopic properties can vary largely depending on the underlying local structures, in spite of the same ingredients. The evaluation of

the effective mechanical properties necessitates the analysis of the local response, which is usually an extremely complex problem with analytical methods. After the seminal work of Eshelby (Eshelby, 1957) on the elastic field of an ellipsoidal inclusion, the theory of micromechanics has been developed, and the homogenization of heterogeneous materials under static loading has been researched extensively. For the elastodynamic homogenization under very low frequencies without any local resonance, the problem is quite similar to the static ones. When the frequency rises, the metamaterials with local soft mode on the sub-wavelength structure tend to have local resonances, which can result in negative effective properties. However, this phenomenon is independent of the periodicity of the material. So the effective properties can be obtained by the local dynamic analysis. When the frequency is so high that the wavelength is comparative or shorter than the characteristic length of the local structure, there is no valid effective material properties since the local structure can be resolved from the resultant wave field. Therefore, for the frequencies under which the stop band is caused by Bragg scattering, the interaction among the local structures is essential for the homogenization. In this work, the interaction is solved numerically to facilitate the computational homogenization. The advantage of explicitly solving the wave field is that more accurate prediction of the local response can be provided, comparing with the approximate solutions in previous works (Nemat-Nasser et al., 2011; Willis, 1997), in which the local response is approximated by using the expansion of Green's function and variational method.

The beginning of multiple scattering analysis may be traced back to the work of Lord Rayleigh on the scattering of light (Rayleigh, 1870). Then multiple scattering problem in various disciplines (e.g. acoustic wave, electromagnetic wave and electron wave) has been studied

extensively. However, due to the mode conversion in elastodynamic problems, the multiple scattering of elastic waves has unique complexity. It is still necessary to develop an accurate and effective technique to evaluate the local stress field when involving large number of inhomogeneities.

Therefore, in this work, an analytical-numerical method for the multiple scattering problem is developed first. Then an efficient method for the eigenstate determination of periodic unit cell is developed for periodic materials. Based on the computed local responses, the computational homogenization techniques are developed. Lastly, the multiscale model is developed by combining the developed techniques.

1.3 Literature Review

1.3.1 Multiple scattering of elastic waves

The multiple scattering problem of waves in inhomogeneous media was first treated by assuming the rays to be trajectories of particles. In 1945, Foldy originally considered the problem by using the wave treatment. The scattering of scalar waves by isotropic scatterers were studied and the “configurational averaging” method was developed to take the average of resulting waves over the ensemble of configurations (Foldy, 1945). Then to determine the wave field explicitly, an important technique called “T-matrix” approach is developed by Waterman (Waterman, 1969). The T-matrix is a linear transformation between the expansion coefficients of incident wave and scattered wave. Based upon that, Varadan proposed the scattering matrix approach to investigate the multiple scattering of elastic waves in a medium with multiple in-

homogeneities with arbitrary cross section (Varadan et al., 1978). Cai and Williams proposed a technique called scatterer polymerization to reduce the actual scatterers to less abstract ones. With the use of T-matrix, they developed a numerical procedure for large-scale multiple scattering problems (Cai and Williams, 1999a,b). Biwa et al. and Sumiya et al. analyzed the multiple scattering of SH wave (Biwa et al., 2004) and P/SV waves (Sumiya et al., 2013) in unidirectional fiber-reinforced composite by using numerical collocation method. Wang and Sudak investigated the multiple scattering of P/SV waves by cylinders with imperfect bonding conditions (Wang and Sudak, 2007). By using the boundary integral method, Benites et al. (Benites et al., 1992, 1997) and Dravinski and Yu (Dravinski and Yu, 2011) studied the multiple scattering of elastic waves by multiple inhomogeneities with circular or arbitrary cross section.

1.3.2 Elastodynamic homogenization

A major part of the works on the elastodynamic homogenization are focused on the heterogeneous materials with periodic local structures. The static problems of periodic material have been well studied by the method of asymptotic homogenization (Arabnejad and Pasini, 2013; Sabina et al., 2002). In the dynamic context, with the assumption that the materials are perfect periodic and infinitely extended, Bloch waves are admitted as the solutions. The asymptotic homogenization method was extended to the dynamic problems at low frequencies (Parnell and Abrahams, 2006). And recently, it has been extended to higher frequencies (Antonakakis et al., 2014; Hui and Oskay, 2014). In the phononic crystal research field, the periodicity of the local structures and the wave forms is also assumed inherently, and various numerical techniques have been developed to determine the dispersion relations. These include the plane

wave expansion method (Kushwaha et al., 1993; Sigalas and Economou, 1992), the multiple scattering theory method (Liu et al., 2002; Mei et al., 2003), the finite-difference time-domain method (Sigalas and Garcia, 2000), variational methods (Srivastava and Nemat-Nasser, 2014), etc. Since the works are mainly focused on the band structures, the Bloch wave vector is prescribed and the frequency of the incident wave is computed as the eigenvalue. In addition, the Bloch wave vector is usually limited to the boundary of the irreducible Brillouin zone. So the methods are inefficient to determine the effective wave fields under prescribed incident waves.

For the heterogeneous materials with random local structures, the configurational averaging method was first developed by Foldy to take the average of resulting waves over the ensemble of configurations (Foldy, 1945). Lax generalized the procedure (Lax, 1951) and introduced the quasi-crystalline approximation to determine the effective field (Lax, 1952). Because of the similarity of the wave phenomena, the retrieval method, which began with electromagnetic waves, was subsequently extended to acoustic waves (Fokin et al., 2007) and elastic waves (Zhang et al., 2013). Although the retrieval method is simple in principle, it is unreliable when the frequency is high and the wave number in the heterogeneous medium is unknown. Typical micromechanical models used in static problems, such as self-consistent (Kim, 1996, 2003; Norris and Conoir, 2011; Sabina and Willis, 1988) and generalized self-consistent models (Yang and Mal, 1994, 1996), have also been extended to the dynamic problem for the evaluation of the effective properties. However the existing methods are limited to the low frequencies, low doping ratios or small mismatch of mechanical properties between the matrix and the inhomogeneities.

1.3.3 Multiscale modeling of elastodynamic problem

For multiscale modeling, the most important issue is the upscaling method, by which the effects of fine-scale features can be reproduced. There are two main categories of methods. The first one is based on the effective properties obtained with various homogenization techniques. Many of them are based on the averaging the field variables of local wave field with different assumptions of the constitutive relation (Backus, 1962; Helbig and Schoenberg, 1987; Tsvankin et al., 2010). By applying matrix and group theory, a general effective medium theory is developed by Schoenberg (Schoenberg and Muir, 1989) and tested by comparing the analytical results with the ones obtained with a finite-difference method (Carcione et al., 2012). Later, various numerical approaches have been developed with solving the local problem numerically and averaging the field variables to extract the effective properties (Grechka, 2003; Rijpsma and Zijl, 1998; Zijl et al., 2002). For the periodic fine-scale features, the asymptotic homogenization can also be employed (Allaire, 1992). Since the effective properties should be independent of the boundary condition, the separation of scales have to be assumed. So this category of multiscale methods is preferable for the structures with large difference between the characteristic lengths of two scales.

Instead of computing the effective properties, the other category of methods is based on combining the results computed in fine-scale into the simulations carried out in coarse-scale. One of the most popular and earliest developments is the Multiscale Finite Element Method by Hou and Wu (Hou and Wu, 1997). By constructing basis functions obtained from solving boundary value problem in fine-scale, the effect of the fine-scale features is incorporated through the global stiffness matrix. More recently Gao et al. proposed a General Multiscale

Finite Element Method in which the basis functions are constructed from multiple local problems (Gao et al., 2015a,b). Casadei and Ruzzene et al. developed a Geometric multiscale Finite Element Method (Casadei and Ruzzene, 2012; Casadei et al., 2013, 2014, 2016). The method is based on multi-node elements whose shape functions are computed numerically by means of an auxiliary fine-scale discretization. In this category of multiscale methods, while the assumption of separation of scales is relaxed, the computational cost is higher than that of the homogenization-based methods.

1.4 Research objectives and outline

The overall objective of this work is to develop new multiscale methods for the analysis of the elastic wave propagation in heterogeneous materials consisting of underlying local structures. The multiscale modeling is based on the effective properties obtained by homogenization technique, which depends on the computation of the multiple scattering wave field or the eigenstate of periodic unit cell in the fine-scale. Therefore, the work in this thesis is carried out in following steps:

First, an efficient analytical-numerical method is developed for the multiple scattering problem of elastic waves in the infinite media consisting of significant numbers of circular inhomogeneities under both antiplane and in-plane incident wave loading.

Secondly, for efficiently computing the local response of periodic materials under given loading, an analytical-numerical method for the eigenstate determination of the periodic unit cell is developed.

Based on the explicitly solved wave field, the methods of computational homogenization

are proposed to extract the effective elastodynamic properties of the heterogeneous material. By averaging the computed wave field inside the domain of RVE, two methods are developed. The first one is based on the volume averages of the stress and strain with the averaging scheme modified to consider the effective wave form, in which the effective wave number is determined by self-consistent method. The second one is based on the assumptions of effective wave number and the kinetic energy equivalence.

Then the other kind of computational homogenization method is developed based on matching the boundary response of the RVE. By defining the residue function, which indicates the mismatch between the boundary responses of the RVE and the homogenized substitution, as the objective function, the homogenization is reduced to an optimization problem. Then the numerical optimization methods are employed to minimize the residue function over the complex-valued material properties.

At last, the multiscale modeling method is summarized, which is capable of simulating the scattering of waves with long wavelength relative to the local structures in large scale efficiently, and accurately recovering the local response at any location on demand.

Chapter 2: Multiple scattering of elastic waves

This chapter presents an analytical-numerical method for the two-dimensional multiple scattering problem of elastic composite media with interacting inhomogeneities under time-harmonic elastic incident waves. The main focus is on the detailed evaluation of the effectiveness and accuracy of the method in the determination of the local dynamic behaviour of such composite media with significant numbers of inhomogeneities. The method is based on the eigenfunction expansion of single inhomogeneity problem and the use of a pseudo-incident wave technique, which allows the accurate determination of local stress field caused by the interaction. The accuracy and effectiveness of the method for dealing with multiple interaction problems are discussed in detail. Illustrative examples under different loading and geometric conditions are considered to study the local dynamic field and the behavior of stop-band of wave propagating for periodic inhomogeneity arrangements. Then the method is extended to in-plane problem by introducing Helmholtz decomposition. This chapter stems from the published journal article written by the author under the supervision by Dr. Wang. (Wang and Wang, 2016).

2.1 Introduction

One of the major issues in the study of elastic waves in inhomogeneous media is the accurate determination of the local stress field, which is important for the the damage evaluation of composite materials and for the recent study of elastic waves in periodic structures for filter or resonator applications. For a single inhomogeneity, the scattering can be easily determined by using well-known techniques (Waterman, 1969). The solution of the interaction

problems is usually based on the proper superposition of the scattered waves from different inhomogeneities. The scattering of antiplane shear waves by interacting cylindrical elastic inhomogeneities was studied analytically using Fourier expansion and was used to evaluate the effective properties of the material and the behavior of effective wave propagation (Bose and Mal, 1974). By integrating the geometric relations between inhomogeneities in the solution, an analytical solution is provided. A similar technique was used to investigate the scattering of elastic waves in a medium containing multiple inhomogeneities (Varadan et al., 1978). To deal with the large number of inhomogeneities needed when considering multiple interaction, a multi-stage superposition process, scatterer polymerization, was developed to reduce the number of scatters in each stage (Cai and Williams, 1999a,b). The multiple scattering of SH wave (Biwa et al., 2004) and P/SV waves (Sumiya et al., 2013) in unidirectional fiber-reinforced composite were analyzed using the solutions mentioned in (Bose and Mal, 1974) by simplifying the analytical solutions using collocation points at the fibers and the wave field was determined. The multiple scattering of P/SV waves by cylinders with imperfect bonding conditions has also been studied (Wang and Sudak, 2007). The boundary integral method has been used to study the scattering of elastic waves by multiple inhomogeneities with circular or arbitrary cross section (Benites et al., 1992, 1997; Dravinski and Yu, 2011; Manolis and Dineva, 2015; Parvanova et al., 2013, 2014, 2015; Sheikhhassani and Dravinski, 2014). Although the general methodology for solving these problems have been extensively studied, the main issue that how to accurately evaluate the local stress when large numbers of inhomogeneities still needs to be evaluated carefully.

In the current chapter, a numerical procedure is studied to solve the multiple interaction

between inhomogeneities in elastic heterogeneous media. The main idea is to provide a two-step solution to this type of interaction problems by first developing the single inhomogeneity solution as the building block and then assembling them into the governing equation of the original problem using the pseudo-incident wave method. Heterogeneous media with circular inhomogeneities subjected to antiplane shear wave is studied in detail. The displacement is expressed by Fourier expansion for the single inhomogeneity problem and the interaction problem is formulated by using the pseudo-incident wave technique (Wang and Meguid, 1997), which reduces the multiple scattering problem into coupled solutions of single scattering problems. The accuracy and effectiveness of the scheme are discussed. As the examples of application, the interaction among the inhomogeneities is studied for the determination of local stress field. The feature of wave propagation in heterogeneous media with periodically arranged inhomogeneities is studied and the existence of stop band is demonstrated. At last, the method is extended to in-plane problems by using the Helmholtz decomposition, which decouples the P and SV waves. The current work is limited to cylindrical shaped inhomogeneities with no damping considered. The method can be extended to inhomogeneities with different shapes and different kinds of materials by using the method presented in this chapter with new general solutions, which can be determined analytically or numerically.

2.2 Formulation of the problem

The problem considered is the dynamic interaction among multiple inhomogeneities embedded in an elastic medium subjected to harmonic elastic waves. The inhomogeneities are cylindrical in shape with the radii being R_i . The shear moduli of the matrix and the inhomogeneities

are assumed to be μ_m and μ_i , and the mass densities are ρ_m and ρ_i . A Cartesian coordinate system is used as the global coordinate system and polar coordinate systems are created for each inhomogeneity, with origins at the centers of the inhomogeneities. The system is schematically shown in Figure 2.1.

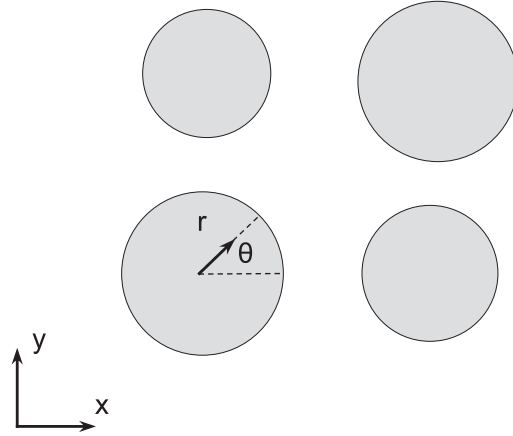


Figure 2.1: Schematic sketch of the model.

The displacement, strain and stress fields corresponding to a steady-state incident elastic wave of frequency ω can be expressed in terms of the frequency ω , such that

$$A^*(x, y, t) = A(x, y)e^{-i\omega t} , \quad (2.1)$$

where A^* represents a field variable, such as displacement or stress. For the sake of convenience, in the following discussion the time factor $e^{-i\omega t}$ will be suppressed.

In what follows, the formulations of single scattering problem of one circular inhomogeneity will be summarized first. The numerical integration method will be developed to simplify the solution and transfer it into a matrix format which is suitable for further evaluation of in-

teracting inhomogeneities. Then the pseudo-incident wave technique will be introduced to deal with the interaction among multiple inhomogeneities.

2.2.1 The single scattering problem

The scattering problem for a single circular inhomogeneity in an elastic matrix is well understood in general. The main formulation of the problem is summarized first in this section to provide the theoretical background for the general interaction problems.

For antiplane problems, the displacement w in the x_3 direction in the matrix and inhomogeneity is governed by the following Helmholtz equation (Achenbach, 1973),

$$(\nabla^2 + k^2) w = 0 \quad (2.2)$$

where ∇^2 is the Laplacian operator, $k = k_m$ or k_i , $k_m = \omega/c_m$ and $k_i = \omega/c_i$ are the wave numbers of the matrix and inhomogeneity, with c_m and c_i being the corresponding shear wave speeds. In the cylindrical coordinate system, the governing equation can be expressed as

$$\left(\frac{\partial^2}{\partial r^2} + \frac{1}{r} \frac{\partial}{\partial r} + \frac{1}{r^2} \frac{\partial^2}{\partial \theta^2} \right) w + k^2 w = 0 \quad (2.3)$$

where r is the distance measured from the center of inhomogeneity and the θ is the angular coordinate measured from x axis of global coordinate system.

The general solution of the governing equation can be expressed in forms of Fourier expan-

sion as (Waterman, 1969)

$$w(r, \theta) = \sum_{n=-\infty}^{\infty} \left[J_n(kr) B_n e^{in\theta} + H_n^{(1)}(kr) A_n e^{in\theta} \right], \quad (2.4)$$

where J_n and $H_n^{(1)}$ are the Bessel functions and the Hankel functions of the first kind, k is the corresponding wave number and A_n and B_n are the unknown constants to be determined from the boundary/interface conditions. For the scattered wave field in the matrix, the radiation condition must be satisfied (Colton and Kress, 2013; Kupradze, 1976),

$$\lim_{r \rightarrow \infty} \sqrt{r} \left(\frac{\partial w}{\partial r} - ik_m w \right) = 0. \quad (2.5)$$

Substituting the equation (2.4) into equation (2.5) indicates that B_n must be zero. For the field in the inhomogeneity, A_n must be zero to ensure that the field has a limited amplitude at the center of the inhomogeneity $r = 0$. The displacements of the scattered wave field in the matrix and the field in the inhomogeneity are

$$w(r, \theta) = \begin{cases} \sum_{n=-\infty}^{\infty} H_n^{(1)}(k_m r) A_n e^{in\theta} & r \geq R \quad \text{In the matrix} \\ \sum_{n=-\infty}^{\infty} J_n(k_i r) B_n e^{in\theta} & r < R \quad \text{In the inhomogeneity.} \end{cases} \quad (2.6)$$

It is further assumed that the inhomogeneity and the matrix are perfectly bonded. The continuity conditions along the interface can then be expressed as

$$w_m|_{inter} = w_i|_{inter}, \quad \tau_m|_{inter} = \tau_i|_{inter}, \quad (2.7)$$

where τ is the shear stress τ_{rz} , and the subscripts m and i represent matrix and inhomogeneity respectively.

When the system is subjected to an incident wave w_{in} , the wave field in the matrix can be considered as the superposition of the incident wave field (w_{in}, τ_{in}) and the scattered wave field (w_{sc}, τ_{sc}), such that

$$w_m = w_{in} + w_{sc} , \quad \tau_m = \tau_{in} + \tau_{sc} . \quad (2.8)$$

Then the continuity conditions become

$$w_{in}|_{inter} + w_{sc}|_{inter} = w_i|_{inter} , \quad \tau_{in}|_{inter} + \tau_{sc}|_{inter} = \tau_i|_{inter} . \quad (2.9)$$

The coefficients A_n and B_n of the scattered wave and the refracted wave in the inhomogeneity can be obtained by using the continuity condition along the interface and the orthogonality of the expansion, such that

$$\begin{Bmatrix} A_n \\ B_n \end{Bmatrix} = [T_n] \int_0^{2\pi} \begin{Bmatrix} w_{in}|_{inter} \\ \tau_{in}|_{inter} \end{Bmatrix} e^{-in\theta} d\theta , \quad (2.10)$$

where

$$[T_n] = -\frac{1}{2\pi} \begin{bmatrix} H_n^{(1)}(k_m R) & -J_n(k_i R) \\ \mu_m k_m H_n^{(1)'}(k_m R) & -\mu_i k_i J_n'(k_i R) \end{bmatrix}^{-1} \quad (2.11)$$

with the prime (') representing the derivative. The displacement of scattered wave and the refracted wave inside the inhomogeneity can then be obtained by substituting the computed A_n and B_n into equation (2.6).

The above relation between the boundary value of the incident wave and the scattered wave can be considered as a transfer function, which depends on the configurations of the inhomogeneity, the material properties, and the incident frequency. For the multiple scattering problem, the expressions of the input wave $w_{in}|_{inter}$ in the local polar coordinate system become very complicated when the effects of the other inhomogeneities are considered.

An efficient way to establish the relation between the incident and the scattered waves is replacing (2.10) by an equivalent discrete linear transformation from the boundary values of the incident wave to the coefficients of the scattered wave. This is achieved by using only the values of the incident wave at limited number of integration points along the interface, e.g. equally spaced points, to complete the integration (Wang and Wang, 2016). As shown in equations (2.10), the transformation will involve the integration of the exponential term $e^{-in\theta}$, which will always fluctuate intensely when the order n becomes high. To ensure the accuracy of the treatment, instead of discretizing the whole integrand, only the boundary value of the incident wave along the interface is discretized and replaced by linear interpolation functions. Then the original integral is replaced with a finite summation of analytical integrals of the piecewise linear interpolation functions multiplied by the exponential factors. For the integration of the displacement, for example,

$$\int_0^{2\pi} w_{in}|_{inter} e^{-in\theta} d\theta \approx \sum_{j=1}^P \int_{\theta_j}^{\theta_j+\Delta\theta} f_j(\theta) e^{-in\theta} d\theta, \quad (2.12)$$

where P is the total number of the integration points, $f_j(\theta)$ is the j th interpolation function, θ_j is the angular coordinate of j th integration point along the interface and $\Delta\theta$ is the interval angle between two neighboring integration points. For uniformly distributed integration points, for

example,

$$\theta_j = \frac{2\pi}{P}(j-1), \quad \Delta\theta = \frac{2\pi}{P}. \quad (2.13)$$

The linear interpolation function of the displacement along the interface between two integration points $\theta^{(j+1)}$ and $\theta^{(j)}$ is

$$f_j(\theta) = a_j\theta + b_j, \quad (2.14)$$

where

$$a_j = \frac{w_{in}^{(j+1)}|_{inter} - w_{in}^{(j)}|_{inter}}{\Delta\theta} \quad (2.15)$$

$$b_j = w_{in}^{(j+1)}|_{inter} - \theta_{j+1} \frac{(w_{in}^{(j+1)}|_{inter} - w_{in}^{(j)}|_{inter})}{\Delta\theta}, \quad (2.16)$$

with $w_{in}^{(j)}|_{inter}$ being the displacement of the incident wave at the j th integration point. The interpolation functions for the incident stress can be obtained similarly. The coefficients of the expansion can then be determined by

$$\begin{Bmatrix} A_n \\ B_n \end{Bmatrix} = [T_n] \sum_{j=1}^P \int_{\theta_j}^{\theta_{j+1}} \begin{Bmatrix} a_j\theta + b_j \\ g_j\theta + h_j \end{Bmatrix} e^{-in\theta} d\theta, \quad (2.17)$$

where g_j and h_j are the counterparts of a_j and b_j for the interpolation functions of the shear stress. By substituting (2.15) and (2.16) into (2.17), the coefficients A_n and B_n can be expressed in terms of the values of the incident field at the integration points as

$$\{A\} = [Q] \{\xi_{in}\}, \quad \{B\} = [R] \{\xi_{in}\}, \quad (2.18)$$

where vector $\{\xi\}$ is called the effect vector in this work, with the subscript indicating the wave

by which the effect is caused, composed as

$$\{\xi_{in}\} = \begin{Bmatrix} \{w_{in|inter}\} \\ \{\tau_{in|inter}\} \end{Bmatrix}, \quad (2.19)$$

where $\{w_{in|inter}\}$ and $\{\tau_{in|inter}\}$ are the vectors comprised by the displacements and the shear stresses at the integration points along the interface due to the incident wave. $[Q]$ and $[R]$ are the known transition matrices, given by

$$Q_{nj} = \begin{cases} C_n T(n, j) & 1 \leq j \leq P \\ D_n T(n, j - P) & P + 1 \leq j \leq 2P. \end{cases} \quad (2.20)$$

where C_n and D_n are

$$C_n = \frac{k_i \mu_i J'_n(k_i R)}{2\pi \left[k_m \mu_m J_n(k_i R) H_n^{(1)'}(k_m R) - k_i \mu_i J'_n(k_i R) H_n^{(1)}(k_m R) \right]}, \quad (2.21)$$

$$D_n = \frac{-J_n(k_i R)}{2\pi \left[k_m \mu_m J_n(k_i R) H_n^{(1)'}(k_m R) - k_i \mu_i J'_n(k_i R) H_n^{(1)}(k_m R) \right]}, \quad (2.22)$$

and $T(n, j)$ is

$$T(n, j) = \begin{cases} \Delta\theta & n = 0 \\ \alpha(n, 1) + \beta(n, P) & n \neq 0, j = 1 \\ \alpha(n, j) + \beta(n, j - 1) & n \neq 0, j > 1, \end{cases} \quad (2.23)$$

with

$$\alpha(n, j) = \left[\frac{1}{n^2 \Delta\theta} (1 - e^{-in\Delta\theta}) - \frac{i}{n} \right] e^{-in(j-1)\Delta\theta}, \quad (2.24)$$

$$\beta(n, j) = \left[-\frac{1}{n^2 \Delta \theta} + \left(\frac{i}{n} + \frac{1}{n^2 \Delta \theta} \right) e^{-in \Delta \theta} \right] e^{-in(j-1) \Delta \theta}. \quad (2.25)$$

The element of matrix $[R]$ is

$$R_{nj} = \begin{cases} E_n T(n, j) & 1 \leq j \leq P \\ F_n T(n, j - P) & P + 1 \leq j \leq 2P, \end{cases} \quad (2.26)$$

where

$$E_n = \frac{k_m \mu_m H_n^{(1)'}(k_m R)}{2\pi \left[k_m \mu_m H_n^{(1)'}(k_m R) J_n(k_i R) - k_i \mu_i H_n^{(1)}(k_m R) J_n'(k_i R) \right]}, \quad (2.27)$$

$$F_n = \frac{-H_n^{(1)}(k_m R)}{2\pi \left[k_m \mu_m H_n^{(1)'}(k_m R) J_n(k_i R) - k_i \mu_i H_n^{(1)}(k_m R) J_n'(k_i R) \right]}. \quad (2.28)$$

Matrices $[Q]$ and $[R]$ provide direct transformations from the the values of the incident wave at the integration points to the parameters A_n and B_n . From this relation the wave field due to a single inhomogeneity in the matrix and in the inhomogeneity can be calculated.

2.2.2 Interaction of multiple inhomogeneities

For an elastic medium with N inhomogeneities, the wave field in the matrix can be considered as the superposition of the incident wave and the scattered waves from each inhomogeneity.

$$w = w_0 + \sum_{i=1}^N w_{sc}^{(i)}, \quad (2.29)$$

where w_0 represents the incident wave, $w_{sc}^{(i)}$ represents the scattered wave from the i^{th} inhomogeneity and N is the total number of inhomogeneities. For the k^{th} inhomogeneity, it is subjected

to a pseudo-incident wave $w_{ps}^{(k)}$ which is the superposition of the real incident wave w_0 and the scattered waves from other inhomogeneities (Wang and Meguid, 1997), such that

$$w_{ps}^{(k)} = w_0 + \sum_{\substack{i=1 \\ i \neq k}}^N w_{sc}^{(i)}, \quad \tau_{ps}^{(k)} = \tau_0 + \sum_{\substack{i=1 \\ i \neq k}}^N \tau_{sc}^{(i)}, \quad (2.30)$$

where $\tau_{sc}^{(i)}$ is the shear stress due to the scattered wave from i^{th} inhomogeneity. As a result of this pseudo-incident wave, the scattered wave from the k^{th} inhomogeneity can be obtained from equations (2.18), considering the pseudo-incident wave $w_{ps}^{(k)}$ as the incident wave in the single scattering problem, such that

$$\{A^{(k)}\} = [Q]_k \{\xi_{ps}^{(k)}\}, \quad (2.31)$$

where $\{A^{(k)}\}$ is the vector composed of the expansion coefficients of the scattered wave from the k^{th} inhomogeneity, $\{\xi_{ps}^{(k)}\}$ is the effect vector of the pseudo-incident wave to the k^{th} inhomogeneity. It is composed of the components of displacement and traction due to the pseudo-incident wave at the integration points of k^{th} inhomogeneity.

As shown in equation (2.30), the effect vector of the pseudo-incident wave is the superposition of the ones of the original incident wave and the scattered waves from all the other inhomogeneities, such that

$$\{\xi_{ps}^{(k)}\} = \{\xi_0^{(k)}\} + \sum_{\substack{i=1 \\ i \neq k}}^N [M]_{ki} \{A^{(i)}\}, \quad (2.32)$$

where $\{\xi_0^{(k)}\}$ is the effect vector of the incident wave to the k^{th} inhomogeneity. $[M]_{ki} \{A^{(i)}\}$ is the vector corresponding to the effects of i^{th} inhomogeneity on the k^{th} , i.e. the scattered field

from the i^{th} inhomogeneity at the integration points of the k^{th} inhomogeneity. Matrix $[M]_{ki}$ is the matrix formed by the wave modes of the scattered field of the i^{th} inhomogeneity, i.e. Hankel functions. The element of matrix $[M]_{ki}$ are given by

$$M_{st}^{(ki)} = H_t^{(1)}(k_m r_{ski}) e^{ir\theta_{ski}} \quad (2.33)$$

$$M_{(s+P_i)t}^{(ki)} = \cos(\theta_{ski} - \theta_{skk}) \mu_m \frac{\partial M_{st}^{(ki)}}{\partial r_{ski}} - \sin(\theta_{ski} - \theta_{skk}) \frac{\mu_m}{r_{ski}} \frac{\partial M_{st}^{(ki)}}{\partial \theta_{ski}}, \quad (2.34)$$

where r_{ski} and θ_{ski} are the coordinates of the s^{th} integration point of the k^{th} inhomogeneity in the local polar coordinate system of the i^{th} inhomogeneity, and P_i is the number of integration points of the i^{th} inhomogeneity.

Then the set of linear equations for the expansion coefficients can be obtained by combining the above equations and collecting the unknown coefficients, as

$$\begin{bmatrix} [I]_1 & -[Q]_1[M]_{12} & \cdots & -[Q]_1[M]_{1N} \\ -[Q]_2[M]_{21} & [I]_2 & \cdots & -[Q]_2[M]_{2N} \\ \vdots & \vdots & \ddots & \vdots \\ -[Q]_N[M]_{N1} & -[Q]_N[M]_{N2} & \cdots & [I]_N \end{bmatrix} \begin{Bmatrix} \{A^{(1)}\} \\ \{A^{(2)}\} \\ \vdots \\ \{A^{(N)}\} \end{Bmatrix} = \begin{Bmatrix} [Q]_1 \{\xi_0^{(1)}\} \\ [Q]_2 \{\xi_0^{(2)}\} \\ \vdots \\ [Q]_N \{\xi_0^{(N)}\} \end{Bmatrix} \quad (2.35)$$

where the matrices $[I]_k$ are the identity matrices with dimension $2 \times N_T + 1$, where N_T is the highest order the expansion is truncated to. The expansion coefficients can then be determined by solving equation (2.35), from which the displacement and stress of the wave field in the matrix can be computed. Then the refracted wave field coefficients in any inhomogeneity can be determined by using its matrix $[R]$ as shown in (2.18).

2.3 Verification of the method

The computational errors of the developed procedure are mainly caused by the numerical integral process and the truncation of the infinite series. The two types of error are analyzed respectively in the following subsections. The developed method is then tested under some limiting cases. The robustness and the limitations of the method are discussed.

2.3.1 Evaluation of numerical integration

In the developed method, the integral along the interface, as shown in equations (2.10), is replaced by the numerical integration shown in equation (2.18). In order to evaluate the accuracy of the numerical integration, the problem of single scattering is considered, since the scattered wave in this simple situation can be obtained analytically.

The computational model is composed of an infinitely extended matrix and a circular inhomogeneity with radius R . The incident wave is a plane wave with unit displacement amplitude propagating in the positive y direction, such that

$$w_{in} = e^{ik_m r \sin(\phi)} \quad (2.36)$$

where k_m is the wave number in the matrix, r and ϕ are the polar coordinates. The material properties are set as $\mu_i/\mu_m = 4$ and $\rho_i/\rho_m = 2$, and the frequency is selected with dimensionless parameter $k_m R = 2.4\pi$.

The analytical solution is obtained by evaluating equations (2.10) using Mathematica. The

series are truncated at 40th order, $N_T = 40$. The procedure using numerical integration is shown in equations (2.18) to (2.28). The first 40 orders are computed for comparison.

Since only the incident wave (or the pseudo-incident wave in the multiple scattering problem) is discretized and replaced by linear interpolation functions, the error of the numerical integration depends on the distance between the numerical points compared with the wave length in the matrix (λ_m). The ratio is defined as

$$\delta = \frac{\lambda_m}{\frac{2\pi R}{P}} = \frac{P}{k_m R} \quad (2.37)$$

with P being the number of integration points. The maximum deviation of the computed coefficients compared with the analytical ones is then evaluated, which is defined as

$$D = \max | A_n^{(ana)} - A_n^{(num)} | \quad (2.38)$$

where $A_n^{(ana)}$ and $A_n^{(num)}$ represent the n^{th} order coefficients computed with analytical and numerical method, respectively. The maximum deviations with different δ are shown in Figure 2.2

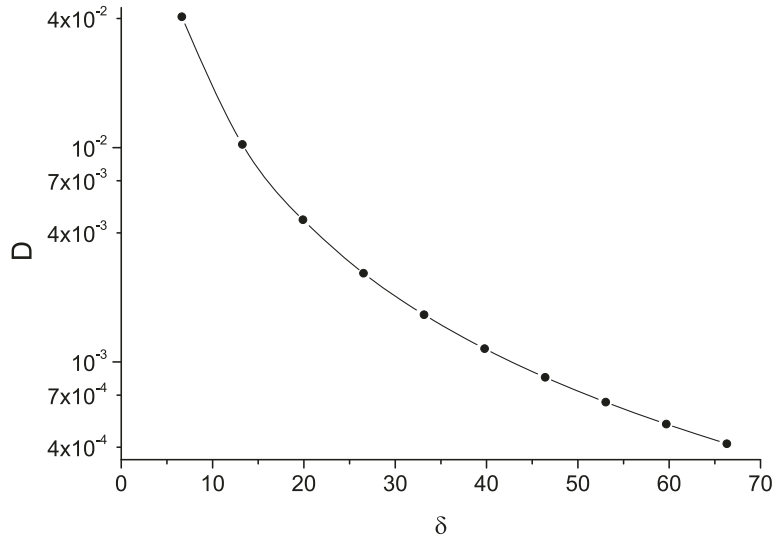


Figure 2.2: Deviation of the computed coefficients compared with the analytical ones.

As shown in the figure, the maximum deviation of the numerical results reduce to less than 1×10^{-3} when the wavelength-to-distance ratio $\delta = 45$, and it can be further decreased as long as δ is large enough. Figure 2.3 shows the normalized shear stresses along the interface computed by the numerical method with $\delta = 45$ and by the analytical method. The accuracy of the numerical method is shown to be sufficient with the difference between the two sets of results being insignificant.

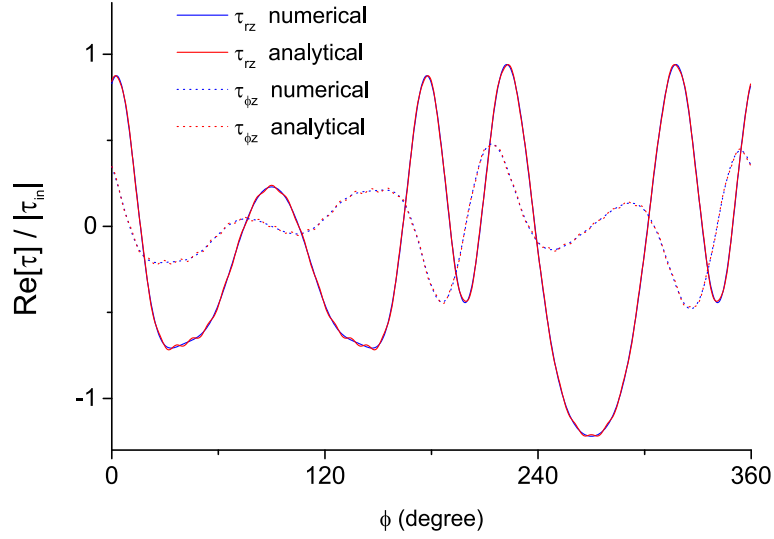


Figure 2.3: Comparison of the computed stresses from numerical and analytical results.

2.3.2 Convergence of the series

The error caused by truncating the infinite summation depends on the convergence of the series. In order to examine the convergence, the difference made by each additional term of the series is evaluated. The difference made by the k^{th} order term can be indicated by the absolute difference of displacements computed by the series with $N_T = k$ and $N_T = k - 1$. The displacements are collected at the same points, and the average of the absolute difference ϵ_k is calculated,

$$\epsilon_k = \langle |w_k - w_{k-1}| / |w_{in}| \rangle, \quad (2.39)$$

where w_k and w_{in} are the calculated displacements for $N_T = k$ and the incident wave, respectively. The angular brackets represent taking the average among the locations where the displacements are collected.

The example evaluated here contains two inhomogeneities with the same radius R , subjected to an antiplane wave propagating in x direction. The configurations of the model are $k_m R = 2.4\pi$, $\mu_i/\mu_m = 4$, $\rho_i/\rho_m = 2$, $D/R = 1$ with D being the distance between the two inhomogeneities, as shown by L1 in Figure 2.4. A total of 1000 points equally spaced along the path between the inhomogeneities are selected, at which the displacements are collected. The incident wave is assumed to be plane wave with unit displacement amplitude propagating along the positive x direction.

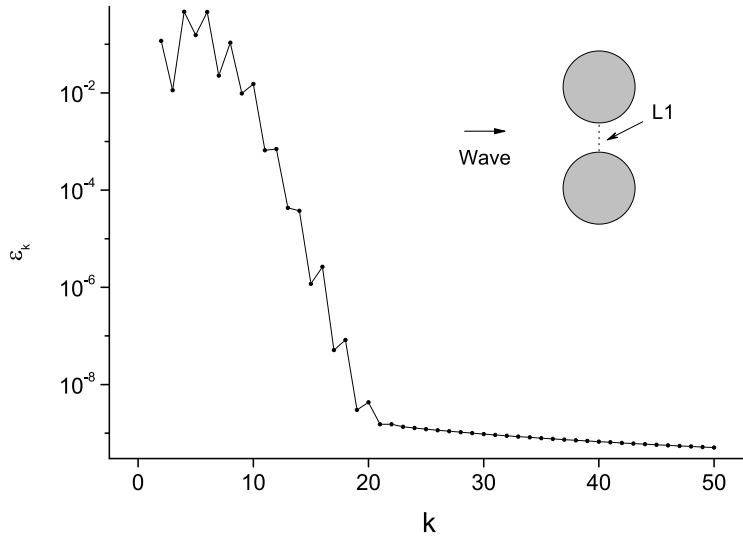


Figure 2.4: Convergence of the series

The dependence of ε_k on k is shown in Figure 2.4 with a logarithmic axis. As shown in the figure, the first 10 terms are important to the result. The differences made by the 10^{th} -to- 20^{th} terms decay rapidly. For higher order terms, the trend changes remarkably and becomes monotonically decreasing. But extremely high order terms should be avoided since they may cause numerical instability because of the precision limit of the computation. Considering that the necessity of high order terms may vary as the frequency changes, N_T could be taken around 20

to achieve reasonable convergent results for typical problems.

2.3.3 Comparison with existing results

To further evaluate the current method, the static and dynamic interaction of two circular inhomogeneities are considered and compared with the corresponding analytical results (Wu, 2000) and numerical results (Parvanova et al., 2014), respectively.

In the static case, the inhomogeneities, with identical radius and shear modulus, are arranged along the x axis, and are subjected to an antiplane shear stress τ_0 applied at a 45° angle from the x axis. The ratio of the shear modulus of the inhomogeneities to that of the matrix is 23.48. Figure 2.5 shows the comparison of the normalized stress τ_{rz} from the current method and that from the analytical solution around the left inhomogeneity for different distances between the inhomogeneities d , which has been normalized by the radius of the inhomogeneities, where ϕ represents the circumferential direction. The comparison of the normalized stress $\tau_{\phi z}$ is also shown in Figure 2.6. Excellent agreement is observed for both stress components.

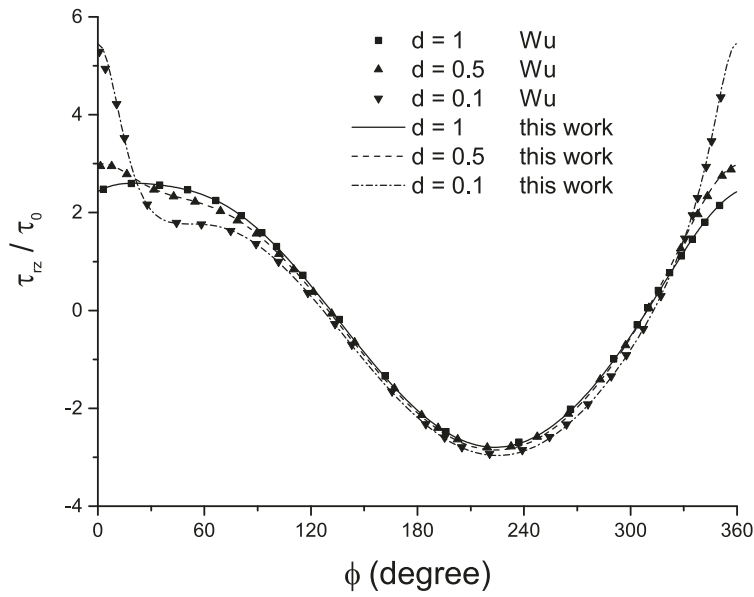


Figure 2.5: Normalized stress τ_{rz} around the left inhomogeneity, compared with the analytical solution.

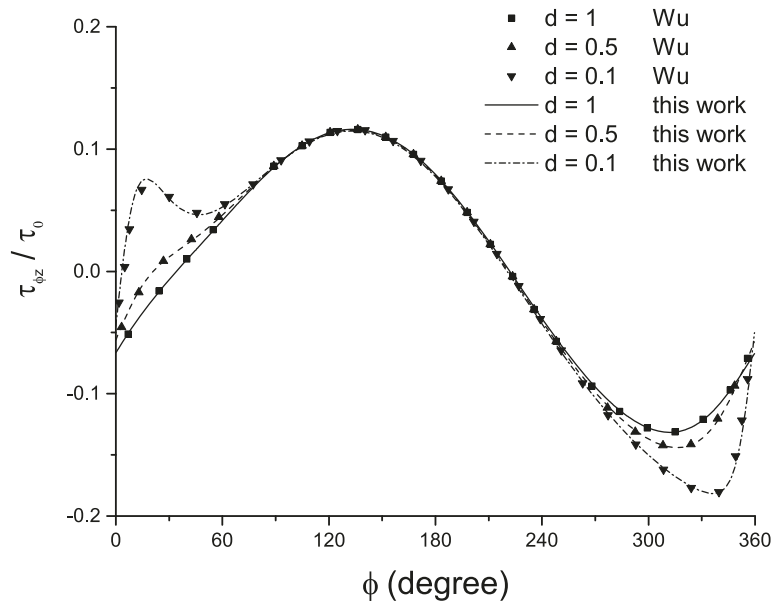


Figure 2.6: Normalized stress $\tau_{\phi z}$ around the left inhomogeneity, compared with the analytical solution.

In the dynamic case, the interaction of two circular cavities, which are simulated by setting

the mass density and shear modulus to negligible small, with radius $r_1 = 1$ and $r_2 = 2$ is computed. The cavities are arranged along the y axis. Three different distances, $d = 2, 0.1, 0.01$, are considered. The incident wave is propagating along the positive y direction, with frequency $k_m r_1 = 0.001$. The stresses $\tau_{\phi z}$ normalized by the incident wave around the smaller cavity are shown in Figure 2.7. The results are compared with the ones computed by Parvanova et al. with boundary element method in (Parvanova et al., 2014), and the results are in excellent agreement.

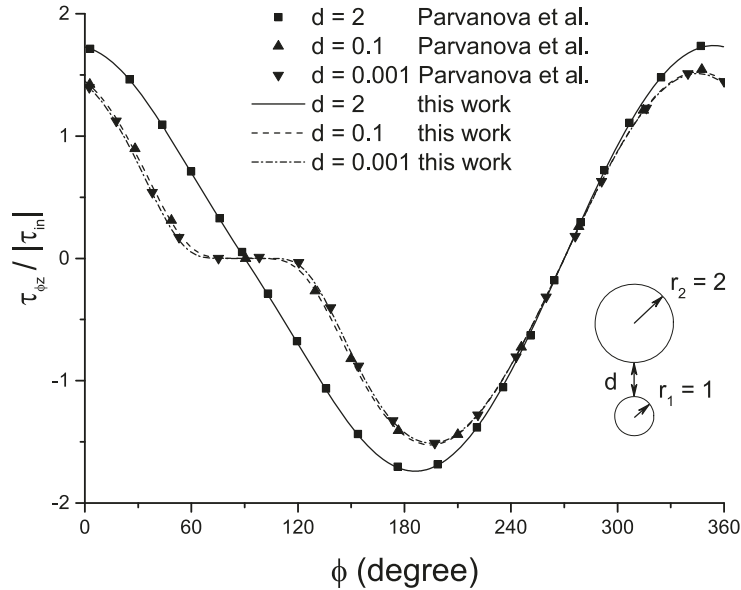


Figure 2.7: Normalized stress $\tau_{\phi z}$ around the smaller cavity, compared with the BEM results.

2.3.4 Limiting cases

In this section, the developed method is tested under several limiting conditions and the continuity conditions along the interfaces are checked to examine the accuracy and the robustness.

The first limiting case considered is to make the materials of the inhomogeneities and the matrix to be same. Theoretically, the multiple scattering problem is reduced to the propagation

of plane wave in a homogeneous medium, and the refracted wave becomes a plane wave as well and the scattered waves are supposed to vanish. However, the computed scattered wave results won't be exactly zero due to various computational errors. So the computed scattered wave indicates the level of the error. The same model as the one in section 2.3.2 is considered except that the materials are set to be same. In the vicinity of the inhomogeneities, the displacement amplitude of the scattered wave normalized by the amplitude of incident wave is computed, and it is in a range of $0-3.953 \times 10^{-7}$. The maximum stress mismatch along the interfaces is 7.858×10^{-5} , normalized by the stress amplitude of incident wave.

In order to test the method with large material mismatch, the second limiting case considered is to make the frequency to be very high and the distance between the inhomogeneities are very small. The considered model is composed of two steel inhomogeneities embedded in the rubber matrix. The inhomogeneities are vertically arranged with distance $2 \mu\text{m}$ and the radii are both 10 mm . The material constants used are: $\rho_{steel} = 7670 \text{ kg m}^{-3}$, $\mu_{steel} = 80.070 \text{ GPa}$, $\rho_{rubber} = 1300 \text{ kg m}^{-3}$, $\mu_{rubber} = 0.832 \text{ GPa}$. The incident wave is propagating along the positive x direction with amplitude of $1 \mu\text{m}$, and the frequency is 400 kHz . So the dimensionless parameter $k_m R$ here is 10π , which is rather high for common applications.

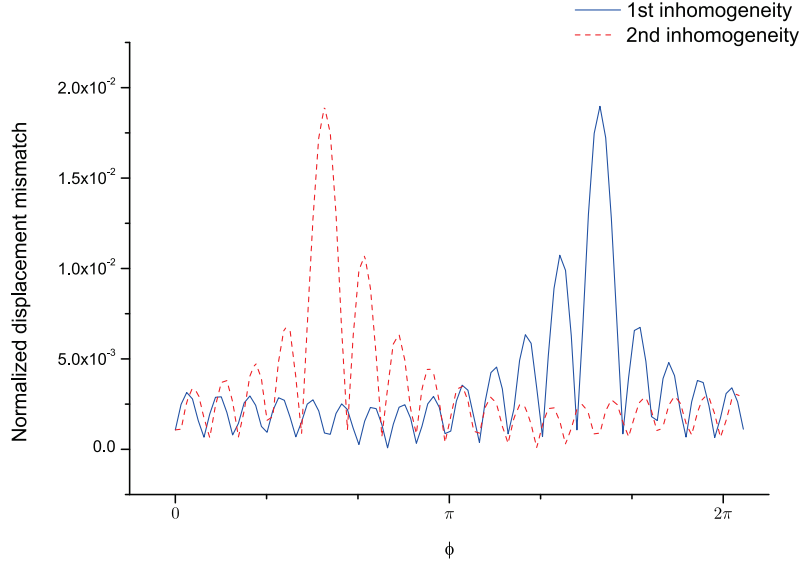


Figure 2.8: The mismatch of normalized displacement under limiting condition.

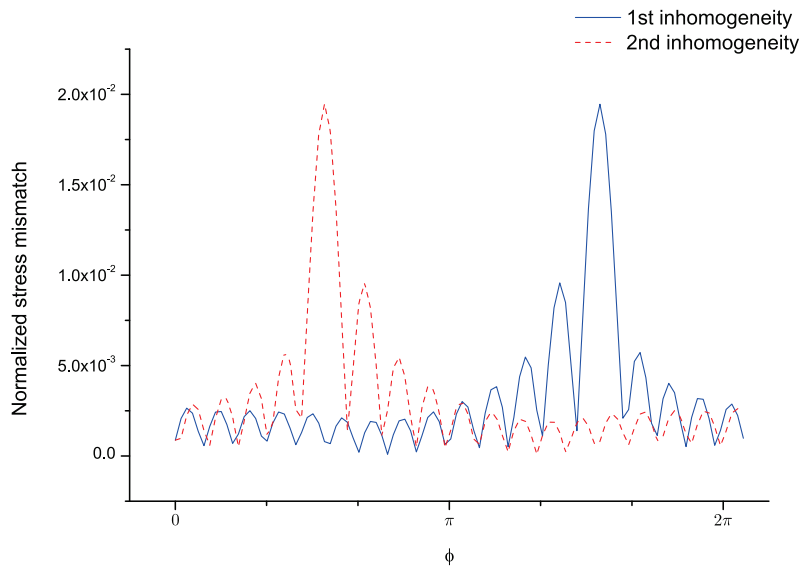


Figure 2.9: The mismatch of normalized τ_{rz} under limiting condition.

Figure 2.8 and Figure 2.9 show the continuity condition between the different media along the two interfaces. The maximum stress mismatch normalized by the stress amplitude of incident wave is 1.946×10^{-2} . A noteworthy feature of the mismatch distribution along the interface is that the peak appears at the nearest point to the other inhomogeneity, where the

stress is concentrated. It is because the radii are large and the distance is very small, indicating very strong interaction.

2.4 Application examples

2.4.1 General case example

In this section, the general model considered is composed of infinitely extended matrix and three inhomogeneities with different materials and radii. The material constants used are: $\rho_1 = 2730 \text{ kg m}^{-3}$, $\mu_1 = 28.658 \text{ GPa}$, $\rho_2 = 7670 \text{ kg m}^{-3}$, $\mu_2 = 80.070 \text{ GPa}$, $\rho_3 = 11400 \text{ kg m}^{-3}$, $\mu_3 = 8.431 \text{ GPa}$, $\rho_m = 1300 \text{ kg m}^{-3}$, $\mu_m = 0.832 \text{ GPa}$. The selection of these material properties is to introduce different kinds of material mismatch: the wave speeds of matrix and inhomogeneity 3 are similar, but are very different from that of media 1 and 2. The incident wave is propagating along the positive x direction with amplitude of $1 \mu\text{m}$, and the frequency is 200 kHz . The radii of the three inhomogeneities are $R_1 = 4 \text{ mm}$, $R_2 = 5.5 \text{ mm}$, $R_3 = 7 \text{ mm}$, respectively, and the position of their centers are $(-8.5 \text{ mm}, 0 \text{ mm})$, $(0 \text{ mm}, -10 \text{ mm})$, $(14 \text{ mm}, 0 \text{ mm})$, as shown in Figure 2.10.

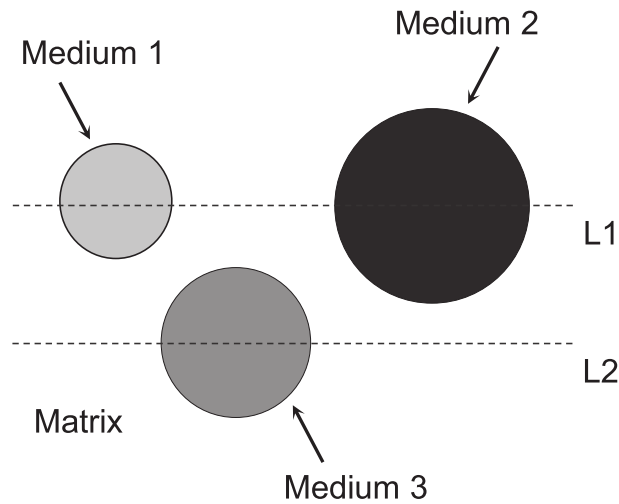


Figure 2.10: Computational model of the general case.

The distribution of amplitudes of displacement, shear stress τ_{xz} and τ_{yz} are shown in Figures 2.11, 2.12 and 2.13. Figure 2.14 shows the distribution of stress amplitudes along lines L1 and L2. As shown in the figures, in the matrix, standing waves are formed by the superposition of the incident wave and the reflected wave from the inhomogeneities, and shadows are formed behind the inhomogeneities. Inside the inhomogeneities, the fields are quite different because of the material variance. For medium 3, standing waves are formed by the refracted wave and the wave length is similar to the one in the matrix, since the wave speeds are similar. For media 1 and 2, the distribution of the fields show clearly stress concentration along the interfaces due to the large material mismatch.

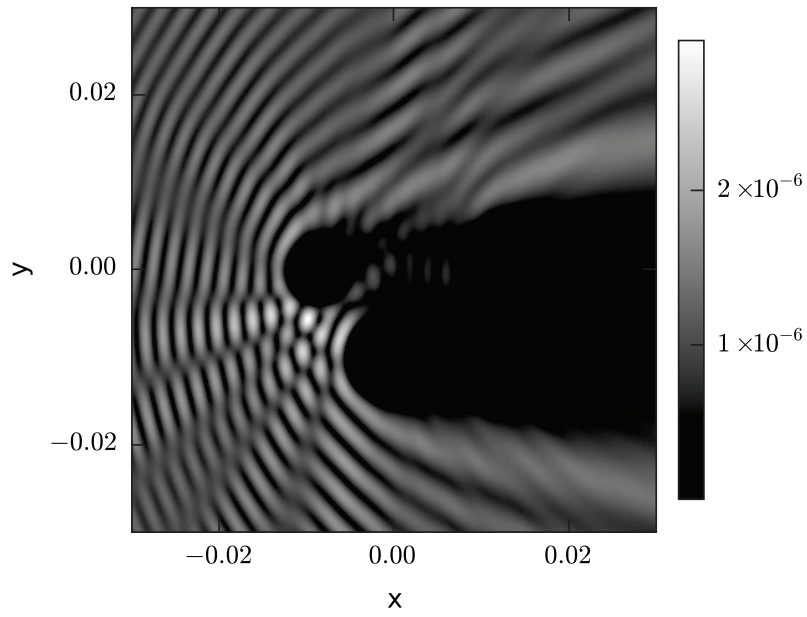


Figure 2.11: Displacement amplitude of the general case.

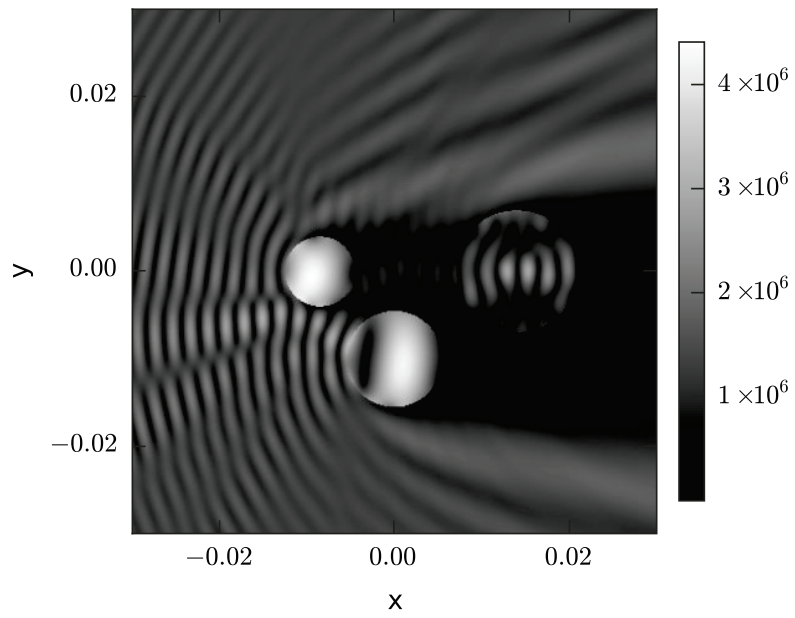


Figure 2.12: τ_{xz} amplitude of the general case.

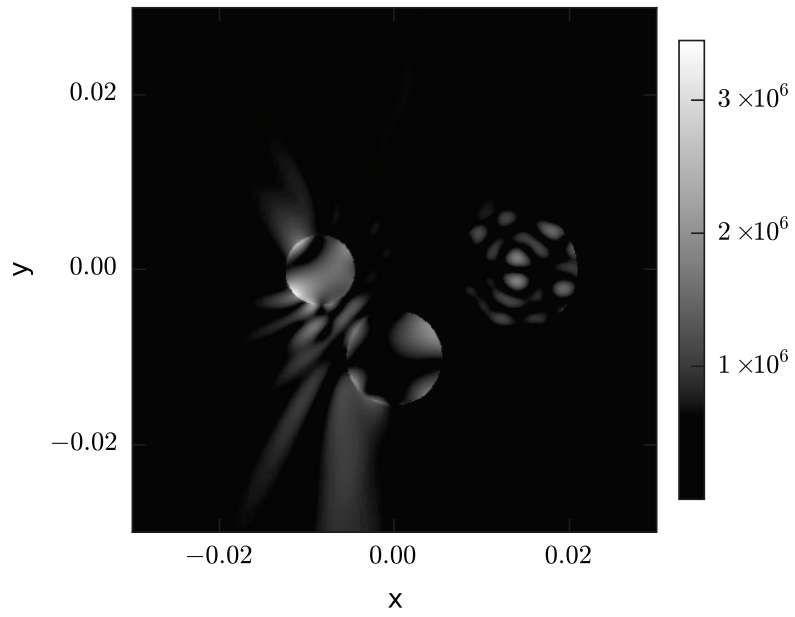


Figure 2.13: τ_{yz} amplitude of the general case.

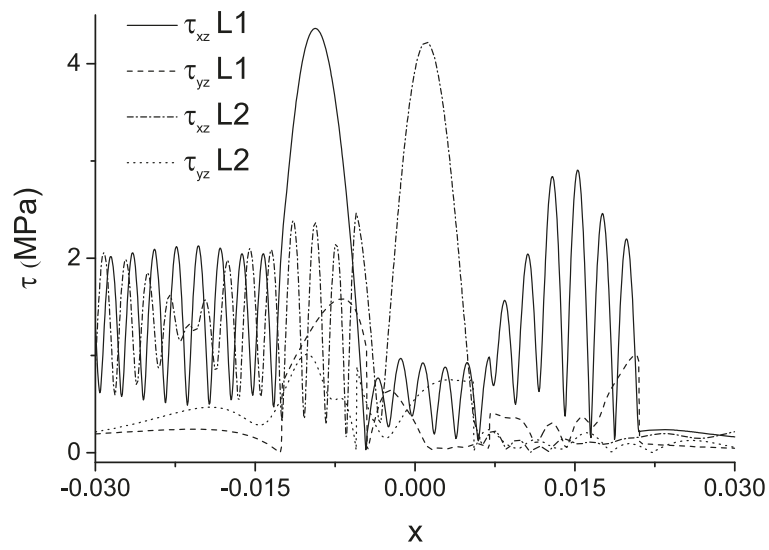


Figure 2.14: Stress amplitudes along L1 and L2.

2.4.2 Interactions among the inhomogeneities

In this section, the effects of interactions among the inhomogeneities are evaluated. The model is composed of infinitely extended matrix and two rows of identical inhomogeneities aligned along the x direction. The materials of the matrix and inhomogeneities are same as media 1 and 2 in section 2.4.1. The radius is 6 mm and the distance between two adjacent inhomogeneities is 3 mm. The incident wave is propagating along the positive x direction with amplitude of $1 \mu\text{m}$. The shear stress τ_{rz} along the interfaces in one row are computed and plotted in Figures 2.15 and 2.16, for the cases with 6 and 8 inhomogeneities, respectively.

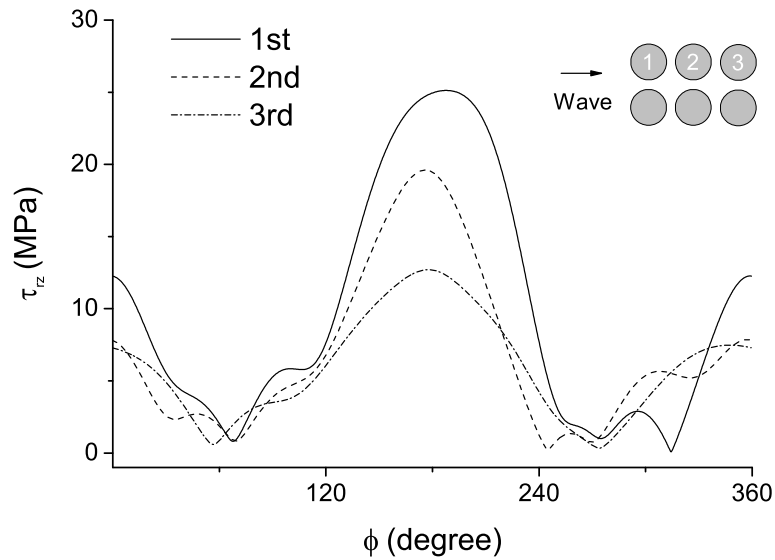


Figure 2.15: Stress amplitudes along each interface in the model with 6 inhomogeneities.

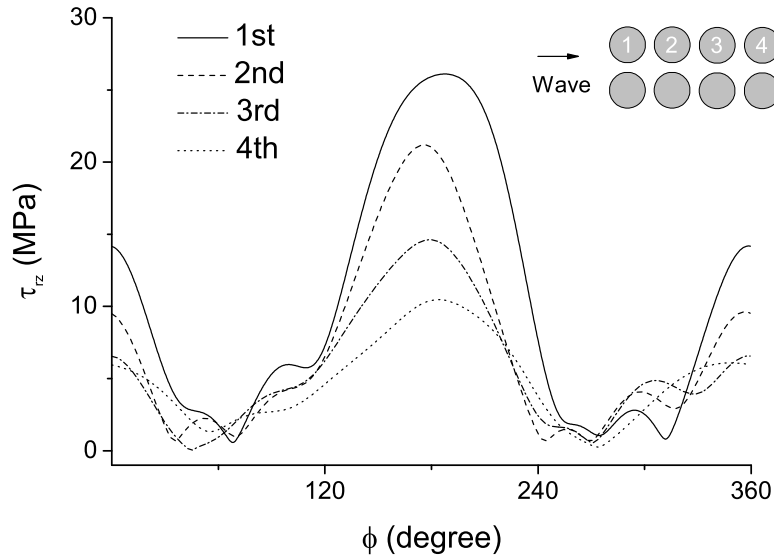


Figure 2.16: Stress amplitudes along each interface in the model with 8 inhomogeneities.

The maximum of the stress appears around the most front of each inhomogeneity, and the value decreases as the inhomogeneity position turns backward, since the effect of blocking made by the front ones. Due to the existence of the inhomogeneities in the other row, the distributions are not symmetric about 180° . From the comparison between the two cases, it can be observed that the stress along the first and the second inhomogeneity are not much affected by the addition of the fourth one. However, for the third inhomogeneity, the stress distribution becomes more similar to the second one, since it is replaced from the last one. And the stress distributions of the last inhomogeneities in both cases are similar.

2.4.3 Stop band

In order to investigate the stop band feature, a model is set with a square arrangement with 6 inhomogeneities in the x direction and 15 inhomogeneities in the y direction, as shown in Figure 2.17. The material constants used are $\mu_m = 1.73 \text{ GPa}$, $\rho_m = 1200 \text{ kg m}^{-3}$, $\mu_i = 8.36 \text{ GPa}$

and $\rho_i = 11\,300\text{ kg m}^{-3}$. The volume fraction $\phi = 0.25$. The incident wave is propagating along the positive x direction. The amplitude of displacement at the points along the lines shown in Figure 2.17 are collected. The normalized average value of the points along L1 are plotted against $k_m R$ in Figure 2.18.

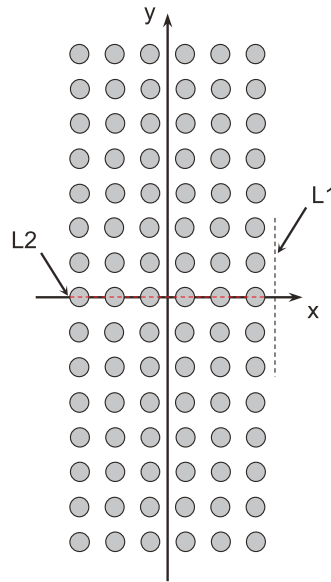


Figure 2.17: Computational model for showing stop band.

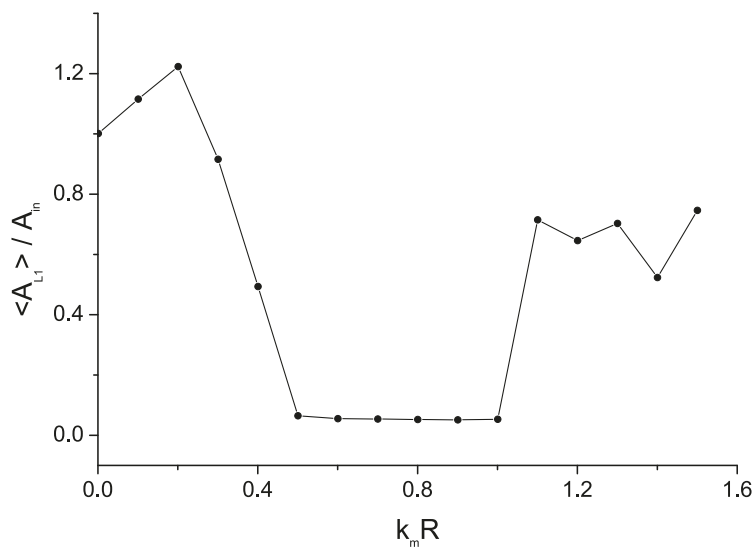


Figure 2.18: Displacement amplitude of the points right behind the arrangement.

Figure 2.19 shows the amplitude of displacement collected along L2 at three typical frequencies, $k_m R = 0.2, 0.8, 1.2$, and the corresponding distributions of displacement amplitude of the fields are plotted in Figures 2.20, 2.21, 2.22. As shown in the figures, the incident wave is able to pass the arrangement with little attenuation when the frequency is relative low. For the frequency in a higher range, the incident wave attenuates rapidly and barely pass the arrangement. When the frequency is high enough, the energy can be transmitted.

For the current results, the incident wave is in the positive x direction. Changing the angle of the incident wave is equivalent to changing the characteristic length of the structure. Later results for different structures show similar stop bands if this characteristic length remains in the same level.

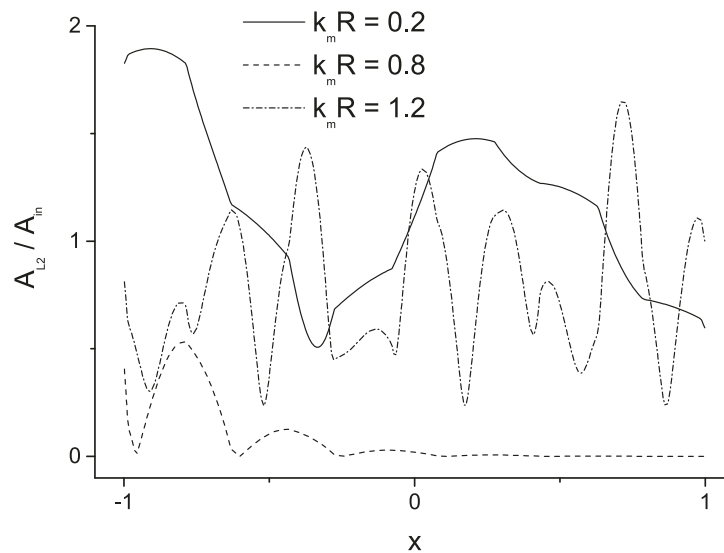


Figure 2.19: Displacement amplitude decays for the specific frequency.

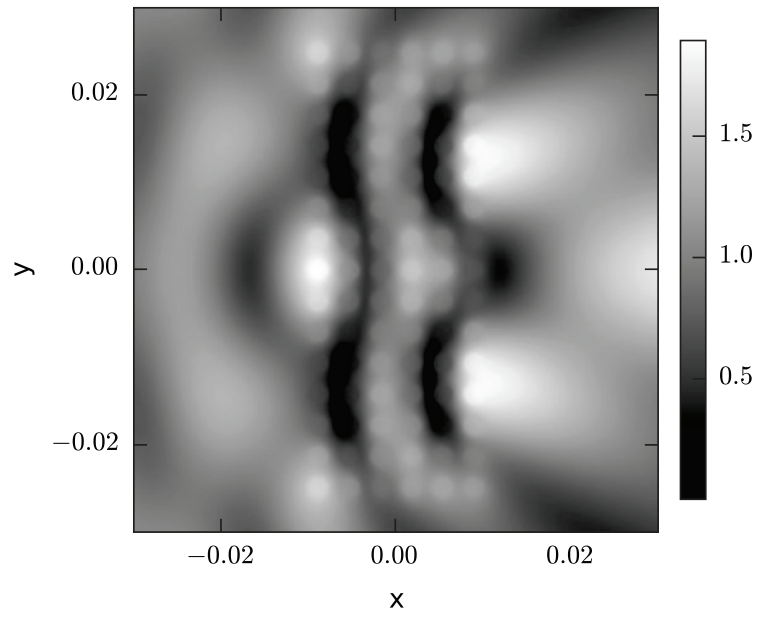


Figure 2.20: Distribution of displacement amplitude when $k_m R = 0.2$.

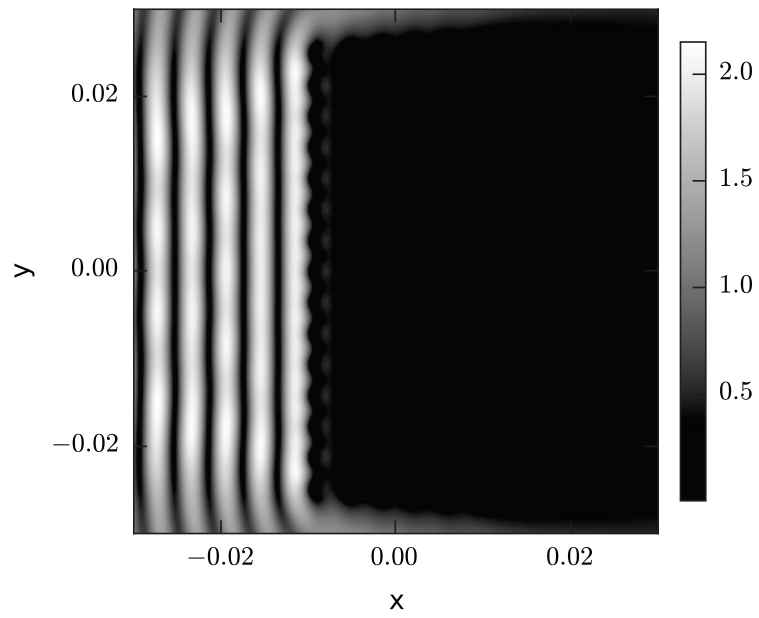


Figure 2.21: Distribution of displacement amplitude when $k_m R = 0.8$.

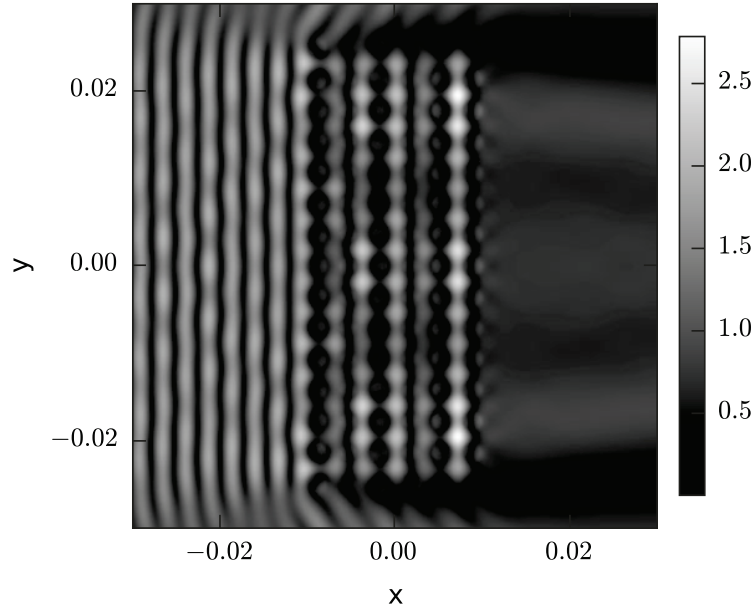


Figure 2.22: Distribution of displacement amplitude when $k_m R = 1.2$.

2.5 In-plane problem

2.5.1 Formulation of the problem

In this section, the developed numerical method for the multiple scattering of antiplane waves is expanded to in-plane problems. For the harmonic in-plane problem, the governing equation in terms of the displacement vector \mathbf{u} in the matrix or any inhomogeneities is

$$\mu \nabla^2 \mathbf{u} + (\lambda + \mu) \nabla (\nabla \cdot \mathbf{u}) + \rho \omega^2 \mathbf{u} = \mathbf{0} , \quad (2.40)$$

where μ and λ are the Lamé constants of the matrix or the inhomogeneities.

By using Helmholtz decomposition,

$$\mathbf{u} = \nabla\varphi + \nabla \times \boldsymbol{\psi} , \quad (2.41)$$

where φ and $\boldsymbol{\psi}$ are the displacement potentials, the displacement vector field can be decomposed into an irrotational vector field and a solenoidal vector field, which represent the longitudinal wave and transverse wave, respectively. In the two-dimensional problem with cylindrical coordinate system, the displacement field can be expressed as,

$$u_r = \frac{\partial\varphi}{\partial r} + \frac{1}{r} \frac{\partial\psi}{\partial\theta} , \quad u_\theta = \frac{1}{r} \frac{\partial\varphi}{\partial\theta} - \frac{\partial\psi}{\partial r} , \quad (2.42)$$

where ψ is the z component of the vector potential $\boldsymbol{\psi}$ in equation (2.41). Then the governing equation becomes two decoupled Helmholtz equations,

$$\nabla^2\varphi + k_L^2\varphi = 0 , \quad \nabla^2\psi + k_T^2\psi = 0 , \quad (2.43)$$

where k_L and k_T are the wave numbers of longitudinal wave and shear wave in the matrix or inhomogeneities, which depend on the frequency and wave speeds, as

$$k_L = \frac{\omega}{c_L} , \quad k_T = \frac{\omega}{c_T} , \quad (2.44)$$

where

$$c_L = \sqrt{\frac{\lambda + 2\mu}{\rho}} , \quad c_T = \sqrt{\frac{\mu}{\rho}} . \quad (2.45)$$

The solutions of the governing equations are in the form of Fourier expansion,

$$\varphi(r, \theta) = \sum_{n=-\infty}^{\infty} \left[B_n J_n(k_L r) e^{in\theta} + A_n H_n^{(1)}(k_L r) e^{in\theta} \right], \quad (2.46)$$

$$\psi(r, \theta) = \sum_{n=-\infty}^{\infty} \left[D_n J_n(k_T r) e^{in\theta} + C_n H_n^{(1)}(k_T r) e^{in\theta} \right]. \quad (2.47)$$

where A_n, B_n, C_n and D_n are the unknown constants to be determined from the boundary condition. For the scattered wave fields in the matrix, the radiation conditions must be satisfied (Colton and Kress, 2013; Kupradze, 1976),

$$\lim_{r \rightarrow \infty} \sqrt{r} \left(\frac{\partial \varphi}{\partial r} - ik_{Lm} w \right) = 0, \quad (2.48)$$

$$\lim_{r \rightarrow \infty} \sqrt{r} \left(\frac{\partial \psi}{\partial r} - ik_{Tm} w \right) = 0. \quad (2.49)$$

Substituting equation (2.46) into equation (2.48) and equation (2.47) into equation (2.49) indicates that B_n and D_n must be zero. For the field in the inhomogeneity, A_n and C_n must be zero to get limited amplitudes at the center. Therefore, the solution of the governing equations can be expressed as

$$\varphi(r, \theta) = \begin{cases} \sum_{n=-\infty}^{\infty} A_n H_n^{(1)}(k_{Lm} r) e^{in\theta} & r \geq R \quad \text{In the matrix} \\ \sum_{n=-\infty}^{\infty} B_n J_n(k_{Li} r) e^{in\theta} & r < R \quad \text{In the inhomogeneity.} \end{cases} \quad (2.50)$$

$$\psi(r, \theta) = \begin{cases} \sum_{n=-\infty}^{\infty} C_n H_n^{(1)}(k_{Tm}r) e^{in\theta} & r \geq R \quad \text{In the matrix} \\ \sum_{n=-\infty}^{\infty} D_n J_n(k_{Ti}r) e^{in\theta} & r < R \quad \text{In the inhomogeneity.} \end{cases} \quad (2.51)$$

Along the interface, the continuity conditions of displacement and traction are assumed.

$$\mathbf{u}_{ps}|_{inter} + \mathbf{u}_{sc}|_{inter} = \mathbf{u}_{re}|_{inter}, \quad \mathbf{t}_{ps}|_{inter} + \mathbf{t}_{sc}|_{inter} = \mathbf{t}_{re}|_{inter}, \quad (2.52)$$

where displacement vector \mathbf{u} is $(u_r, u_\theta)^T$ and traction vector \mathbf{t} is $(\sigma_{rr}, \sigma_{r\theta})^T$, and the subscripts (ps , sc and re) represent the pseudo-incident wave, scattered wave and refracted wave, respectively.

By substituting the displacement and traction of the scattered and refracted waves with the potentials and using the numerical technique developed above, the transformation from the effect vector of pseudo-incident wave to the unknown coefficients for k^{th} inhomogeneity can be obtained as

$$\begin{Bmatrix} A^{(k)} \\ C^{(k)} \end{Bmatrix} = [Q_k] \left\{ \xi_{ps}^{(k)} \right\}, \quad \begin{Bmatrix} B^{(k)} \\ D^{(k)} \end{Bmatrix} = [R_k] \left\{ \xi_{ps}^{(k)} \right\}, \quad (2.53)$$

where the effect vector of pseudo-incident wave is composed as,

$$\left\{ \xi_{ps}^{(k)} \right\} = \begin{Bmatrix} \left\{ u_r^{(ps)}|_{inter} \right\} \\ \left\{ u_\theta^{(ps)}|_{inter} \right\} \\ \left\{ \sigma_{rr}^{(ps)}|_{inter} \right\} \\ \left\{ \sigma_{r\theta}^{(ps)}|_{inter} \right\} \end{Bmatrix}_k, \quad (2.54)$$

and the $[Q_k]$ and $[R_k]$ are the transition matrices of k^{th} inhomogeneity. With considering the interactions among inhomogeneities, the effect vector $\left\{ \xi_{ps}^{(k)} \right\}$ is composed of the effects of incident wave and other scattered waves, such as

$$\left\{ \xi_{ps}^{(k)} \right\} = \left\{ \xi_0^{(k)} \right\} + \sum_{\substack{i=1 \\ i \neq k}}^N [M_{ki}] \left\{ \begin{matrix} A^{(i)} \\ C^{(i)} \end{matrix} \right\}, \quad (2.55)$$

where matrix $[M_{ki}]$ represents the influence of the i^{th} inhomogeneity to the k^{th} . Then, a set of linear equations for the expansion coefficients can be obtained in the same form of equation (2.35). By solving the linear equations, the potentials can be determined, and then the displacement and stress fields can be computed directly.

2.5.2 General example

The model in section 2.4.1 is considered here again as a general example. The incident wave is a harmonic plane P wave propagating along the positive x direction with amplitude $1 \mu\text{m}$.

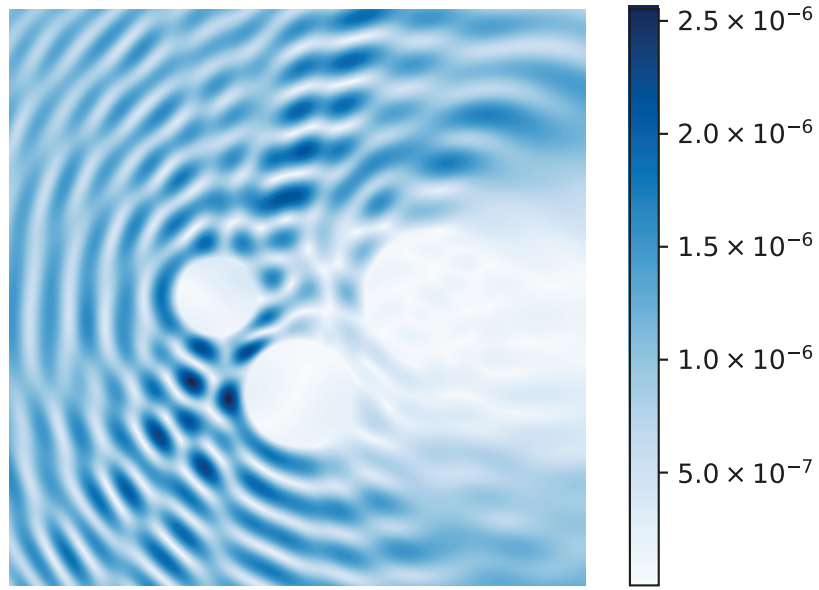


Figure 2.23: Amplitude of displacement in x direction (m).

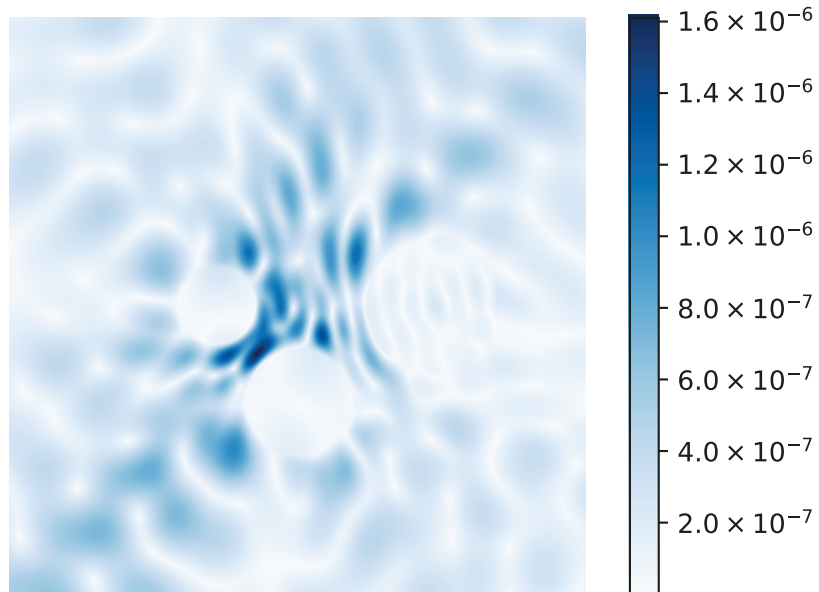


Figure 2.24: Amplitude of displacement in y direction (m).

The amplitude of displacements in x and y direction are shown in Figure 2.23 and Figure 2.24. It can be observed that, due to the large mismatch on the longitudinal wave speed, the displacement in x direction is weak. However, for the displacement in y direction, which

is mainly caused by the SV wave, can be observed with the standing wave pattern inside the medium 3 where the transverse wave speed is similar as the matrix. The distributions of the amplitude of stress σ_{xx} , σ_{yy} and σ_{xy} are shown in Figure 2.25, Figure 2.26 and Figure 2.27. The stress concentration due to the material mismatch can be observed along the interfaces. The comparison between these results with the ones of the antiplane problem reveals that the in-plane wave fields are distributed in more complicated patterns, which indicates the mode transition occurs between P and SV wave.

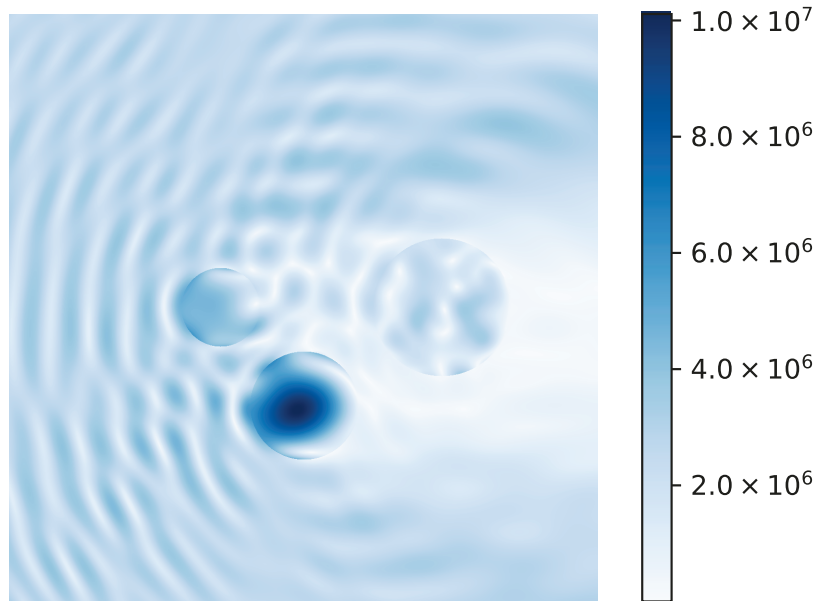


Figure 2.25: Amplitude of stress σ_{xx} (Pa).

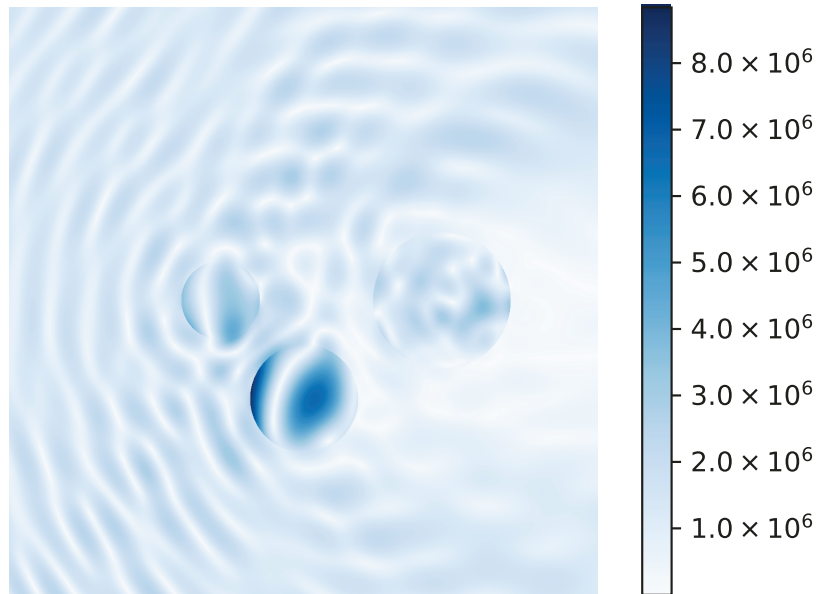


Figure 2.26: Amplitude of stress σ_{yy} (Pa).

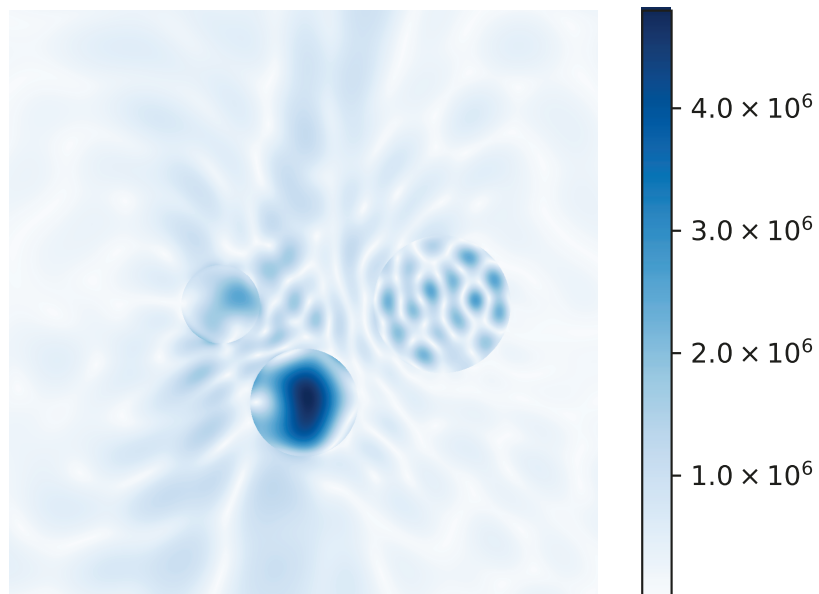


Figure 2.27: Amplitude of stress σ_{xy} (Pa).

The continuity condition across the interfaces are checked for showing the validity of the method. As shown in Figure 2.28, the normalized mismatch can be controlled below 3.238×10^{-3} .

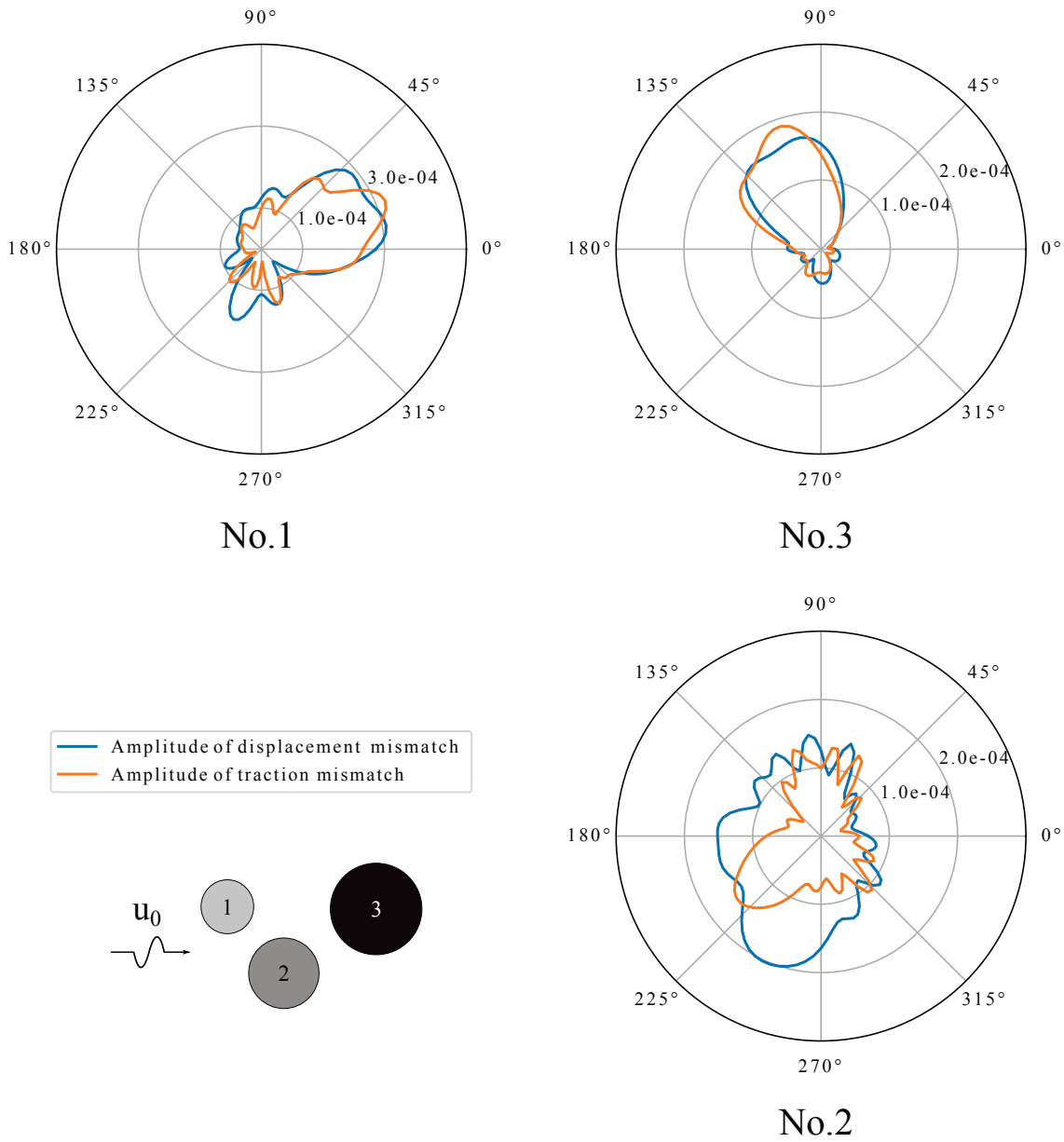


Figure 2.28: The mismatch of normalized displacement and traction.

2.6 Conclusion

In this chapter, a computational procedure for simulating the multiple scattering of P/SV/SH wave in composite media is presented. The procedure is based upon the use of pseudo-incident

wave method and the simplification of scattering problem. By discretizing the superposition of scattered wave fields, the scattering mechanism can be simplified to a linear transformation and then the expansion coefficients can be obtained by solving the linear equations. The validity and robustness of the procedure have been demonstrated by verifications and tests under limiting conditions. This procedure is proved to be capable of simulating the multiple scattering by a large number of circular inhomogeneities with various properties. Furthermore, the wave propagations in the medium with periodically arranged inhomogeneities are simulated and the stop band is demonstrated.

Chapter 3: Elastic waves in periodic materials

This chapter presents an analytical-numerical method for the determination of eigenstates of the periodic unit cell with one circular inhomogeneity under designated frequency and angle of the wave propagation. The method is based on the eigenfunction expansion in Chapter 2 and the use of the Newton's method for solving the nonlinear eigenvalue problem. The accuracy of the method is verified by comparing the results with the finite element method. This chapter stems from the journal paper in preparation: "Computational homogenization for antiplane wave propagation in heterogeneous materials", written by the author under the supervision by Dr. Wang.

3.1 Introduction

The determination of local response of the microscopic structure is essential for the homogenization process. For the computational homogenization, since the local response is computed explicitly from the solution of a specific model, the effect of the boundary condition should be eliminated to avoid the loss of generality. For a heterogeneous material with periodic microscopic structures, the unit cell with periodic boundary condition is equivalent to the one inside a piece of the periodic material which is infinitely extended in all directions. Therefore, the local response of the unit cell with periodic boundary condition is ideal for the homogenization of the periodic material.

The local response is comprised by the eigenstates of the periodic unit cell, which is determined by the solution of eigenvalue problem. The existing works on solving the eigenvalue

problem for periodic materials are mainly focusing on the band structure determination. The most used methods include plane wave expansion method (Kushwaha et al., 1993; Sigalas and Economou, 1992), the multiple scattering theory method (Liu et al., 2002; Mei et al., 2003), the finite-difference time-domain method (Sigalas and Garcia, 2000), the finite element method (Axmann and Kuchment, 1999; Huang and Chen, 2011; Oudich et al., 2010), variational methods (Srivastava and Nemat-Nasser, 2014), etc. However, the methods for band structure determination are inefficient for computing the eigenstates for a specific frequency, which is evaluated as the eigenvalue with the Bloch wave vector designated.

For calculating the wave number as the eigenvalue with the frequency and propagation direction designated, various methods have been developed, which include the Dirichlet-to-Neumann map method (Zhen et al., 2012), boundary element method (Li et al., 2012), and finite element method (Veres et al., 2013). However, since the band structure determination only requires the wave vectors on the edge of irreducible Brillouin zone, these works only apply to the polynomial eigenvalue problems which can be solved through linearization (Mehrmann and Voss, 2004). Moreover, since the dimensions of matrices in these numerical methods depend on the fine meshes, the problem of stability and computational cost may arise.

In this chapter, an analytical-numerical method for the determination of the periodic unit cell under the given frequency and propagation direction is developed. By using the eigenfunction expansion, the nonlinear eigenvalue problem with the expansion coefficients being the eigenvector is established. Then the Newton's method is employed to solve the nonlinear eigenvalue problem. The accuracy is discussed through the comparison with finite element method.

3.2 Formulation of the problem

In periodic materials, which can be assumed to be continuous with periodically varying properties, the elastic waves are in the form of Bloch wave (Kittel, 2004), as

$$w(\mathbf{r}) = \tilde{w}(\mathbf{r})e^{i\mathbf{k}^* \cdot \mathbf{r}}, \quad \sigma_{ij}(\mathbf{r}) = \tilde{\sigma}_{ij}(\mathbf{r})e^{i\mathbf{k}^* \cdot \mathbf{r}}, \quad (3.1)$$

where \mathbf{k}^* is the Bloch wave vector, \tilde{w} and $\tilde{\sigma}_{ij}$ are periodic functions with the same periodicity as the lattice. So, for the unit cell shown in Figure 3.1,

$$\begin{aligned} w_3(y) &= w_1(y)e^{ik^* \cos(\theta)a}, & w_4(x) &= w_2(x)e^{ik^* \sin(\theta)a}, \\ t_3(y) &= -t_1(y)e^{ik^* \cos(\theta)a}, & t_4(x) &= -t_2(x)e^{ik^* \sin(\theta)a}, \end{aligned} \quad (3.2)$$

where w_i and t_i ($i = 1 - 4$) are the antiplane displacement and traction along the edges, θ is the angle between \mathbf{k}^* and the horizontal positive direction, and a is the lattice constant.

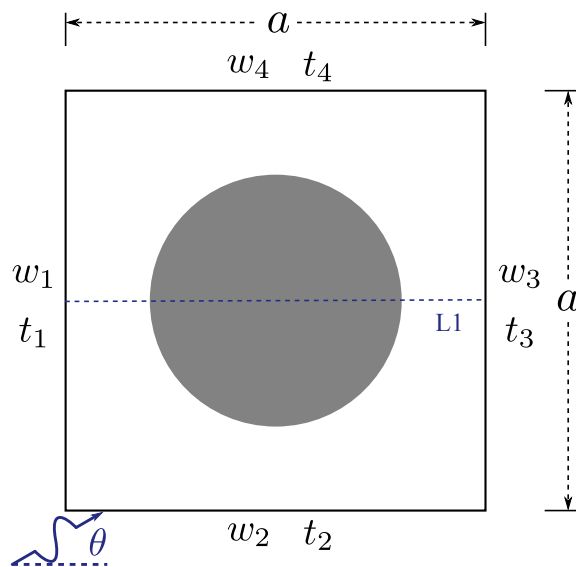


Figure 3.1: Model of unit cell under periodic boundary condition

In the local structure, the materials of the inhomogeneity and the matrix are homogeneous. The governing equations for the displacement fields in both media are the Helmholtz equations, as shown in equation (2.3), with different wave numbers. Therefore, by using the eigenfunction expansion as in equation (2.6) and additionally expanding the incident wave, the displacement field can be expressed as

$$w(r, \varphi) = \begin{cases} \sum_{n=-\infty}^{\infty} A_n H_n^{(1)}(k_m r) e^{in\varphi} + \sum_{n=-\infty}^{\infty} B_n J_n(k_m r) e^{in\varphi} & r \geq R \quad \text{In the matrix} \\ \sum_{n=-\infty}^{\infty} C_n J_n(k_i r) e^{in\varphi} & r < R \quad \text{In the inhomogeneity} \end{cases} \quad (3.3)$$

where r and φ are the polar coordinates measured from the center of the inhomogeneity, J_n and $H_n^{(1)}$ are the Bessel functions and Hankel functions of the first kind, k_m and k_i are the corresponding wave numbers. A_n , B_n and C_n are the unknown constants to be determined from the boundary/interface conditions.

Since the inhomogeneity and the matrix are perfectly bonded, the continuity condition along the interface of the inhomogeneity and matrix can be given as,

$$w_m|_{r=R} = w_i|_{r=R}, \quad \tau_m|_{r=R} = \tau_i|_{r=R}, \quad (3.4)$$

where τ denotes the shear stress τ_{rz} , and the subscripts m and i represent matrix and inhomogeneity respectively. By substituting the solution in equation (3.3) and using the orthogonality

of the expansion, for any n ,

$$\begin{cases} A_n H_n^{(1)}(k_m R) + B_n J_n(k_m R) = C_n J_n(k_i R) \\ \mu_m k_m [A_n H_n^{(1)'}(k_m R) + B_n J_n'(k_m R)] = \mu_i C_n k_i J_n'(k_i R) \end{cases} \quad (3.5)$$

Then the coefficients B_n can be substituted by A_n , and the displacement field in the matrix can be completely expressed by the expansion with A_n being the unknown coefficients.

Therefore, after selecting $4M$ collocation points uniformly along the unit cell boundary and truncating the series at the order of N , the vectors of boundary values at the collocation points can be represented by A_n as,

$$\begin{cases} w_1 \\ w_2 \\ -t_1 \\ -t_2 \end{cases}_{4M} = [Z_1]_{4M \times N} \{A\}_N, \quad \begin{cases} w_3 \\ w_4 \\ t_3 \\ t_4 \end{cases}_{4M} = [Z_2]_{4M \times N} \{A\}_N, \quad (3.6)$$

where $[Z_1]$ and $[Z_2]$ are the matrices which are formed by the series basis for displacement or traction at the node positions, as

$$\begin{aligned} [Z_\alpha]_{(p,n)} &= [H_n^{(1)}(k_m r_p) + T_n J_n(k_m r_p)] e^{in\phi_p} \\ [Z_\alpha]_{(p+2M,n)} &= (-1)^\alpha \mu_m k_m [H_n^{(1)'}(k_m r_p) + T_n J_n'(k_m r_p)] e^{in\phi_p} n_{r_p} + \\ & \quad (-1)^\alpha \mu_m (in) [H_n^{(1)}(k_m r_p) + T_n J_n(k_m r_p)] e^{in\phi_p} n_{\phi_p}, \end{aligned} \quad (3.7)$$

where $\alpha = 1$ or 2 , $p \in [1, 2M]$ indicates the p th node, n_r and n_ϕ are the cosines of the outward

normal vector at the node relative to the positive r and φ direction, and the T_n is the relation between A_n and B_n as

$$T_n = \frac{\mu_i k_i J'_n(k_i R) H_n(k_m R) - \mu_m k_m J_n(k_i R) H_n^{(1)'}(k_m R)}{\mu_m k_m J_n(k_i R) J'_n(k_m R) - \mu_i k_i J'_n(k_i R) J_n(k_m R)} \quad (3.8)$$

Then, by using the periodic boundary condition (PBC) in equation (3.2), the nonlinear general eigenvalue problem with non-square matrices ($4M \times N$) is derived as

$$[Z_2] \{A\} = [S][Z_1] \{A\} , \quad (3.9)$$

where $[S]$ is the diagonal matrix composed of the $2M$ factors for the phase shift in x direction and $2M$ factors for the phase shift in y direction, as

$$[S] = \begin{bmatrix} e^{ik^* \cos(\theta)a} & & & & \\ & \ddots & & & \\ & & & & \\ & & & e^{ik^* \sin(\theta)a} & \\ & & & & \ddots \end{bmatrix} . \quad (3.10)$$

By decomposing the matrix $[Z_2]$ with singular value decomposition,

$$[Z_2] = [U][\Sigma][V^*] , \quad (3.11)$$

and multiplying the conjugate transpose of matrix $[U]$ on both sides, the dimension of the matrix

can be reduced, and the nonlinear eigenvalue problem can be derived as

$$[U^*SZ_1 - \Sigma V^*]\{A\} = [Z]\{A\} = 0, \quad (3.12)$$

where matrix $[Z]$ nonlinearly depends on the Bloch wave number k^* , with dimension of $N \times N$.

When the frequency is in the pass-band, the normalized Bloch wave number k^*a can be obtained as the real eigenvalue and the coefficients A_n are obtained as the elements of the eigenvector.

In the numerical implementation, for the frequencies under the higher limit of first stop band, convergence tests were conducted for the selection of the series top order N . Based on these tests, $N = 14$ is selected with the number of collocation points being $20N$ or $M = 70$. The Newton's method is used for solving the nonlinear eigenvalue problem numerically. Since the dimension of the problem is reduced to N , the determinant of the matrix $[Z]$ can be computed directly. So the approximation of the eigenvalue is obtained accurately by scanning the determinants of matrix $|Z|(k^*a)$ and selecting the k^*a at which the determinant is minimum. The scanning range is $k^*a \in [0, \pi)$ because the $|Z|(k^*a)$ is periodic and symmetric about π . Then, the iterations are carried out, as

$$T^{(i)} = [Z]^{-1}[Z']A^{(i)}, \quad A^{(i+1)} = T^{(i)}/|T^{(i)}|, \quad (3.13)$$

where $[Z']$ is the derivative of matrix $[Z]$ with respect to k^*a , such as,

$$[Z'] = [U^*S'Z_1 - \Sigma V^*], \quad (3.14)$$

3.3 Verification of the method

In order to verify the method, the dispersion relation and eigenstates of a periodic material are evaluated and compared with the results obtained by using finite element method (FEM). The commercial software COMSOL Multiphysics 5.2a is utilized.

The considered model is composed of circular inhomogeneities, with the radius $R_i = 6$ mm, embedded with square lattice, with the lattice constant $a = 20$ mm, in an elastic matrix. The unit cell is shown in Figure 3.1 schematically. The material constants used are $\rho_m = 7670 \text{ kg m}^{-3}$, $\mu_m = 84.3 \text{ GPa}$, $\rho_i = 11400 \text{ kg m}^{-3}$, $\mu_i = 8.43 \text{ GPa}$. The direction of the Bloch wave is set to be the positive x direction, and the first two branches are computed.

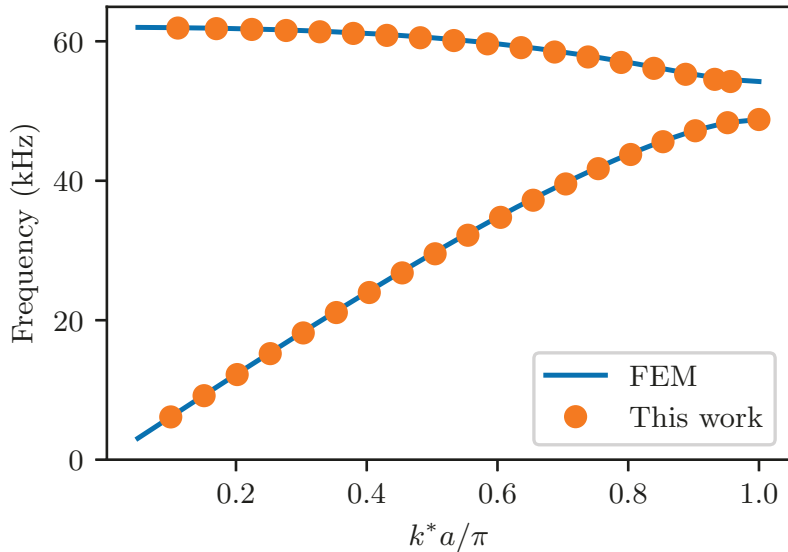


Figure 3.3: Dispersion relation comparison.

Figure 3.3 shows the comparison of the dispersion relation computed by using the method developed and FEM with 29288 triangular elements. It can be observed that the results agree well on both the branches, which means that the eigenvalues can be obtained accurately for a

large frequency range.

For validating the eigenvectors, which is the series coefficients of scattering wave, the eigenstate of the unit cell is computed and compared with the one obtained by using FEM with 29288 triangular elements. The considered model is the same as the previous one. The frequency is set to be 35.015 kHz so that the $k^*a = 0.6$, and the angle of the Bloch wave vector is set to be 30° . Along the horizontal center line, as shown in Figure 3.1, the normalized amplitude of the antiplane displacement $|w|$, stress $|\tau_{xz}|$ and $|\tau_{yz}|$ of the eigenstate are plotted in Figure 3.4, Figure 3.5 and Figure 3.6. As shown in the figures, the results obtained by the developed method can well match the ones computed by FEM.

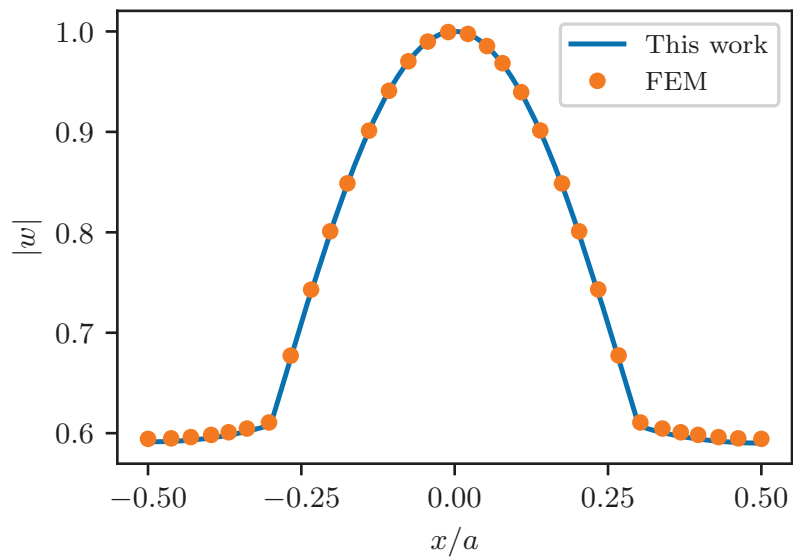


Figure 3.4: Normalized displacement amplitude $|w|$ along L1.

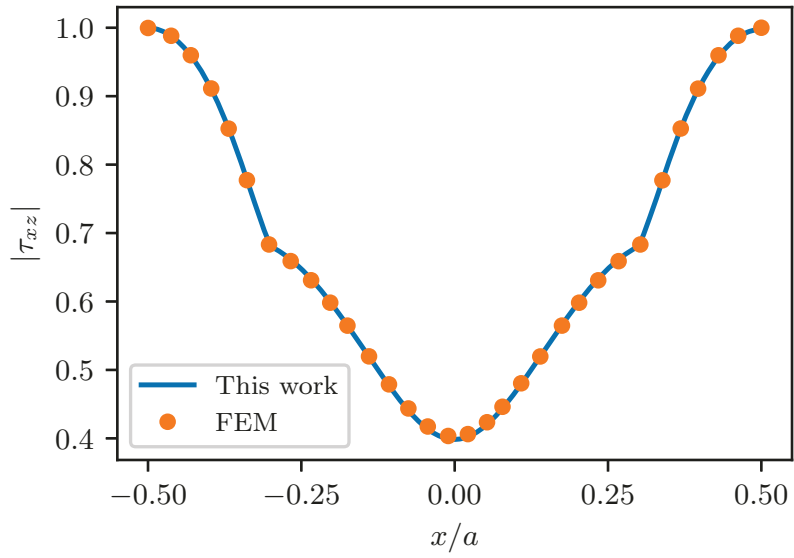


Figure 3.5: Normalized stress amplitude $|\tau_{xz}|$ along L1.

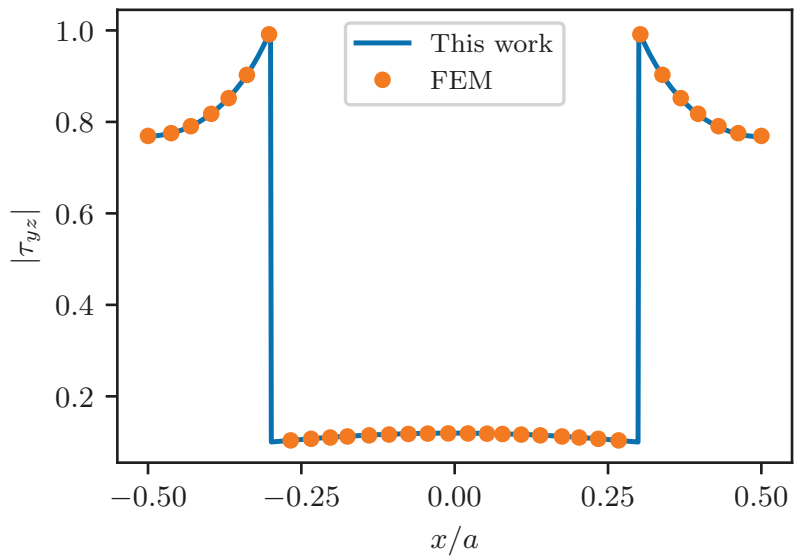


Figure 3.6: Normalized stress amplitude $|\tau_{yz}|$ along L1.

3.4 Conclusion

In this chapter, a computational method for evaluating the eigenstates of unit cell with periodic boundary condition is developed. Based on the eigenfunction expansion of the wave field, the nonlinear eigenvalue problem with the Bloch wave number being the eigenvalue is established. And, by using the expansion coefficients as the eigenvector, the dimension of the problem can be reduced so that the nonlinearity caused by the arbitrarily specified propagation angle can be handled efficiently. The accuracy of the method is validated by comparing the results with the ones obtained by using FEM.

Chapter 4: Homogenization based on domain averaging

This chapter presents two homogenization methods for periodic heterogeneous materials with averaging the explicitly solved wave fields. The first one is based on the volume averages of the stress and strain field, and the second one is based on the kinetic energy equivalence of the wave fields in the domain of unit cell. The first section of this chapter stems from the published journal article written by the author under the supervision by Dr. Wang. (Wang and Wang, 2016). The second section of this chapter stems from the journal paper in preparation: “A computational homogenization method based on the energy equivalence”, written by the author under the supervision by Dr. Wang.

4.1 Volume average

The effective properties of the heterogeneous materials can be determined based on the volume averages of the field variables. In this section, the formulations of the elastostatic homogenization with volume averages will be summarized first. By expanding the formulations to the harmonic elastodynamic cases, the physical meaning of the volume averages of the wave fields is shown. Then the computational homogenization method based on the concept of self-consistent across different scales is developed.

4.1.1 Basic concepts of the elastostatic homogenization

Since the length scale of the load is much larger than that of the RVE, an RVE can be considered only as a material point in the macroscopic field. Thus, the point possesses a stress state σ_{ij}^*

and a strain state ε_{ij}^* . The asterisk superscript means macroscopic fields. The objective of homogenization is to find the moduli C_{ijkl}^* , which represents the relation between σ_{ij}^* and ε_{ij}^* . However, in the microscopic view, the RVE occupies a domain in which the stress σ_{ij} and strain ε_{ij} may vary, as shown in Figure 4.1. The general idea of finding C_{ijkl}^* is to establish the relation between $(\sigma_{ij}^*, \varepsilon_{ij}^*)$ and $(\sigma_{ij}, \varepsilon_{ij})$ by defining boundary condition of the RVE and averaging method, and the relation between σ_{ij} and ε_{ij} by solving the boundary value problem of the RVE (Mura, 1987; Qu and Cherkaoui, 2006).

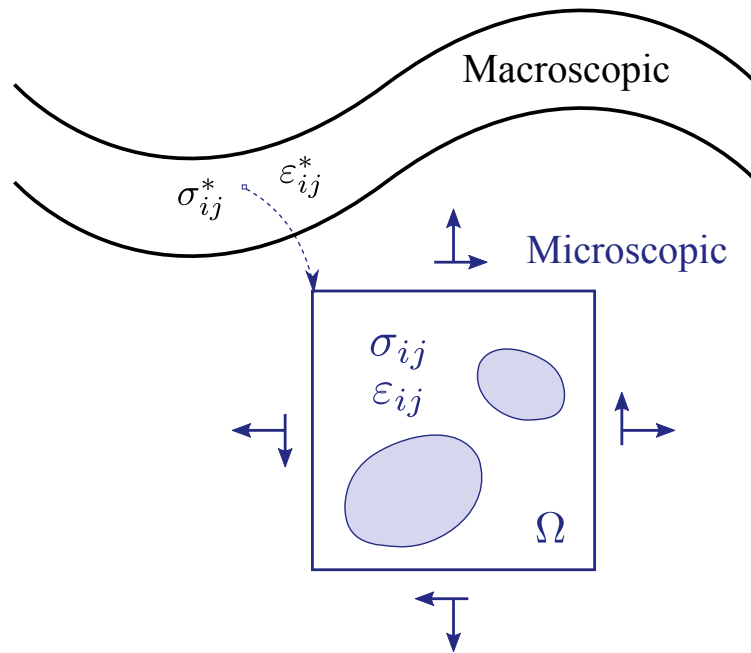


Figure 4.1: RVE for elastostatic homogenization.

Under the assumption that the length scale of the load is much larger than the dimensions of RVE, the variation of stress and strain in the vicinity of the RVE can be neglected. So, from the continuity of traction and displacement,

$$\sigma_{ij}(\mathbf{x})n_j \Big|_{\partial\Omega} = \sigma_{ij}^*n_j \Big|_{\partial\Omega}, \quad u_i(\mathbf{x}) \Big|_{\partial\Omega} = \varepsilon_{ij}^*x_j \Big|_{\partial\Omega}, \quad (4.1)$$

where Ω is the domain of the RVE, \mathbf{x} is the position vector defined in Ω and \mathbf{n} is the outward normal along the boundary $\partial\Omega$. If the material in the RVE is homogeneous, the stress and strain will trivially equal to the macroscopic stress and strain regardless of the RVE shape (Hashin, 1972),

$$\sigma_{ij}(\mathbf{x}) = \sigma_{ij}^*, \quad \varepsilon_{ij}(\mathbf{x}) = \varepsilon_{ij}^*. \quad (4.2)$$

For the RVEs composed of heterogeneous materials, the stress or strain won't be trivially constant under the boundary conditions in equation (4.1). But the volume average of stress and strain still equal to the macroscopic ones,

$$\langle \sigma_{ij}(\mathbf{x}) \rangle = \sigma_{ij}^*, \quad \langle \varepsilon_{ij}(\mathbf{x}) \rangle = \varepsilon_{ij}^*, \quad (4.3)$$

where the angle brackets are defined as volume average operator,

$$\langle f(\mathbf{x}) \rangle = \frac{1}{V} \int_{\Omega} f(\mathbf{x}) dv, \quad (4.4)$$

where V is volume of domain Ω . These can be respectively proved as follows.

Firstly, the corollary of divergence theorem used in the following discussion is

$$\int_{\Omega} f_{i,j} dv = \int_{\partial\Omega} f_i n_j ds, \quad (4.5)$$

where \mathbf{n} is the outward normal vector. This is because, for any constant vector \mathbf{a} , we have

$$\int_{\Omega} f_{i,j} a_j dv = \int_{\Omega} (f_i a_j)_{,j} dv. \quad (4.6)$$

And by using the divergence theorem,

$$\int_{\Omega} f_{i,j} a_j dv = \int_{\partial\Omega} f_i n_j a_j ds . \quad (4.7)$$

Since this holds for any constant vector a , the equation (4.5) must be true.

Under the equilibrium condition, the divergence of stress is zero, so

$$(\sigma_{ik} x_j)_{,k} = \sigma_{ik,k} x_j + \sigma_{ik} \delta_{jk} = \sigma_{ij} . \quad (4.8)$$

Substitute the σ_{ij} in to the volume average,

$$\langle \sigma_{ij} \rangle = \frac{1}{V} \int_{\Omega} \sigma_{ij} dv = \frac{1}{V} \int_{\Omega} (\sigma_{ik} x_j)_{,k} dv . \quad (4.9)$$

By using the divergence theorem,

$$\langle \sigma_{ij} \rangle = \frac{1}{V} \int_{\partial\Omega} \sigma_{ik} x_j n_k ds \quad (4.10)$$

Under the traction boundary condition defined in equation (4.1), we have

$$\langle \sigma_{ij} \rangle = \frac{1}{V} \sigma_{ik}^* \int_{\partial\Omega} x_j n_k ds \quad (4.11)$$

After using the divergence theorem again,

$$\langle \sigma_{ij} \rangle = \frac{1}{V} \sigma_{ik}^* \int_{\Omega} x_{j,k} dv = \sigma_{ik}^* \delta_{jk} = \sigma_{ij}^* \quad (4.12)$$

Corresponding to the equilibrium condition for the stress, the strain is under kinematically admissible condition, so

$$\langle \boldsymbol{\varepsilon}_{ij} \rangle = \frac{1}{2V} \int_{\Omega} (u_{i,j} + u_{j,i}) dv \quad (4.13)$$

By using divergence theorem,

$$\langle \boldsymbol{\varepsilon}_{ij} \rangle = \frac{1}{2V} \left[\int_{\partial\Omega} u_i n_j ds + \int_{\partial\Omega} u_j n_i ds \right] \quad (4.14)$$

Under the displacement boundary condition defined in equation (4.1), we have

$$\langle \boldsymbol{\varepsilon}_{ij} \rangle = \frac{1}{2V} \left[\boldsymbol{\varepsilon}_{ik}^* \int_{\partial\Omega} x_k n_j ds + \boldsymbol{\varepsilon}_{jk}^* \int_{\partial\Omega} x_k n_i ds \right] \quad (4.15)$$

After using the divergence theorem again,

$$\langle \boldsymbol{\varepsilon}_{ij} \rangle = \frac{1}{2V} \left[\boldsymbol{\varepsilon}_{ik}^* \int_{\Omega} x_{k,j} dv + \boldsymbol{\varepsilon}_{jk}^* \int_{\Omega} x_{k,i} dv \right] = \frac{1}{2} \left[\boldsymbol{\varepsilon}_{ik}^* \boldsymbol{\delta}_{kj} + \boldsymbol{\varepsilon}_{jk}^* \boldsymbol{\delta}_{ki} \right] = \boldsymbol{\varepsilon}_{ij}^* \quad (4.16)$$

Therefore, by averaging the local stress and strain fields, the macroscopic stress and strain can be evaluated, from which the effective constitutive relation can be obtained.

4.1.2 Basic concepts of the elastodynamic homogenization

For elastodynamic problems, the strain is also kinematically admissible. So the relation between the volume average of strain in RVE and the macroscopic strain still holds. However, the relation for stress doesn't hold because of the inertial force, as shown in Figure 4.2.

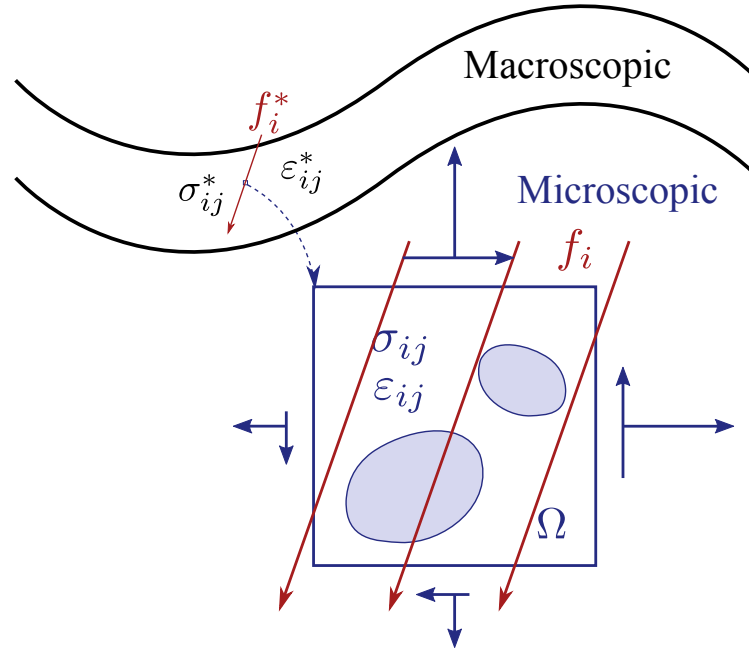


Figure 4.2: RVE for elastodynamic homogenization.

In the macroscopic field, the governing equation of stress becomes

$$\sigma_{ij,j}^* + f_i^* = 0 \quad , \quad (4.17)$$

where the body force $f_i^* = -\rho \ddot{u}^*$ represents the inertial force. So, comparing with the static case, the material point in macroscopic view has the body force as one more state in addition to the stress and strain. Similarly, under long wavelength assumption, the microscopic body force f_i is assumed to be constant all over the RVE with the same magnitude and direction of the macroscopic body force f_i^* , as

$$f_i(\mathbf{x}) = f_i^* = -\sigma_{ij,j}^* \quad . \quad (4.18)$$

Since the macroscopic field becomes static after applying the inertial force, the RVE should be

static as well. So the body force in RVE should be balanced by the resultant force applying along the boundary. Therefore the stress in the vicinity of the RVE cannot be assumed as constant anymore otherwise the resultant force of the traction will be zero,

$$\sigma_{ij}(\mathbf{x})n_j \Big|_{\partial\Omega} = \sigma_{ij}^* n_j \Big|_{\partial\Omega} \implies \int_{\partial\Omega} \sigma_{ij}(\mathbf{x})n_j ds = \sigma_{ij}^* \int_{\partial\Omega} n_j ds = 0 . \quad (4.19)$$

So, instead of a constant, the stress in the vicinity of the RVE is assumed as a linear function. Accordingly, the boundary condition becomes

$$\sigma_{ij}(\mathbf{x})n_j \Big|_{\partial\Omega} = \left(\sigma_{ij}^* + \sigma_{ij,k}^* x_k \right) n_j \Big|_{\partial\Omega} , \quad (4.20)$$

where $\sigma_{ij,k}^*$ is the macroscopic stress gradient, which is a constant three-order tensor in the RVE. Then the resultant of the traction becomes

$$\begin{aligned} \int_{\partial\Omega} \sigma_{ij}(\mathbf{x})n_j ds &= \int_{\partial\Omega} \left(\sigma_{ij}^* + \sigma_{ij,k}^* x_k \right) n_j ds \\ &= \sigma_{ij,k}^* \int_{\partial\Omega} x_k n_j ds \\ &= \sigma_{ij,k}^* \delta_{jk} V \\ &= \sigma_{ij,j}^* V , \end{aligned} \quad (4.21)$$

which balances the resultant of the body force, as

$$\int_{\partial\Omega} \sigma_{ij}(\mathbf{x})n_j ds + \int_{\Omega} f_i(\mathbf{x}) dv = \sigma_{ij,j}^* V + f_i^* V = 0 . \quad (4.22)$$

So, subjected to the body force defined in equation (4.18) and the traction defined in (4.20), the

RVE will be in equilibrium.

Now, consider the stress volume average of the RVE under such traction boundary condition. Due to the body force f_i , the divergence of stress becomes $-f_i$. Thus the equation (4.8) becomes

$$(\sigma_{ik}x_j)_{,k} = \sigma_{ik,k}x_j + \sigma_{ik}\delta_{jk} = \sigma_{ij} - f_ix_j . \quad (4.23)$$

So the volume average of stress becomes

$$\begin{aligned} \langle \sigma_{ij} \rangle &= \frac{1}{V} \int_{\Omega} \sigma_{ij} dv = \frac{1}{V} \int_{\Omega} [(\sigma_{ik}x_j)_{,k} + f_ix_j] dv \\ &= \frac{1}{V} \int_{\partial\Omega} (\sigma_{ik}x_j)n_k ds + \frac{1}{V} \int_{\Omega} f_ix_j dv . \end{aligned} \quad (4.24)$$

Substitute the traction boundary condition defined in equation (4.20) and body force defined in equation (4.18),

$$\langle \sigma_{ij} \rangle = \frac{1}{V} \int_{\partial\Omega} (\sigma_{ik}^* + \sigma_{ik,l}^*x_l)x_j n_k ds - \frac{1}{V} \sigma_{ik,k}^* \int_{\Omega} x_j dv . \quad (4.25)$$

The position vector of the centroid of RVE (\mathbf{c}) is defined as

$$c_i = \frac{1}{V} \int_{\Omega} x_i dv . \quad (4.26)$$

Thus,

$$\begin{aligned}
\langle \sigma_{ij} \rangle &= \frac{1}{V} \int_{\partial\Omega} \sigma_{ik}^* x_j n_k ds + \frac{1}{V} \int_{\partial\Omega} \sigma_{ik,l}^* x_l x_j n_k ds - \sigma_{ik,k}^* c_j \\
&= \frac{1}{V} \sigma_{ik}^* \int_{\Omega} x_{j,k} dv + \frac{1}{V} \sigma_{ik,l}^* \int_{\Omega} (x_l x_j)_{,k} dv - \sigma_{ik,k}^* c_j \\
&= \sigma_{ik}^* \delta_{jk} + \sigma_{ik,l}^* (\delta_{kl} c_j + \delta_{jk} c_l) - \sigma_{ik,k}^* c_j \\
&= \sigma_{ij}^* + \sigma_{ik,k}^* c_j + \sigma_{ij,l}^* c_l - \sigma_{ik,k}^* c_j \\
&= \sigma_{ij}^* + \sigma_{ij,l}^* c_l .
\end{aligned} \tag{4.27}$$

By selecting the centroid of RVE as the origin, c_l becomes zero.

Therefore, in the dynamic problems with long wavelength assumption and selecting the centroid of RVE as the origin, the macroscopic stress can also be obtained by the volume average of stress in the RVE. However, when the frequency is high, the RVE has a non-uniform body force distribution, and the volume average of the local stress differs from the macroscopic stress.

4.1.3 Formulations and results

This section presents a computational homogenization method based on the explicitly solve wave fields and the concept of self-consistent across different scales. The considered heterogeneous models are composed of an isotropic elastic matrix with periodically embedded circular inhomogeneities, under harmonic antiplane incident wave.

With the long wavelength assumption, the macroscopic wave field can be considered as propagating plane waves in an effective medium, as shown in Figure 4.3 schematically, with the field variables in the form of

$$f^*(\mathbf{x}) = A^* e^{i\mathbf{k}^* \cdot \mathbf{x}} , \tag{4.28}$$

where A^* is the complex amplitude of the macroscopic field and \mathbf{k}^* is the effective wave vector.

Then the effective properties can be obtained by the relation among the complex amplitudes.

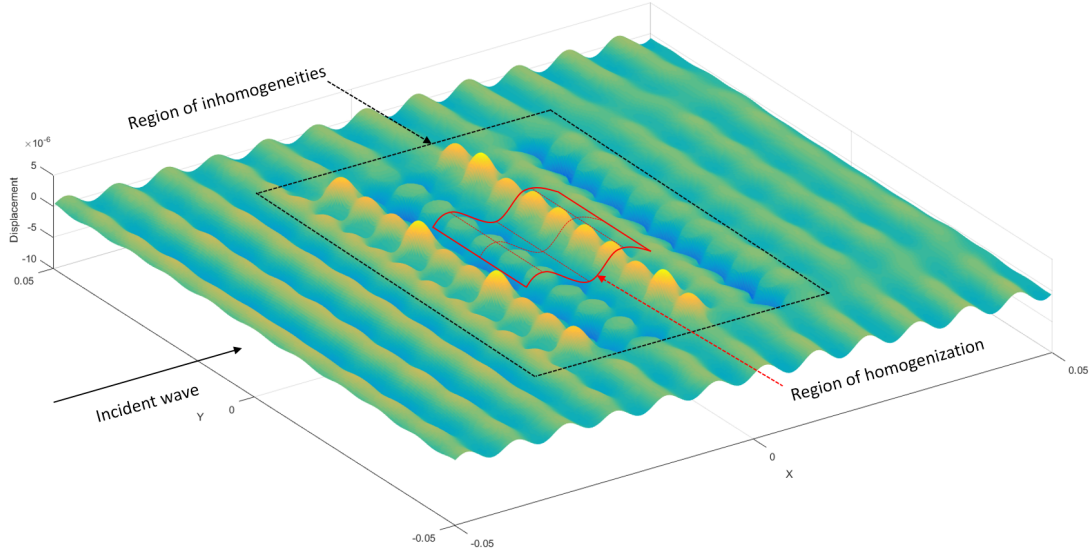


Figure 4.3: Computational model of homogenization.

In such expression, the exponential term represents the overall waveform and the local response of the microscopic structure is encapsulated in the complex amplitude. Accordingly, by assuming the real wave field to be in the form of

$$f(\mathbf{x}) = \tilde{A}(\mathbf{x})e^{i\mathbf{k}^* \cdot \mathbf{x}} , \quad (4.29)$$

the microscopic wave field is represented by the function $\tilde{A}(\mathbf{x})$. Then, as employed in (Wang and Gan, 2002), the complex amplitude of macroscopic wave field is assumed to be the volume average of the microscopic wave field,

$$A^* = \langle \tilde{A}(\mathbf{x}) \rangle = \frac{1}{V} \int_V f(\mathbf{x})e^{-i\mathbf{k}^* \cdot \mathbf{x}} dV . \quad (4.30)$$

where, instead of taking the volume average directly, the overall fluctuation of the effective wave is eliminated before the averaging.

The average field variable f in the heterogeneous medium, representing both displacement and shear strains, can be expressed in terms of the corresponding average values in the matrix and the inhomogeneities as

$$\langle f \rangle = \phi \langle f \rangle_i + (1 - \phi) \langle f \rangle_m , \quad (4.31)$$

where ϕ is the volume fraction of the inhomogeneities, and the subscripts i and m represent averaging in the inhomogeneities and the matrix, respectively.

Based on the currently developed solution of interacting inhomogeneities, the relation between the strains and displacements of inhomogeneity and matrix can be obtained, by selecting a proper RVE, as

$$\langle w \rangle_i = M \langle w \rangle_m \quad (4.32)$$

$$\begin{bmatrix} \langle \gamma_{xz} \rangle_i \\ \langle \gamma_{yz} \rangle_i \end{bmatrix} = \begin{bmatrix} N_1 & N_2 \\ N_2 & N_1 \end{bmatrix} \begin{bmatrix} \langle \gamma_{xz} \rangle_m \\ \langle \gamma_{yz} \rangle_m \end{bmatrix} , \quad (4.33)$$

where matrix N has only two independent elements N_1 and N_2 for an isotropic homogenized material. Then the average displacement and shear strains can be expressed in terms of the average value in the matrix as

$$\langle w \rangle = (\phi M + 1 - \phi) \langle w \rangle_m , \quad (4.34)$$

$$\begin{bmatrix} \langle \gamma_{xz} \rangle \\ \langle \gamma_{yz} \rangle \end{bmatrix} = \begin{bmatrix} \phi N_1 + 1 - \phi & \phi N_2 \\ \phi N_2 & \phi N_1 + 1 - \phi \end{bmatrix} \begin{bmatrix} \langle \gamma_{xz} \rangle_m \\ \langle \gamma_{yz} \rangle_m \end{bmatrix} . \quad (4.35)$$

Using the constitutive relations given by

$$p = -i\omega\rho w \quad (4.36)$$

$$\begin{bmatrix} \tau_{xz} \\ \tau_{yz} \end{bmatrix} = \begin{bmatrix} \mu & 0 \\ 0 & \mu \end{bmatrix} \begin{bmatrix} \gamma_{xz} \\ \gamma_{yz} \end{bmatrix}, \quad (4.37)$$

with p being the momentum density, the average moment density $\langle p \rangle$ and shear stresses $[\langle \gamma_{xz} \rangle, \langle \gamma_{yz} \rangle]^T$ can be expressed as

$$\langle p \rangle = -i\omega[\rho_i\phi M + \rho_m(1 - \phi)] \langle w \rangle_m, \quad (4.38)$$

$$\begin{bmatrix} \langle \tau_{xz} \rangle \\ \langle \tau_{yz} \rangle \end{bmatrix} = \begin{bmatrix} \mu_i\phi N_1 + \mu_m(1 - \phi) & \mu_i\phi N_2 \\ \mu_i\phi N_2 & \mu_i\phi N_1 + \mu_m(1 - \phi) \end{bmatrix} \begin{bmatrix} \langle \gamma_{xz} \rangle_m \\ \langle \gamma_{yz} \rangle_m \end{bmatrix}. \quad (4.39)$$

Then the effective mass density and effective elastic constants can be obtained as

$$\rho_e = \frac{-i\omega[\rho_i\phi M + \rho_m(1 - \phi)]}{\phi M + 1 - \phi}, \quad (4.40)$$

$$[C] = \begin{bmatrix} \mu_i\phi N_1 + \mu_m(1 - \phi) & \mu_i\phi N_2 \\ \mu_i\phi N_2 & \mu_i\phi N_1 + \mu_m(1 - \phi) \end{bmatrix} \begin{bmatrix} \phi N_1 + 1 - \phi & \phi N_2 \\ \phi N_2 & \phi N_1 + 1 - \phi \end{bmatrix}^{-1}. \quad (4.41)$$

By using the element of the principal diagonal of the matrix $[C]$ as the shear modulus, the effective wave number k^* can be obtained, which is supposed to be equal to the one used in the volume average defined in equation (4.30). So, in order to make it to be consistent with the assumed value, the computed k^* is used in the next iteration step until the effective wave number converges. The computed effective wave number is a complex number, with the real

part k_{re} corresponding to the phase velocity $c = \omega/k_{re}$ and the imaginary part k_{im} corresponding to the attenuation of the wave.

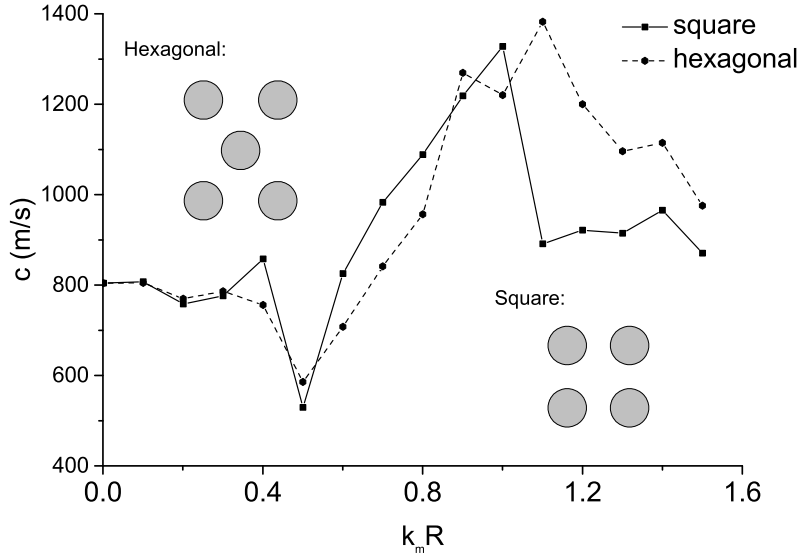


Figure 4.4: Effective phase velocity for the square and hexagonal arrangement

In Figure 4.4, the effective phase velocity is plotted as a function of the dimensionless parameter $k_m R$, which is corresponding to the frequency of incident wave. Two models with same material constants and different arrangements, square and hexagonal, are considered. The averages of field variables are taken in the center unit cell which is surrounded by three layers of inhomogeneities. The numbers of inhomogeneities are 49 and 37 in the cubic and hexagonal arrangements. The material constants used are $\mu_m = 1.73 \text{ GPa}$, $\rho_m = 1200 \text{ kg m}^{-3}$, $\mu_i = 8.36 \text{ GPa}$ and $\rho_i = 11300 \text{ kg m}^{-3}$. The volume fraction $\phi = 0.25$. Figure 4.5 shows the attenuation of the material under incident waves with different frequencies. A considerable increase can be observed when $k_m R = 0.4-1.1$, corresponding to the first stop band. Since the two models have the same volume fraction and the same characteristic length, similar stop bands are observed, indicating that the phenomenon is not sensitive to the details of the lattice

structure.

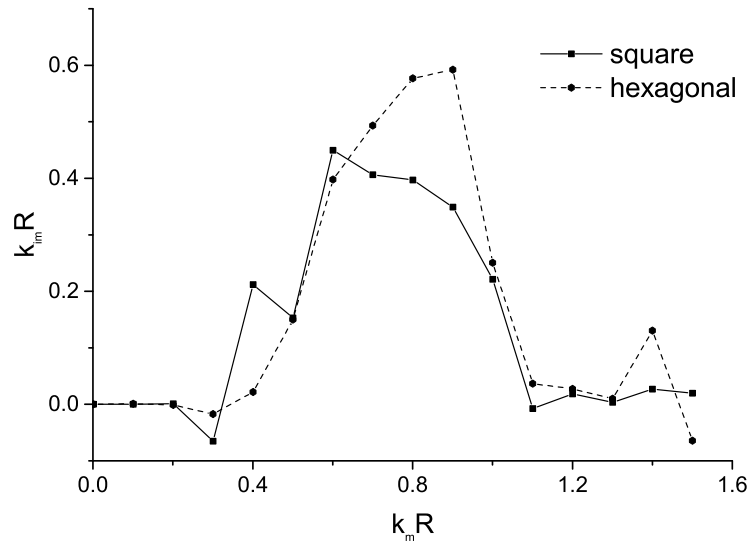


Figure 4.5: Attenuation of the square and hexagonal arrangement

4.2 Energy equivalence

In this section, another computational homogenization method for periodic materials by averaging the computed wave field is developed based on the kinetic energy equivalence. In the following discussion, the formulations will be introduced in detail, and the validity of the method is verified by comparing the obtained effective properties with the existing results under quasi-static limit load, and comparing the simulation results of the original heterogeneous material and its homogenized substitution. Then, as an example, the method is applied to compute the effective material properties under different frequencies in the first pass-band.

4.2.1 Formulations

The considered model is composed of isotropic elastic matrix with circular inhomogeneities embedded periodically in a square lattice. If the periodic material is assumed to extend infinitely, the wave field is in the form of Bloch wave, as shown in equation (3.1). The comparison of this wave form with that of the effective wave shown in equation (4.28) reveals that the exponential term of the Bloch wave represents the macroscopic wave motion, and the Bloch wave number can be used as the wave number of the effective wave.

Therefore, by modeling the RVE with the unit cell and solving the eigenvalue problem by using the method shown in Section 3, the effective wave number k^* can be obtained as the eigenvalue. With assuming the effective material to be isotropic, the wave speed and the relation between material properties of the effective material can be determined as

$$c^* = \frac{\omega}{k^*} = \sqrt{\frac{\mu^*}{\rho^*}}, \quad (4.42)$$

where ω is the frequency, μ^* and ρ^* denote the shear modulus and effective mass density, respectively.

After solving the eigenvalue problem, the eigenstate of the unit cell is also obtained, with which the kinetic energy of the unit cell can be obtained as

$$T = \iint_A \frac{1}{2} \rho \omega^2 \bar{w} w da, \quad (4.43)$$

where w is the antiplane displacement and the superscript bar denotes the complex conjugate.

Then, hypothetically, the local response in that region can be replaced by an effective wave field w^* , which possesses the same kinetic energy as

$$T = T^* = \frac{1}{2} \rho^* \omega^2 \iint_A \bar{w}^* w^* da \quad (4.44)$$

where the w^* denotes the effective displacement field.

In addition, the effective displacement field in the region is assumed to have the minimum mismatch with the one of the real local response. So the effective displacement field can be obtained by fitting an assumed wave form to the displacement distribution of the eigenstate in the unit cell region. Then, by substituting the obtained w^* and T^* into the equation (4.44), the effective mass density can be obtained, and then the effective shear modulus can be evaluated by using the relation in equation (4.42).

In this work, two wave forms are considered. One is the linear function,

$$w^*(\mathbf{x}) = \mathbf{a} \cdot \mathbf{x} + w_0, \quad (4.45)$$

which is corresponding to the constant strain assumption. And the other is the plane wave,

$$w^*(\mathbf{x}) = w_0 e^{i\mathbf{k}^* \cdot \mathbf{x}}. \quad (4.46)$$

The \mathbf{a} and w_0 are the constants to be determined by using the least square method.

In the numerical implementation, a vector of displacement values are collected from an array of points in the unit cell. For the linear distribution, the Moore-Penrose inverse of the

matrix composed of row vectors $[x_1, x_2, 1]$ are used to get the constants. For the plane wave distribution, because the Bloch wave vector is used as the effective wave vector \mathbf{k}^* , the constant w_0 can be directly determined by the inner product of the vector of displacement and the vector composed of $e^{-i\mathbf{k}^* \cdot \mathbf{x}}$, divided by the dimension of the vector.

Since the eigenstate is corresponding to an unidirectional wave propagation, for canceling the effect of the direction to get the isotropic material properties, multiple cases with different angles between $0^\circ - 45^\circ$ are computed, and the averages are used as the isotropic effective material properties.

4.2.2 Verification of the method

In order to validate this method, the effective material properties at the quasi-static limit frequency are computed and compared with the existing results. The material of the matrix and inhomogeneities are steel ($\rho_m = 7670 \text{ kg m}^{-3}$, $\mu_m = 84.3 \text{ GPa}$) and lead ($\rho_i = 11400 \text{ kg m}^{-3}$, $\mu_i = 8.43 \text{ GPa}$) respectively. Since the frequency approaches zero, the wave forms in equation (4.45) and equation (4.46) become equivalent.

The computed effective shear moduli for different volume fractions of the inhomogeneity, compared with existing results (Parnell and Abrahams, 2006), are shown in Figure 4.6. The results computed with the method of this work coincide with the ones computed with the asymptotic homogenization method and self-consistent method in the range of low volume fraction. For the materials with volume fraction higher than 0.3, the results of the three methods start to diverge within the range between the lower and upper bounds.

The validity of the elastodynamic homogenization are verified by comparing the direct nu-

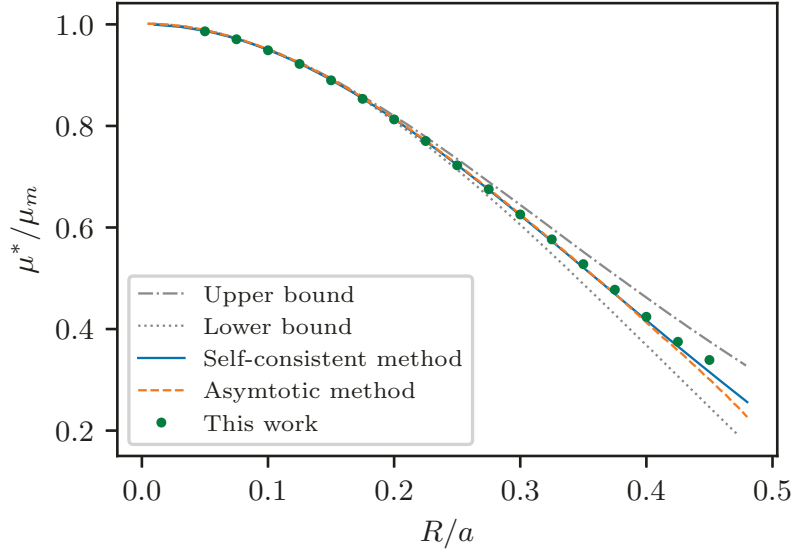
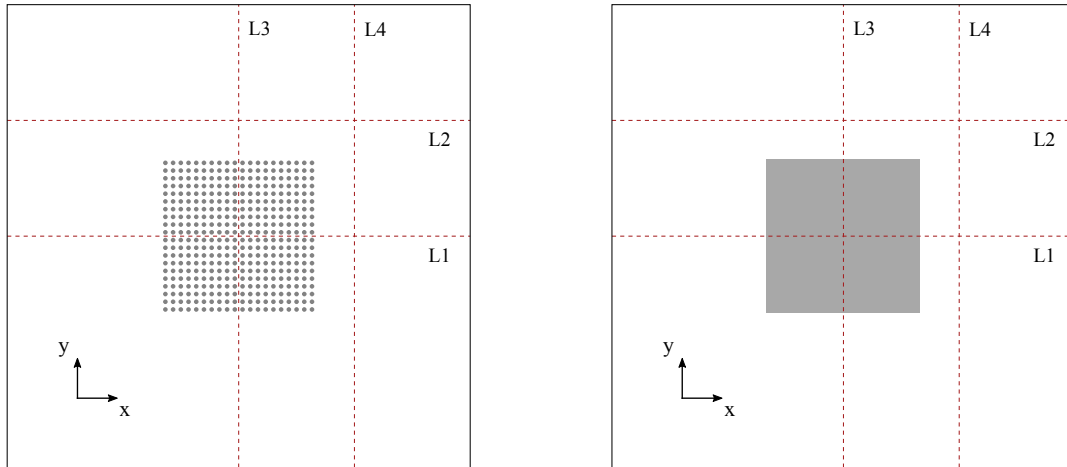


Figure 4.6: Comparison with existing results

merical simulations of the wave fields scattered by multiple inhomogeneities and the homogeneous replacement with the effective properties. As shown in Figure 4.7, the multiple scattering model is composed of an array of circular inhomogeneities arranged in a rectangular lattice. The radius of the inhomogeneities is 6 mm and the lattice constant $a = 20$ mm. The material constants used are $\rho_m = 7670 \text{ kg m}^{-3}$, $\mu_m = 84.3 \text{ GPa}$, $\rho_i = 11400 \text{ kg m}^{-3}$, $\mu_i = 8.43 \text{ GPa}$. The incident wave is a plane SH wave propagating along positive x direction with the frequency which is set to be 26.3818 kHz so that $k_m a = 1$.

The dimension of the array should be large enough to show the properties of the material. To determine the sufficient dimension, models with different dimensions were tested. And, for the frequency $k_m a = 1$, the dimension is set to be 20×20 , which is sufficiently large so that the effective properties become insensitive to the change of dimension of the array.



(a) Multiple scattering model

(b) Homogenized model

Figure 4.7: Direct numerical simulation models for comparison

In the homogenized model, the array of inhomogeneities is replaced by a rectangular inhomogeneity with the same dimensions and effective material properties, which are obtained as 9216.07 kg/m^3 and 53.4968 GPa with the constant strain assumption, or obtained as 9087.92 kg/m^3 and 52.7529 GPa with the plane wave assumption. The multiple scattering model is solved by using the method in the Section 2, and the homogenized models are solved with boundary element method. The displacement distribution of the wave fields at the same phase are shown in Figure 4.8, where only the one with the constant strain assumption is used as the homogenized model.

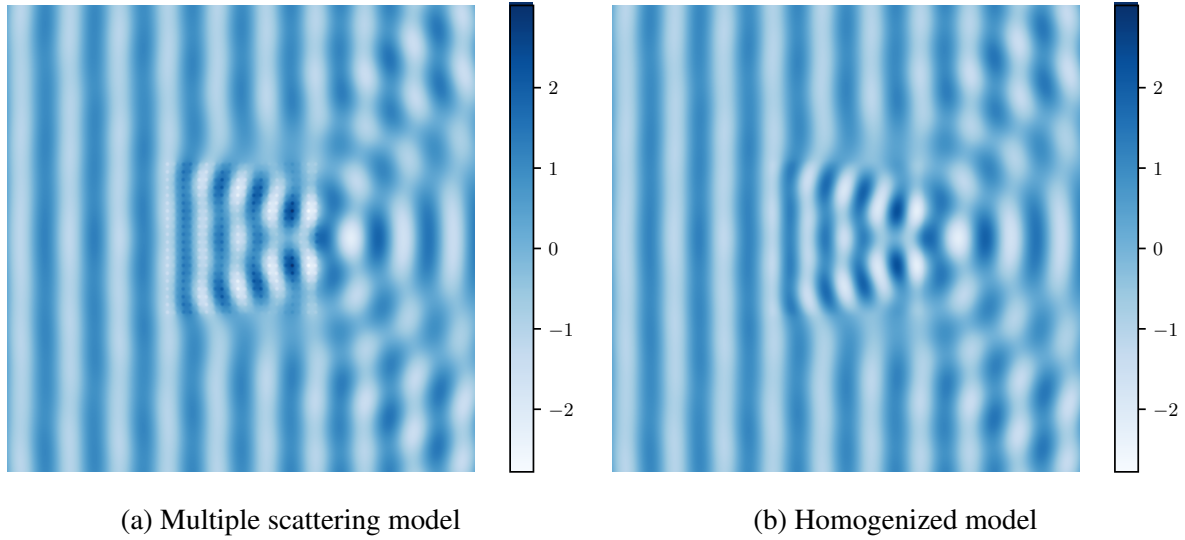


Figure 4.8: Comparison between the displacement fields of the periodic model and homogenized model

The overall displacement distribution of the homogenized model shows good accordance with the one of the model with multiple inhomogeneities, especially for the locations outside of the inhomogeneous region. For the inhomogeneity locations, since the material of the inhomogeneity is softer and heavier than the matrix material, the displacement of multiple scattering model has larger amplitude than that of the homogenized model, in which the material is homogeneous and the displacement varies more smoothly.

The normalized amplitudes of displacement $|w|/|w_0|$ and stress $|\tau_{xz}|/|\tau_0|$ along the lines marked in the Figure 4.7 are plotted in the Figure 4.9 and Figure 4.10 with dashed lines. It can be observed that the fields match well in general.

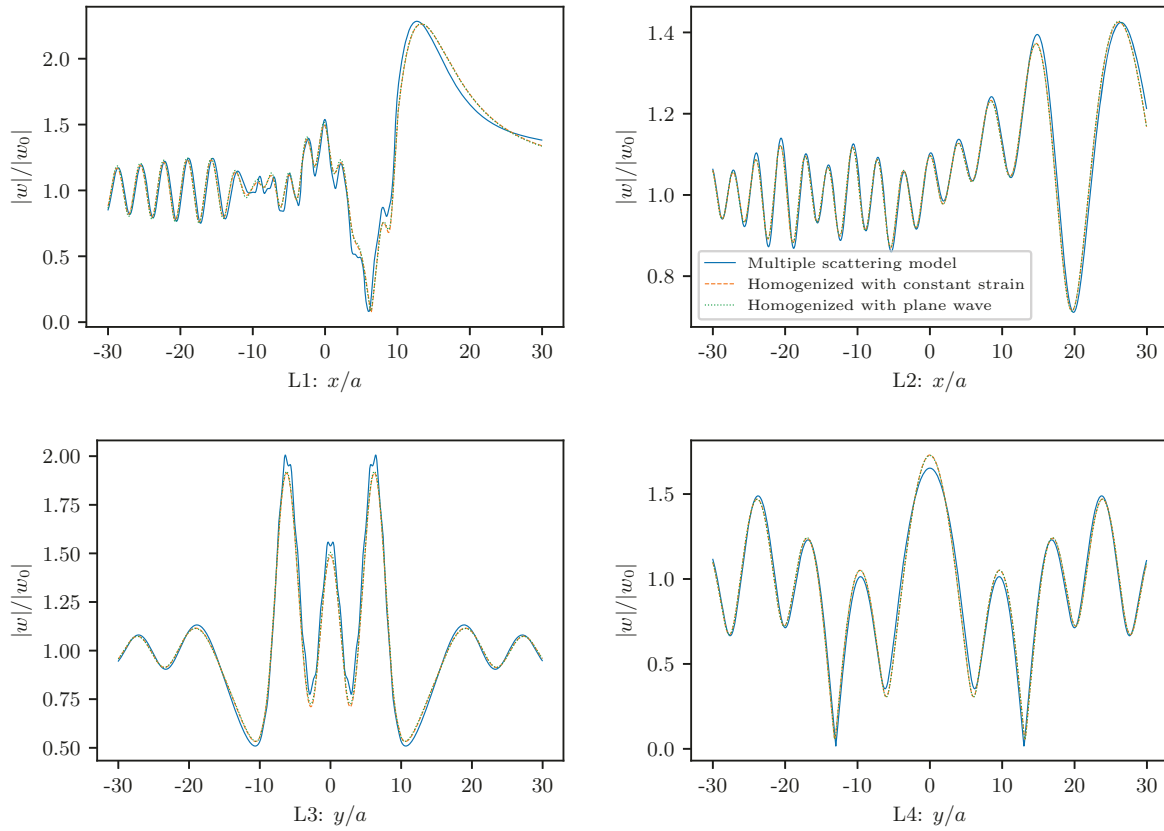


Figure 4.9: Normalized displacement amplitude $|w|$ along the lines

For the displacement distribution inside the region, $-10 < x/a < 10$ and $-10 < y/a < 10$ along L1 and L3, the homogenized model shows larger deviations to the multiple scattering model, while the peak values got approximated accurately.

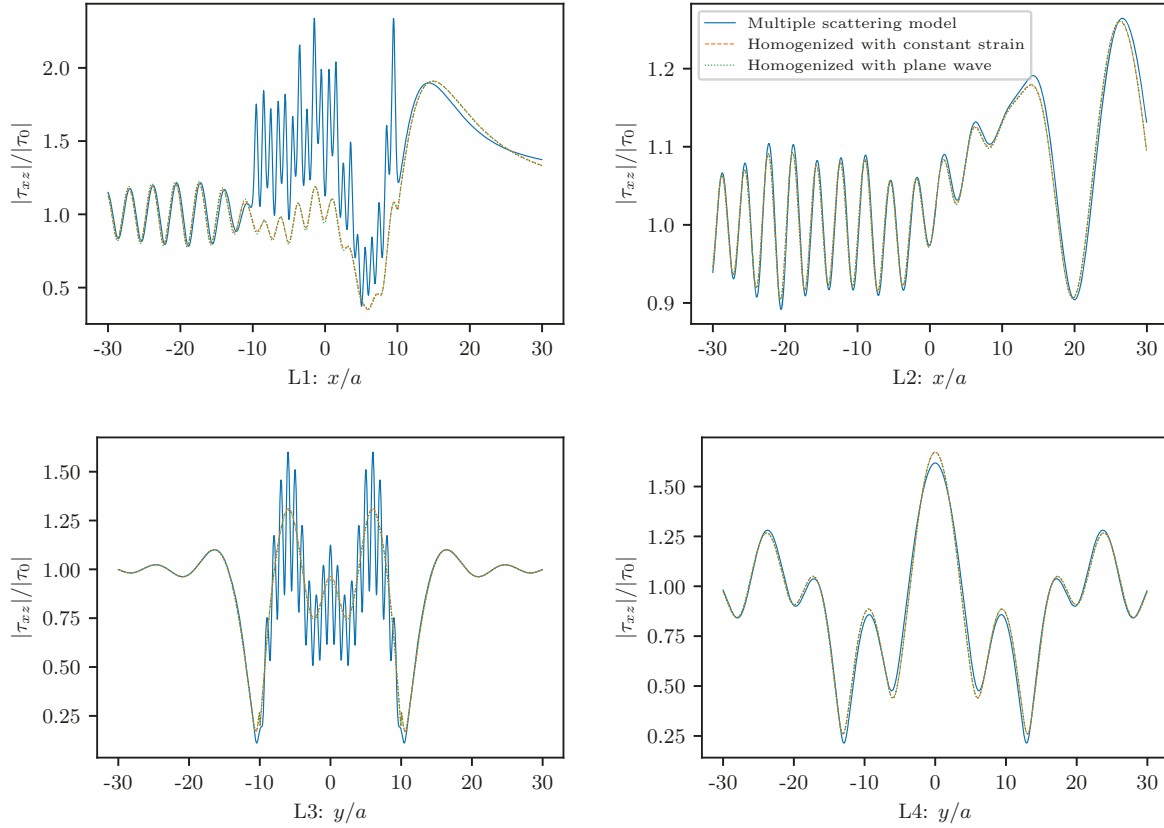


Figure 4.10: Normalized stress amplitude $|\tau_{xz}|$ along the lines

In the comparison of the stress τ_{xz} outside the region of inhomogeneity, there is also a good agreement between the two models. Inside the region, the stress amplitude distribution in the multiple scattering model shows intensive fluctuations, which the homogenized model fails to follow, since the twenty peaks in the curve of the multiple scattering model are corresponding to the twenty inhomogeneities in a row. However, the result of homogenized model can correctly follow the general trend.

From the above comparison, it can be observed that the difference made by using the different fitting wave forms is mainly around the peaks inside of the inhomogeneous region, and is negligible for other locations.

4.2.3 Effective properties

In this section, the effective material properties of the same periodic material as in the Section 4.2.2 under a range of frequencies are evaluated as an example. The considered frequency is ranging from the quasi-static limit to 48.7834 kHz, above which the Bloch wave does not exist for some angles. Two fitting wave forms, equation (4.45) and equation (4.46), are used and the obtained effective mass density and shear modulus are shown in Figure 4.11 and Figure 4.12.

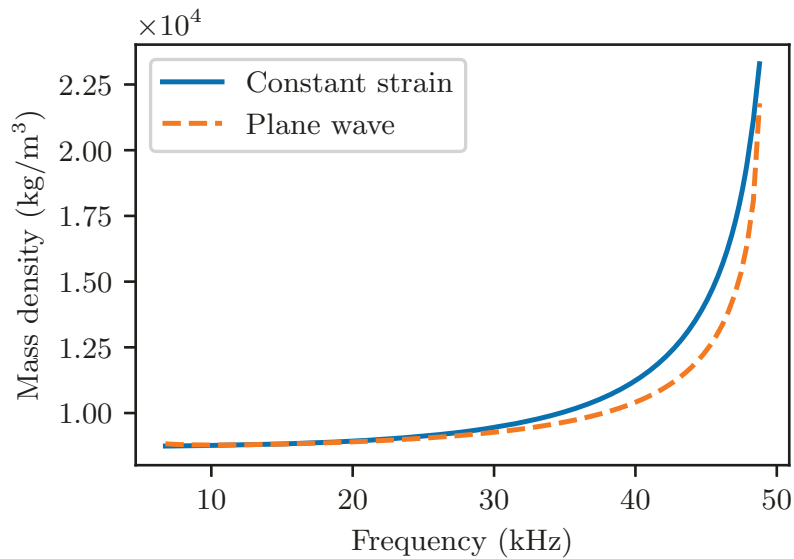


Figure 4.11: Effective mass density.

The effective mass density starts from the static weighted average of the two materials 8724.63 kg/m^3 , and increases monotonically as the frequency increases. The results with two different fitting wave forms both converge to the quasi-static limit and agree well with each other under low frequencies. With increasing the frequency, the effective mass density obtained by using the plane wave assumption becomes lower, because the form of plane wave allows larger displacement which requires less weight to get the same kinetic energy. Equivalently, the

constant strain assumption demands the effective material to be stiffer, which is consistent with the comparison in Figure 4.12.

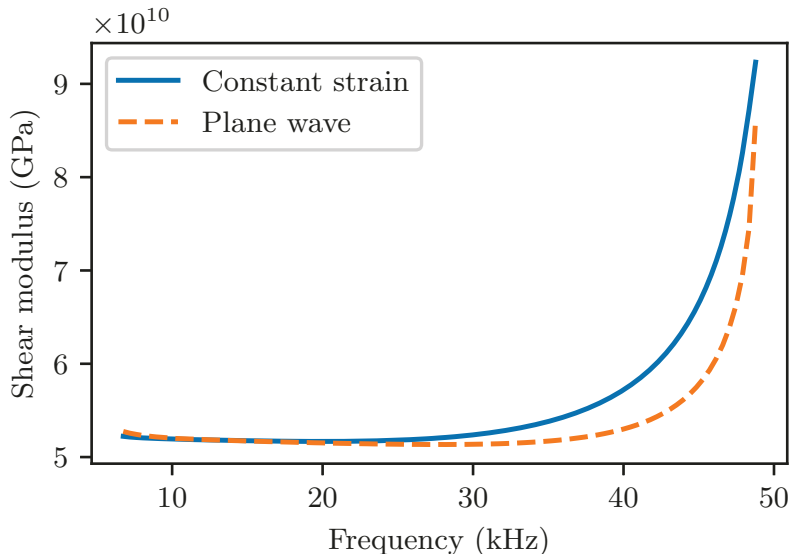


Figure 4.12: Effective shear modulus.

4.3 Conclusion

In this chapter, two elastodynamic homogenization methods are developed based on the domain averaging of the explicitly solved wave fields. In the first method, the volume average scheme with considering the effective wave form is employed, in which the effective wave number is determined by self-consistent method. The effective phase velocity and attenuation of the effective material can be obtained under a wide range of frequency. And the convergence of the effective wave number provides a guideline for the assumption of the effect wave form. Then, by assuming the effective wave number to be the same as the Bloch wave, the second homogenization method for periodic materials is developed based on the kinetic energy equivalence. The homogenization results for both quasi-static and dynamic cases are verified by

comparing with the existing results and the direct numerical simulations. And the applicability of the method is demonstrated by evaluating the effective material properties under a range of frequency.

Chapter 5: Homogenization based on boundary matching

This chapter presents a computational homogenization method for the determination of effective material properties under time-harmonic antiplane incident waves, based upon the optimization of boundary integral of explicitly solved multiple scattering wave fields or eigenstates of unit cell with periodic boundary condition. Depending on the different frequencies and materials, different representative volume elements are modeled for determining the boundary response. The applicability of the method is shown via the homogenization of random materials and periodic materials under a wide range of frequency. The accuracy and effectiveness are discussed through the comparison of direct numerical simulations of homogenized models and the original models with local structures. Illustrative example of the determination of multiple scattering wave field in different scales is considered to study the multiscale modeling of the elastic wave propagation in heterogeneous materials. This chapter stems from the journal paper in preparation: “Computational homogenization for antiplane wave propagation in heterogeneous materials”, written by the author under the supervision by Dr. Wang.

5.1 Introduction

The effective properties of a piece of heterogeneous material can be considered as the transfer characteristics of a black box system, which can be identified by analyzing the relation between the input and output. Based on the concept of system identification, various homogenization methods have been developed, which includes retrieval method (Fokin et al., 2007; Zhang et al., 2013), coherent potential approximation (CPA) methods (Hu et al., 2008; Wu et al., 2007). In

the retrieval method, the experiments or numerical simulations are carried out on a piece of heterogeneous material which is subjected to an incident wave. Then the effective material properties are obtained by analyzing the relation among the incident wave, reflected and transmitted waves which are measured or computed. Although it is simple in principle, the retrieval method becomes unreliable when the frequency is high and the wave number in the heterogeneous material is hard to predict. The CPA method is based on the equivalence of the Green's function or its counterpart, for example, the T-matrix of scatterer. With combining the concept of projection, which is essentially similar to the homogenization, the method based on matching the boundary response in the macroscopic modal space is developed (Yang et al., 2014). Most works on CPA are focused on the analytical solutions, which usually require more assumptions.

This chapter presents a computational method for the elastodynamic homogenization of heterogeneous materials based on the optimization of boundary integral of explicitly computed wave fields. The proposed method is applicable to both periodic materials and random materials under the frequencies beyond the long-wavelength limit, without assuming the macroscopic mode shape functions.

5.2 Methodology

The problem considered is the determination of effective isotropic material properties with which the homogeneous material can be approximately equivalent to the heterogeneous material, which is composed of multiple circular inhomogeneities embedded in an elastic medium, and subjected to harmonic antiplane elastic waves. The model is schematically shown in Figure 5.1.

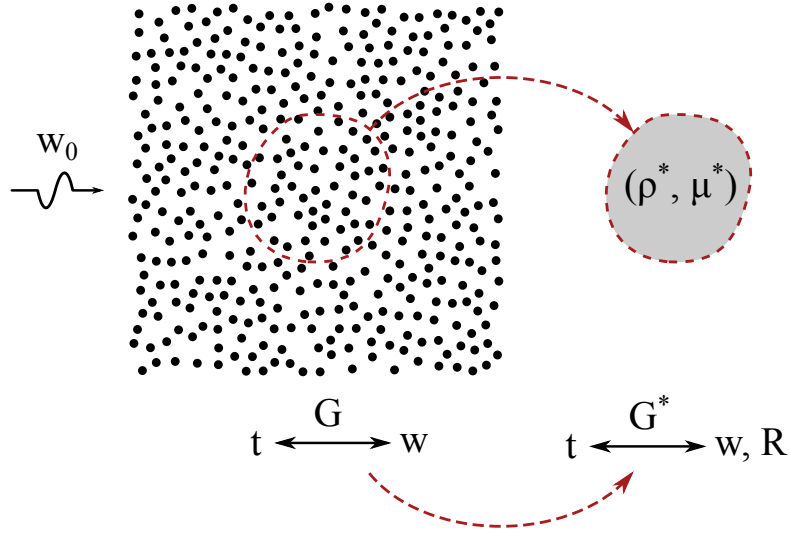


Figure 5.1: Schematic sketch of the model

The properties of macroscopically homogeneous materials can be approximated by those of their RVE. For the periodic heterogeneous materials, any repeating units, which are composed of one or multiple unit cells, can be considered as an RVE. For the random materials with uniformly distributed inhomogeneities, the RVE should be large enough so that its statistical properties become insensitive to its size and location. Since the RVE interacts with the surrounding media only through the interface, the mechanical behavior of the RVE can be encapsulated by its boundary response, which can further be represented by the relation between the two types of boundary conditions, which are the antiplane displacement w and the traction $t = \sigma_{zi}n_i$ in this case, as shown in Figure 5.1. The relation between them can be expressed by the boundary integral equation, as

$$c(\mathbf{x})w(\mathbf{x}) + \int_S \frac{\partial G(\mathbf{x}, \mathbf{y})}{\partial \mathbf{n}(\mathbf{y})} w(\mathbf{y}) ds(\mathbf{y}) = \int_S G(\mathbf{x}, \mathbf{y}) t(\mathbf{y}) ds(\mathbf{y}), \quad (5.1)$$

where S is the boundary of the RVE with the \mathbf{n} being the outward normal vector. The constant $c(\mathbf{x})$ depends on the geometry of the boundary at position \mathbf{x} , and equals to 0.5 if S is smooth around \mathbf{x} . And $G(\mathbf{x}, \mathbf{y})$ is the Green's function in which the local mechanical properties are incorporated.

If the RVE is substituted by a piece of isotropic homogeneous material with effective mass density (ρ^*) and effective shear modulus (μ^*), it can be expected that the relation between w and t can still be established by the fundamental solution for the effective homogeneous material, with introducing a residue $R(\mathbf{x})$, defined as

$$R(\mathbf{x}) = c(\mathbf{x})w(\mathbf{x}) + \int_S \frac{\partial G^*(\mathbf{x}, \mathbf{y})}{\partial \mathbf{n}(\mathbf{y})} w(\mathbf{y}) ds(\mathbf{y}) - \int_S G^*(\mathbf{x}, \mathbf{y}) t(\mathbf{y}) ds(\mathbf{y}), \quad (5.2)$$

where $G^*(\mathbf{x}, \mathbf{y})$ is the fundamental solution of the effective medium, expressed as

$$G^*(\mathbf{x}, \mathbf{y}) = \frac{i}{4} H_0^{(1)}(kr), \quad (5.3)$$

where $H_0^{(1)}$ is the zero order Hankel function of the first kind, k is the wave number of the effective homogeneous material, and the r is the distance between \mathbf{x} and \mathbf{y} . The wave number depends on the frequency ω and the transverse wave speed c , which depends on the mass density ρ^* and shear modulus μ^* of the material,

$$k = \frac{\omega}{c}, \quad c = \sqrt{\frac{\mu^*}{\rho^*}}. \quad (5.4)$$

The comparison between equation (5.1) and (5.2) reveals that when the $R(\mathbf{x})$ vanishes at any

position along the interface for any pair of w and t , the effective fundamental solution $G^*(\mathbf{x}, \mathbf{y})$ will be exactly the same as the Green's function $G(\mathbf{x}, \mathbf{y})$, which is impossible if the effective material is assumed to be homogeneous. However, the amplitude of residue $R(\mathbf{x})$, defined as

$$A(\rho^*, \mu^*) = \sqrt{\int_S \overline{R(\mathbf{x})} R(\mathbf{x}) dx}, \quad (5.5)$$

can indicate how close the effective homogeneous material can respond as the RVE, and the best approximation can be made when $A(\rho^*, \mu^*)$ is minimized by adjusting the effective mass density and shear modulus.

In the numerical implementation, the boundary is discretized into N linear pieces with N nodes, and the boundary integrals are computed by using Gaussian quadrature, which can be linearized as

$$\{R\} = [H]\{w\} - [G]\{t\}, \quad (5.6)$$

where $\{w\}$ and $\{t\}$ are vectors composed of N values of the explicitly computed displacement and traction at the nodes, respectively. When multiple loading cases, such as ones under incident waves with different angles, are considered simultaneously, the residue vector $\{R\}$ can be expanded to a matrix in which each column is corresponding to a loading case,

$$[R] = [R_1, R_2, \dots, R_M] = [H][w_1, w_2, \dots, w_M] - [G][t_1, t_2, \dots, t_M], \quad (5.7)$$

and the amplitude of residue defined in equation (5.5) becomes the Frobenius norm of the

matrix, as

$$A(\rho^*, \mu^*) = \|R\|_F = \sqrt{\sum_{i=1}^N \sum_{j=1}^M \overline{R_{ij}} R_{ij}}. \quad (5.8)$$

Then, by employing the optimization algorithm, the effective properties can be obtained when the minimum A is reached. Since the gradient is hard to obtain, in this work, the Nelder-Mead method is employed for local minimization and the Basin-hopping method is used as the global optimization technique for enlarging the search space.

5.3 RVE modeling

The determination of the RVE response is essential for the developed homogenization method. In this section, two different RVE modeling methods are respectively developed for the materials with inhomogeneities distributed randomly and periodically.

5.3.1 Random material

For random materials, the response of the RVE is collected from the multiple scattering wave field of a large arrangement of circular inhomogeneities randomly embedded in an infinite medium, as shown in Figure 5.1 schematically. The model is solved by using the multiple scattering method developed in Section 2.

Although the integral path in equation (5.2) can be defined arbitrarily, RVEs in circular shape are used in this work for convenience. It is worthy to note that, for the circular RVE, its boundary inevitably crosses the interfaces of inhomogeneities and the matrix. By comparing the results with the ones obtained by the RVE with curve boundary which avoids the crossing,

it can be concluded that the crossing of the interfaces doesn't affect the homogenization in an obvious way.

For random materials with uniformly distributed inhomogeneities, the RVE should be large enough so that its effective properties become insensitive to its size and location. In this work, a number of circular RVEs in different locations are used for determining the appropriate RVE size by examining the coefficients of variation (CV). And the size with which the RVEs render results with CV that is less than 5% is accepted as sufficient. Then the effective properties are obtained by averaging the results from the RVEs with the size.

5.3.2 Periodic material

For the periodic heterogeneous material, when the frequency is in the pass-band, the RVE is defined as the unit cell with periodic boundary condition. And the local response is determined as the eigenstate of the unit cell, which can be computed by using the method developed in Section 3. For the frequencies in the stop-band, there is no traveling Bloch wave exists in the periodic structure. Equivalently, there is no real-valued eigenvalue for the equation (3.12). Although it may be possible to find the complex eigenvalue with sophisticated numerical methods, solving the multiple scattering wave field as in the Section 2 is much easier to obtain the boundary values. With large number of same unit cells surrounding, the RVE can have similar ambient wave field as the one with periodic boundary condition. The details and validity of this model will be discussed in the following section.

In spite of the fact that orthotropic materials are better approximations for the heterogeneous materials with cubic lattice, the isotropic constitutive relation is also adequate for this periodic

material due to the circular shape of the inhomogeneity. So the isotropic constitutive relation is employed for simple Green's function in this work. In order to get the effective isotropic material properties, multiple angles of incident wave are considered simultaneously. Accordingly the matrix of residue defined in equation (5.7) is expanded with each column corresponding to a loading case with a specific incident angle.

5.4 Verification of the method

5.4.1 Random materials

For the random heterogeneous materials, the sufficient size of the RVE should be determined first. In this work, the model is established by embedding 1600 circular inhomogeneities randomly with uniform distribution inside the area of $800 \times 800 \text{mm}^2$ in an infinitely extended matrix, with the radius $R_i = 6 \text{mm}$, as shown in Figure 5.2a.

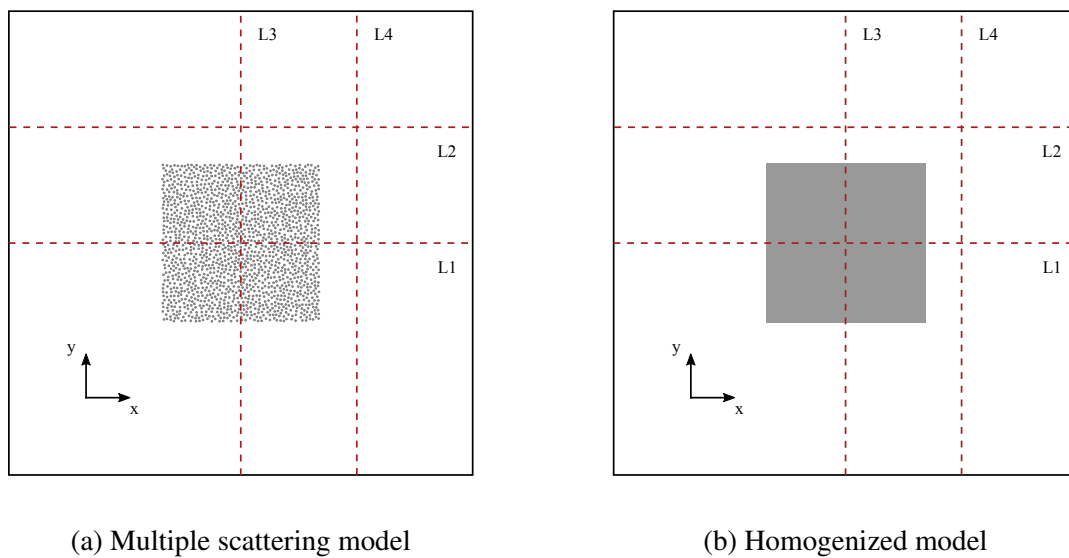


Figure 5.2: Direct numerical simulation models for comparison

The material constants used are $\rho_m = 7670 \text{ kg m}^{-3}$, $\mu_m = 84.3 \text{ GPa}$, $\rho_i = 11400 \text{ kg m}^{-3}$, $\mu_i = 8.43 \text{ GPa}$. The incident wave is a plane SH wave propagating along positive x direction with the frequency which is set to be 17.5879 kHz so that $k_m R_i = 0.2$. In the region, 5×5 equally spaced positions are selected as the centers of the circular RVEs. Then, for each RVE radius R_e , 25 pairs of homogenization results are obtained by the RVEs on 25 different positions. Then the CVs of the results are calculated and plotted in Figure 5.3. Both the CVs of mass density and shear modulus decrease as increasing the radius of RVE. When the RVE radius increases to 10 times of the radius of the inhomogeneity, the CV decreases below 5%, which is deemed as sufficient accurate in this work.

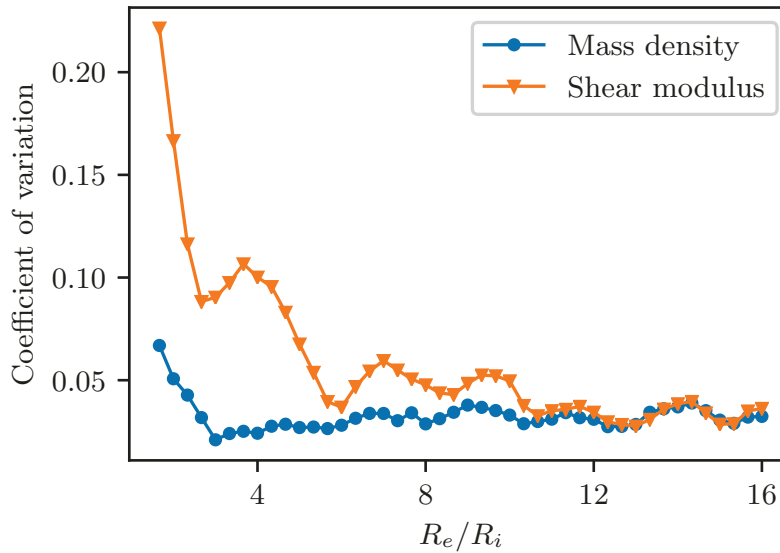


Figure 5.3: Coefficients of variation obtained by RVEs with different radii

The averages of the effective properties among different RVEs with same sizes are plotted in Figure 5.4. It can be observed that the effective properties tend to converge when the RVE radius increases 14 times of the radius of inhomogeneity.

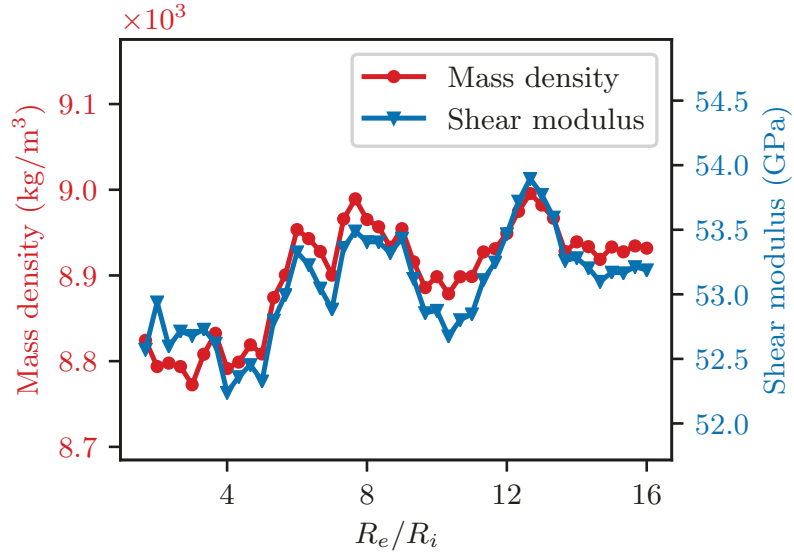


Figure 5.4: Averages of effective properties obtained by RVEs with different radii

The validity of the homogenization results are verified by comparing the direct numerical simulations of the wave fields scattered by multiple inhomogeneities and the homogeneous replacement with the effective properties. As shown in Figure 5.2, in the homogenized model, the array of inhomogeneities is replaced by a rectangular inhomogeneity with the same dimensions and effective material properties, which are obtained as 8899.49 kg/m^3 and 52.9635 GPa . The multiple scattering model is solved by using the method introduced in Section 2, and the homogenized model is solved by using boundary element method.

The displacement distributions of the scattering wave fields at the same phase are shown in Figure 5.5. The overall distributions show good accordance. The difference lies primarily inside the region of inhomogeneities, where the multiple scattering model shows more random perturbations on the general pattern due to the random local structures.

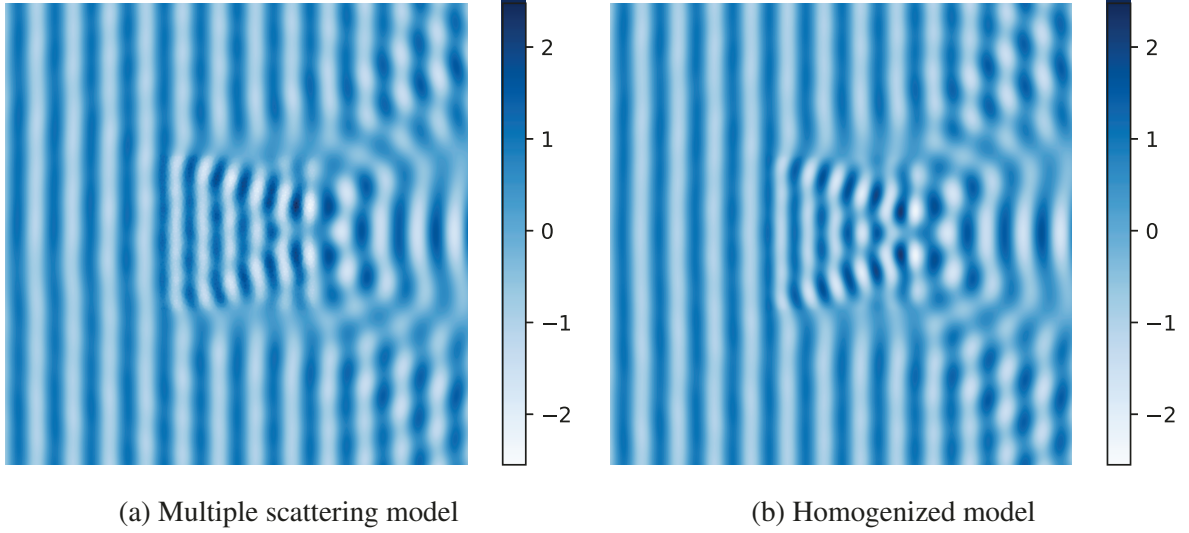


Figure 5.5: Comparison between the displacement fields of the random model and homogenized model

The normalized amplitudes of displacement $|w|/|w_0|$ and stress $|\tau_{xz}|/|\tau_0|$ along the lines marked in the Figure 5.2 are plotted in the Figure 5.6 and Figure 5.7, where the w_0 and $\tau_0 = ik_m \mu_m w_0$ represents the displacement and stress caused by the incident wave. For the wave fields outside the region of inhomogeneities, the general trend in the multiple scattering model can be followed by the homogenized model. And, for the wave fields inside the region, the random fluctuations can be observed due to the randomly distributed inhomogeneities. However, the fluctuations are carried by the pattern which is generally described by the wave fields in the homogenized model.

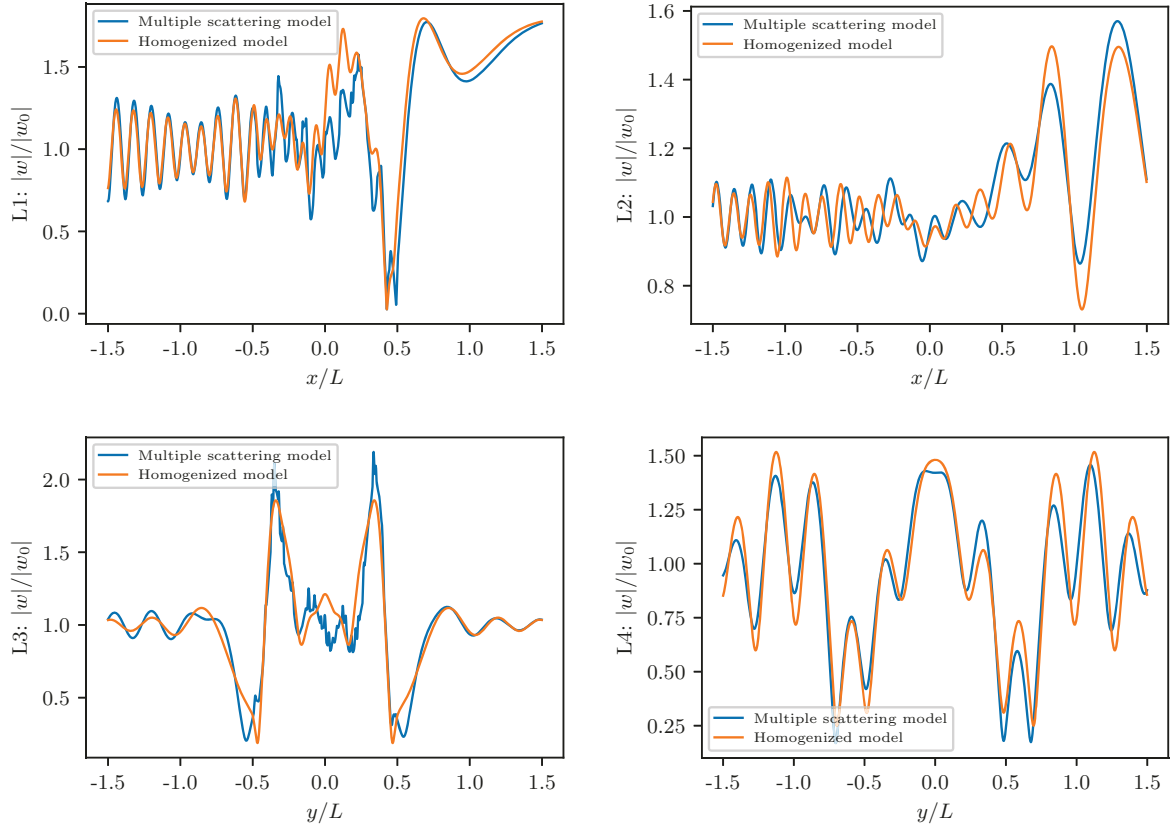


Figure 5.6: Normalized displacement amplitude $|w|$ along the lines in the random model and homogenized model

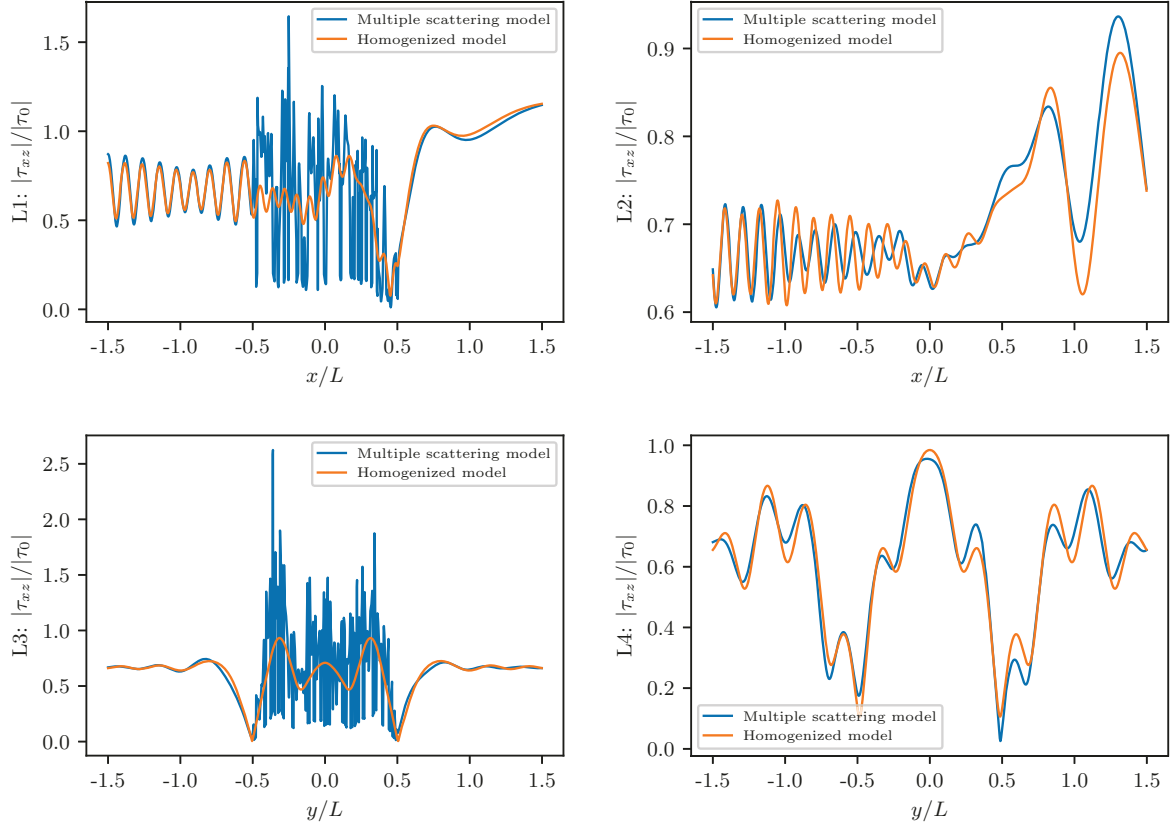
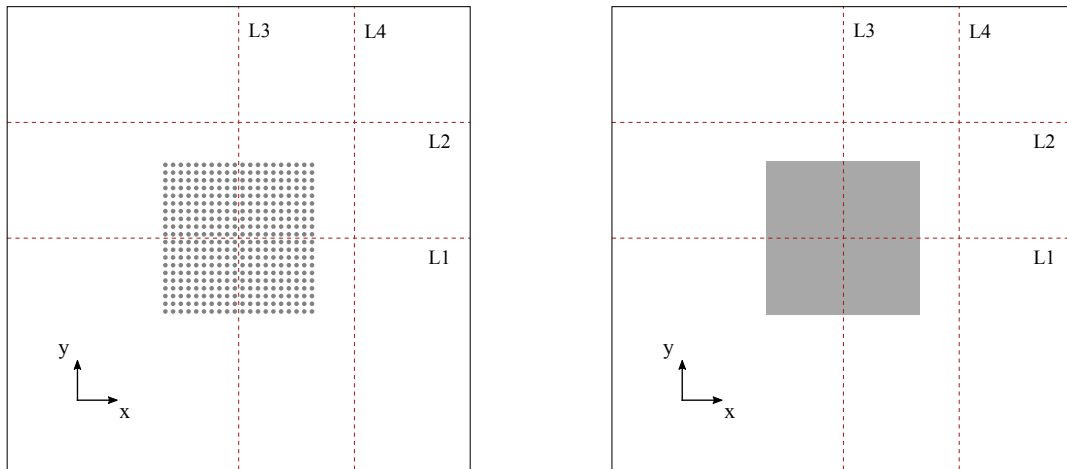


Figure 5.7: Normalized stress amplitude $|\tau_{xz}|$ along the lines in the random model and homogenized model

5.4.2 Periodic materials

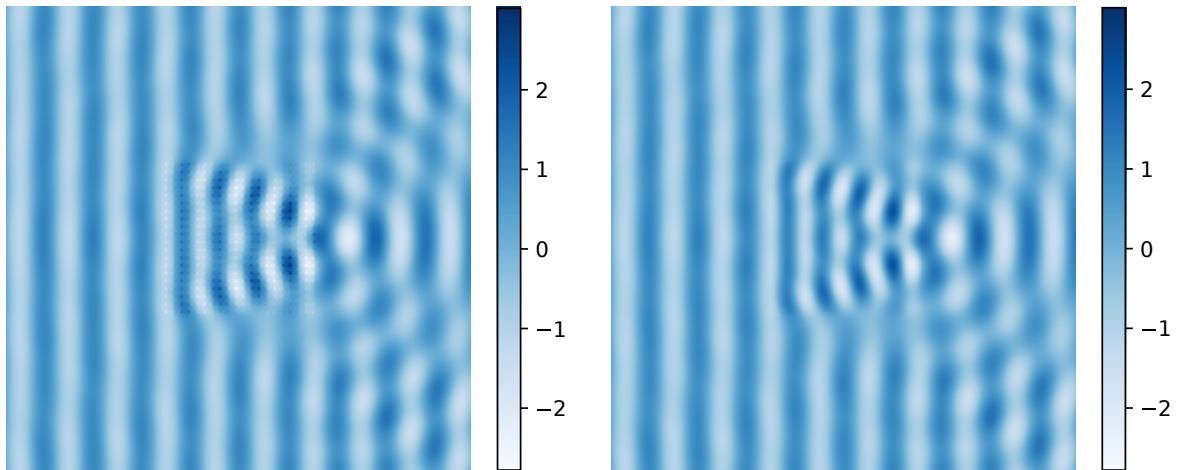
The homogenization methods for periodic materials are also verified by the comparison between the multiple scattering model and the homogenized model. As shown in Figure 5.8, the multiple scattering model is composed of 20×20 identical circular inhomogeneities arranged in a rectangular lattice. The radius of the inhomogeneities is 6mm and the lattice constant $a = 20\text{mm}$. The material constants used are same as in the Section 5.4.1. The incident harmonic SH wave is propagating along the positive x direction. In the homogenized model, the array of inhomogeneities is replaced by a rectangular inhomogeneity with the same dimensions.



(a) Multiple scattering model

(b) Homogenized model

Figure 5.8: Direct numerical simulation models for comparison



(a) Multiple scattering model

(b) Homogenized model

Figure 5.9: Normalized displacement distributions of the two models

For the frequencies in the pass-band, the frequency f is set to be 26.3818 kHz so that $k_m a = 1$. The unit cell with PBC developed in Section 3 is employed and 45 angles ranging from 0 to $\pi/4$ are considered. The effective properties are obtained as: $\rho^* = 9162.13 \text{ kg/m}^3$, $\mu^* = 51.2334 \text{ GPa}$. The computed imaginary parts are less than a hundredth of the real parts, and are

neglected.

Figure 5.9 shows the normalized displacement distribution of the two models at the same phase. Although, at the inhomogeneity locations, the displacement field of the multiple scattering model includes more details comparing to the one of the homogenized model, the overall distributions show good accordance.

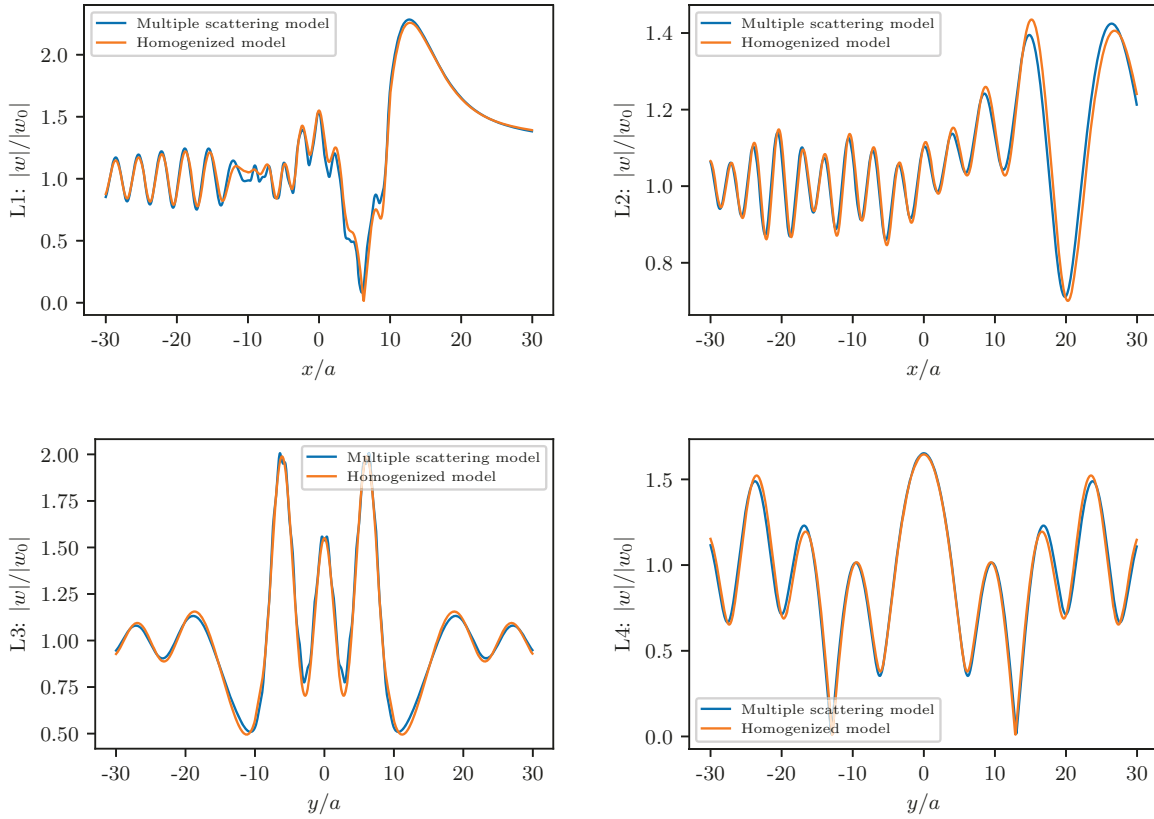


Figure 5.10: Normalized displacement amplitude $|w|$ along the lines in the pass-band

The normalized amplitudes of displacement $|w|/|w_0|$ and stress $|\tau_{xz}|/|\tau_0|$ along the lines marked in the Figure 5.8 are plotted in the Figure 5.10 and Figure 5.11. From the comparison of the results, it can be observed that both the displacement w and stress τ_{xz} match well outside the region of inhomogeneities, which is $-10 < x/a < 10$ and $-10 < y/a < 10$. For the comparisons

inside the region, larger deviations can be observed. The stress amplitude fluctuates intensively in the multiple scattering model, while get smoothed with the correct trend in the homogenized model.

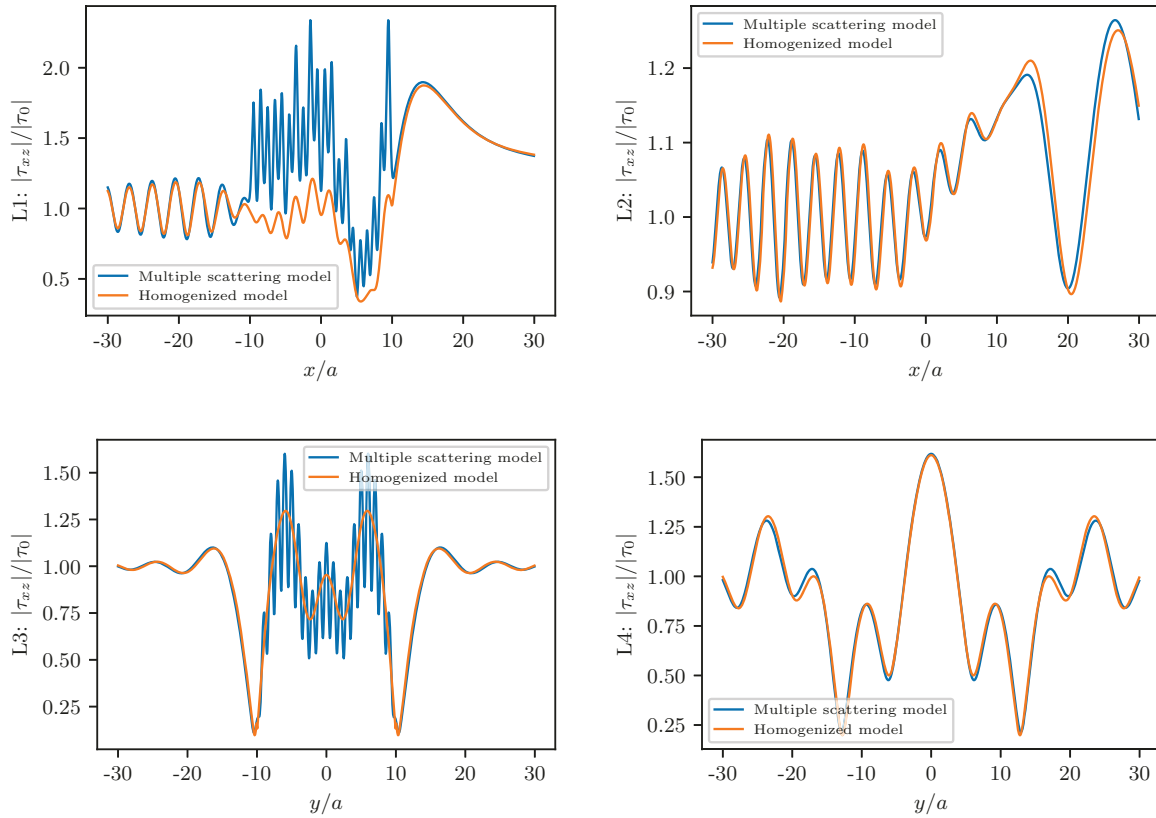


Figure 5.11: Normalized stress amplitude $|\tau_{xz}|$ along the lines in the pass-band

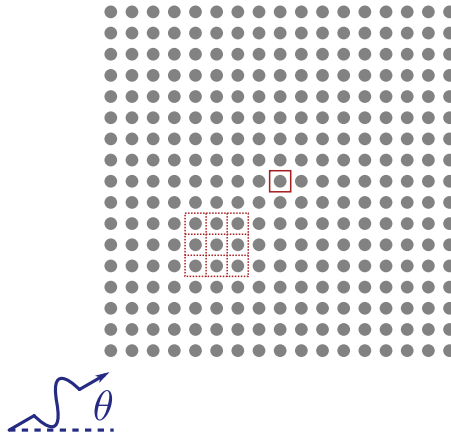


Figure 5.12: Homogenization model for frequencies in the stop-band

As the frequency increases to the first stop-band, because of the difficulty in getting the complex eigenvalue, the RVE model with PBC is substituted by the model with the unit cell surrounded by a number of identical cells for simulating the ambient multiple scattering wave field, as shown by the solid line in Figure 5.12 schematically. In order to validate the approximation, the effective properties obtained by using the center unit cells in the arrays of 7×7 and 17×17 unit cells are compared with the ones obtained by using the RVE with PBC, under a range of frequencies in the pass-band. The results are plotted in Figure 5.13 with triangles. It can be observed that, despite the center unit cell models agree well with the PBC model under the low frequencies, the results diverge when the frequency approaches stop-band.

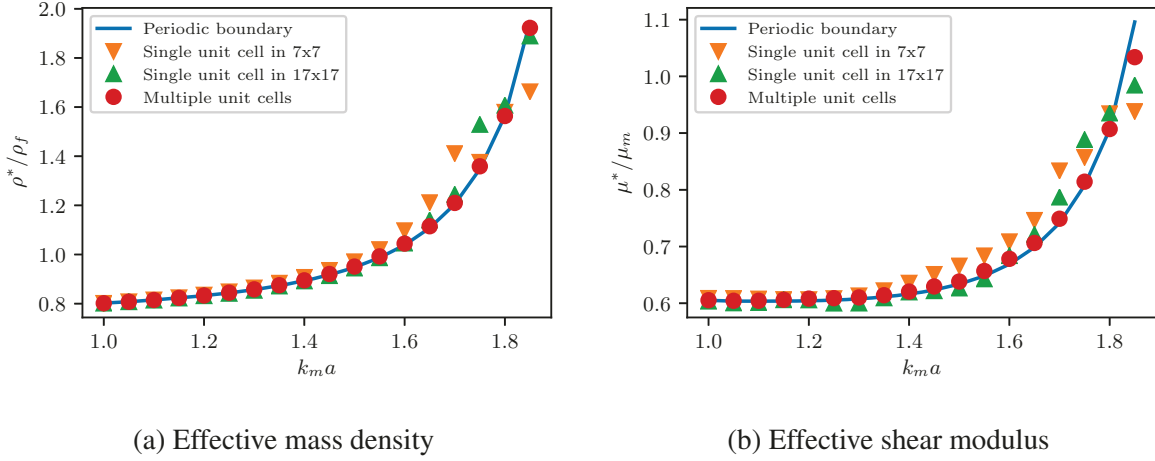


Figure 5.13: Comparison between the effective properties obtained by the RVEs with multiple scattering and PBC

The reason is the effect of the finite size of the array. Since the array can be regarded as an inhomogeneity with finite size, there will be reflections of waves, which put different unit cells into different load environments. Therefore, the effective material properties obtained may alter slightly as selecting different unit cells to be the RVE. In order to cancel this effect, multiple unit cells are used, as shown by the dashed line in Figure 5.12. Then the matrix of residue defined in equation (5.7) is expanded with each column corresponding to a unit cell. The result obtained by using 3×3 adjacent unit cells in an array of 12×12 unit cells is plotted in the Figure 5.13 denoted by circles, which show better accordance. So it can be concluded that the RVE with multiple unit cells embedded in an array is valid as an alternative to the RVE with PBC.

For the validation of the homogenization results obtained by the proposed model, the same comparison by direct numerical simulation as the pass-band case is made. The frequency f is set to be 51.9667 kHz. The obtained effective properties are complex-valued: $\rho^* = (-1002.61 + 8284.78i) \text{kg/m}^3$, $\mu^* = (3.30358 + 34.9685i) \text{kg/m}^3$. The normalized displace-

ment distributions of the two models at the same phase are shown in Figure 5.14.

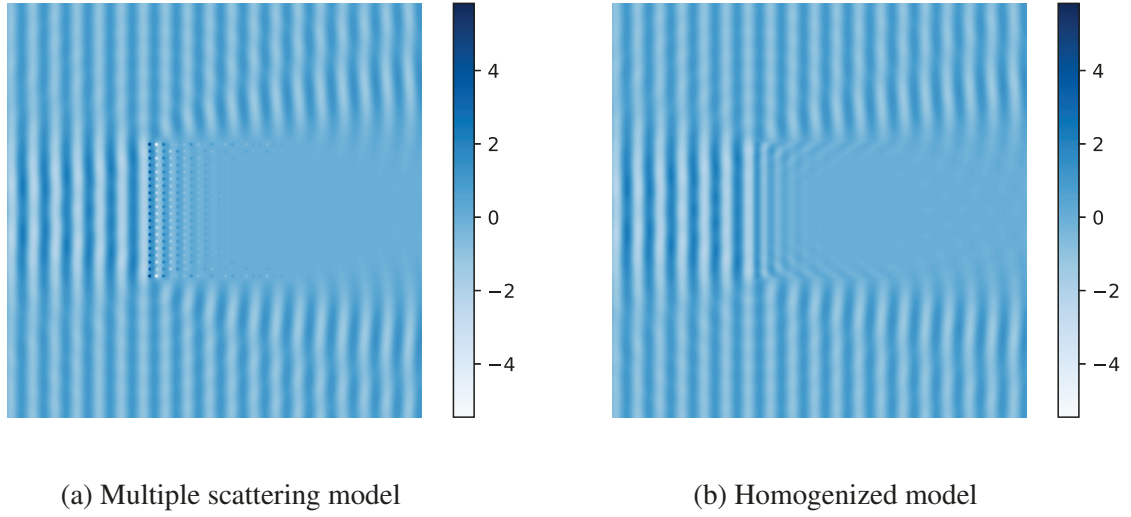


Figure 5.14: Normalized displacement distributions of the two models in stop-band

Similar as the comparison of the pass-band case, the overall distribution show good accordance except for the locations close to the inhomogeneities. The normalized amplitude of displacement $|w|/|w_0|$ and stress $|\tau_{xz}|/|\tau_0|$ along the lines marked in the Figure 5.8 are respectively plotted in the Figure 5.15 and Figure 5.16. From the figures of L1, it can be observed that, inside the region of inhomogeneities, the wave amplitude in homogenized model agrees well with the general trend of the one in multiple scattering model and decays exponentially. There is also a good agreement between the wave fields outside the region of the inhomogeneities of the two models.

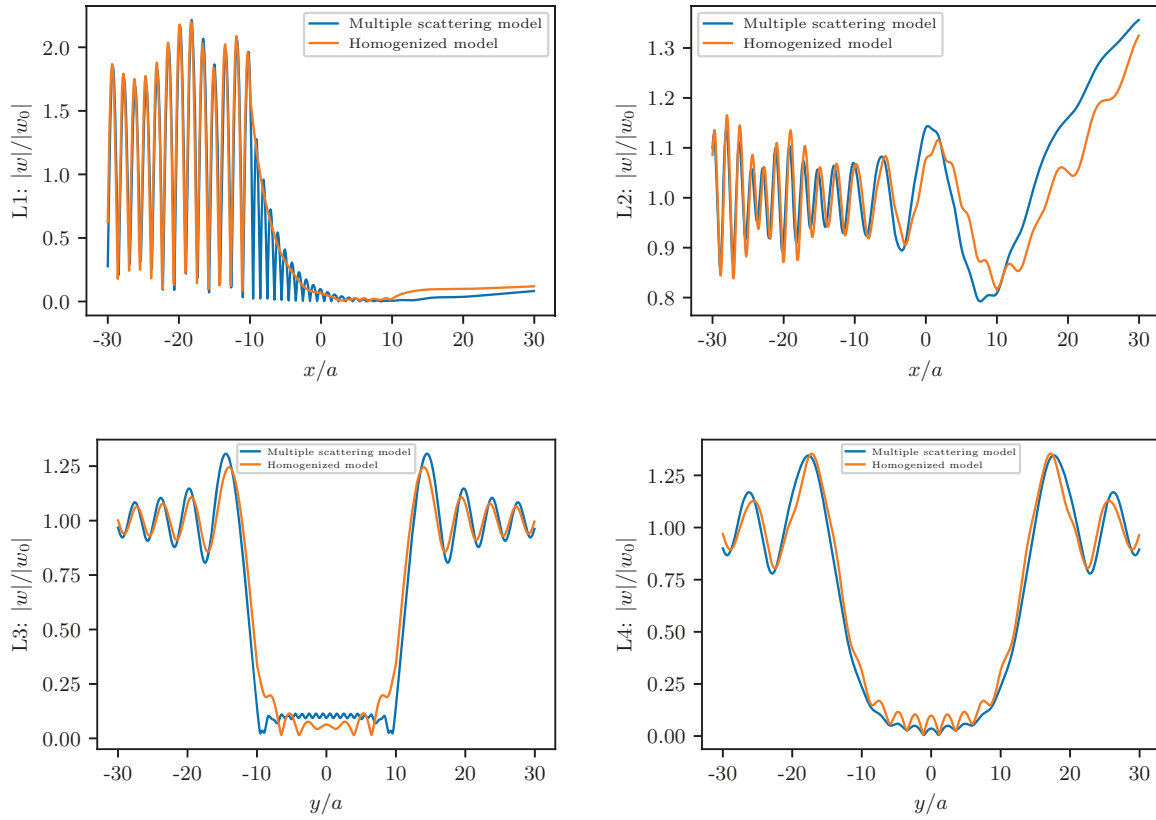


Figure 5.15: Normalized displacement amplitude $|w|$ along the lines in the stop-band

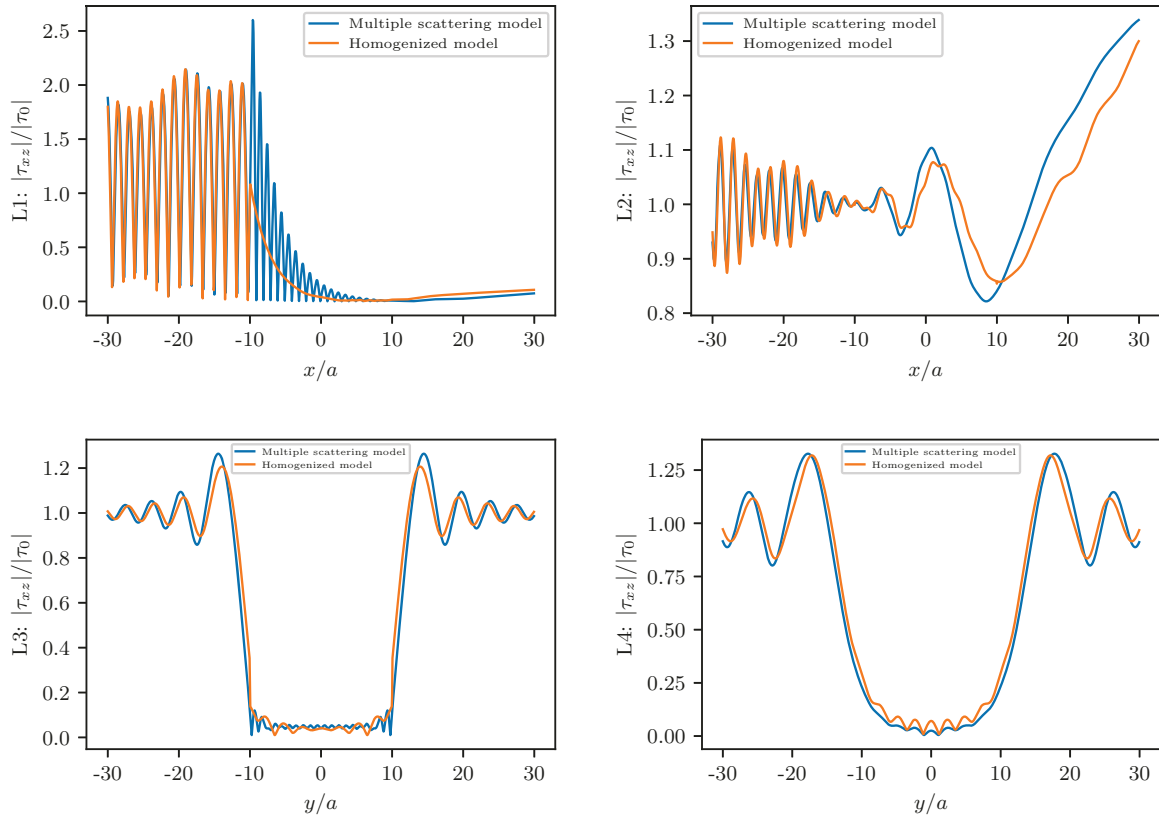


Figure 5.16: Normalized stress amplitude $|\tau_{xz}|$ along the lines in the stop-band

5.5 Effective material properties of periodic material

In this section, the effective material properties of the same periodic material as in the Section 5.4.2 under different frequencies are evaluated. The considered frequency is ranging from the quasi-static limit to the higher boundary of the first stop-band, 0 – 54.2320 kHz. As mentioned above, different RVE models are used according to the frequency. When the frequency is below 48.7832 kHz, which is the limit of the Bloch wave in x direction, the RVE with PBC is used. When the frequency is in the stop-band, 51.5682 – 54.2320 kHz, the RVE with multiple unit cells is used. For the frequencies in between, 48.7832 – 51.5682 kHz, although they are in

the pass-band, real-valued Bloch wave numbers don't exist for some of the angles, so the latter RVE model is used too.

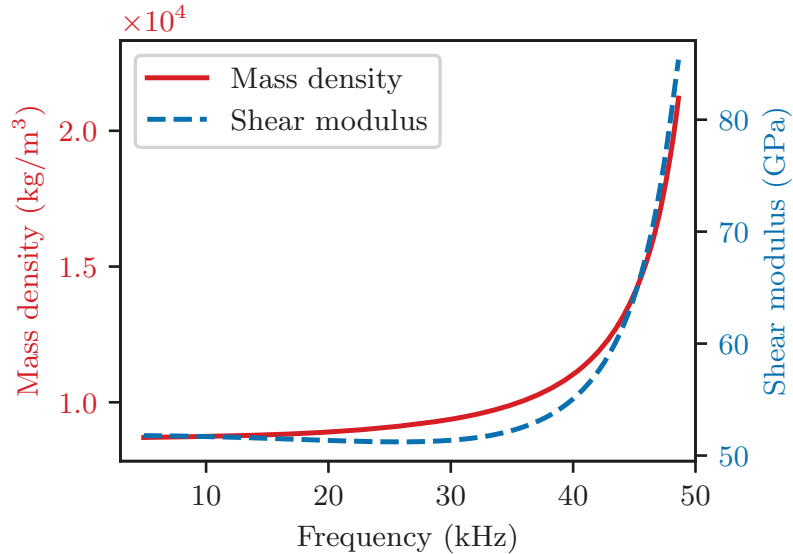


Figure 5.17: Effective material properties in the first pass-band

Figure 5.17 shows the computed effective properties in the first frequency range. The quasi-static limits of the mass density and shear modulus respectively converge to the weighted average of mass density, 8724.63 kg/m^3 , and the effective shear modulus obtained by asymptotic homogenization (Parnell and Abrahams, 2006), 52.6875 GPa , with relative errors of 0.23% and 1.7% at the frequency of 4.9kHz. The effective mass density increases monotonically with increasing the frequency, while the effective shear modulus first shows a slight reduction followed by rising sharply.

The comparison of the results obtained by the current method and by the methods based on energy equivalence, with constant strain and plane wave assumption, introduced in Chapter 4.2 is shown in Figure 5.18 and Figure 5.19. The three methods agree well for the lower frequencies, and tend to converge at the higher limit. For the higher frequencies in between,

larger deviations can be observed, while the result obtained by the current method remains in the middle between the other two.

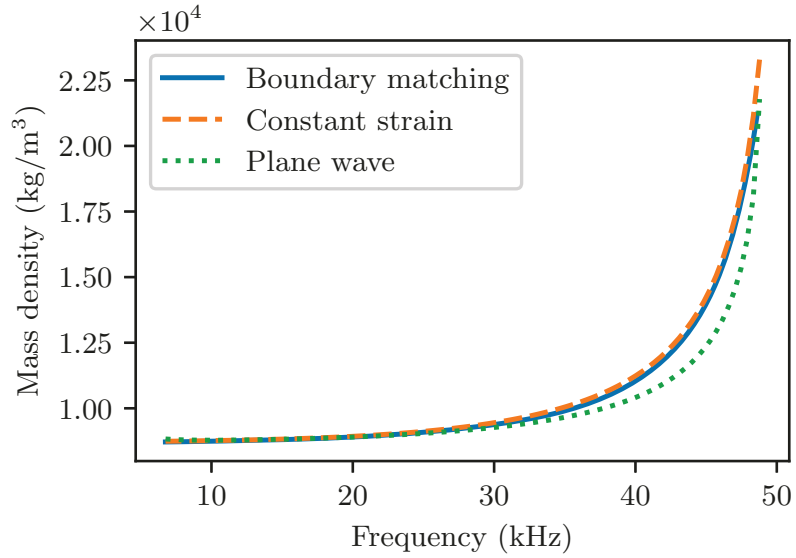


Figure 5.18: Comparison of the effective mass density obtained by different methods

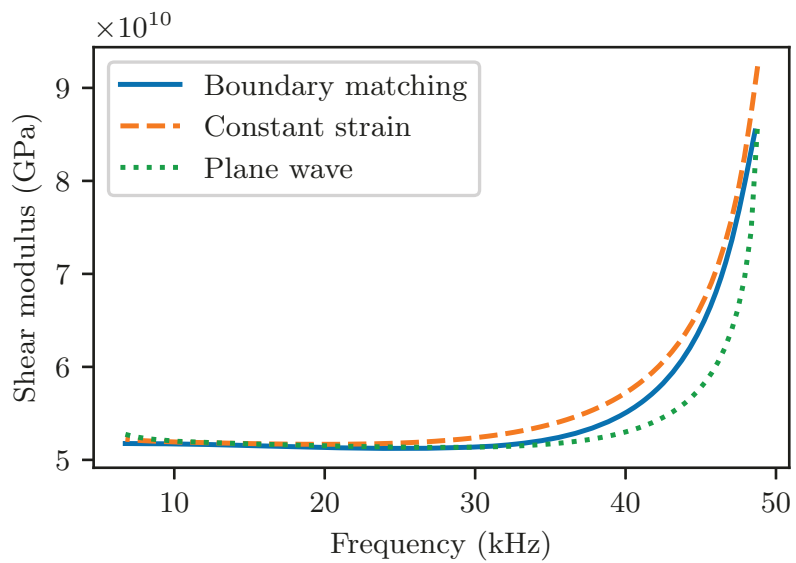


Figure 5.19: Comparison of the effective shear modulus obtained by different methods

By using the RVE with multiple unit cells, the effective properties under the frequencies

in the range of 48.7832 – 54.2320kHz are computed and plotted in Figure 5.20, where the stop-band boundary, 51.5682kHz, is drawn with dash-dot line. It can be observed that the first part of the curves continue the trend in the Figure 5.17. It is worthy to note that the imaginary parts of the effective properties start to increase, which indicates that, for some of the angles, the Bloch waves start to decay due to the complex-valued wave number. When the frequency approaches the lower boundary of the stop-band, the effective properties increase dramatically, which is corresponding to the resonance of the structure. Then, after passing the boundary, the real parts of the effective properties vanish while the imaginary parts drop to nonzero values and vary smoothly with increasing the frequency. For the frequencies around the higher boundary of the stop-band, the optimization process fails to converge to reasonable values. It indicates that the higher limit of the homogenization algorithm is reached.

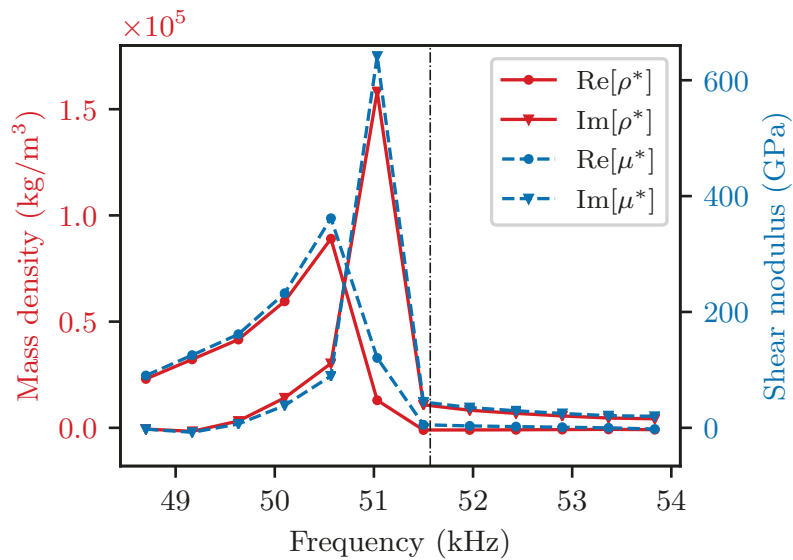


Figure 5.20: Effective material properties in the first stop-band

5.6 Multiscale modeling

In this section, the multiscale modeling method based on the developed computational homogenization method is shown by a general example of multiple scattering in large scale. Then, the recovery of the local response is demonstrated for evaluating the local stress concentration.

5.6.1 Multiple scattering in large scale

As shown in Figure 5.21a, the model considered is composed of three identical regions of inhomogeneities embedded in an infinite medium. The lattice constants, inhomogeneity radius and materials used are the same as the ones in the Section 5.4.2. In the homogenized model, the regions of inhomogeneities are replaced by the rectangular pieces of effective homogeneous material, as shown in Figure 5.21b. The incident wave is a harmonic SH plane wave propagating along the positive x direction with wave number $k_m a = 1$.

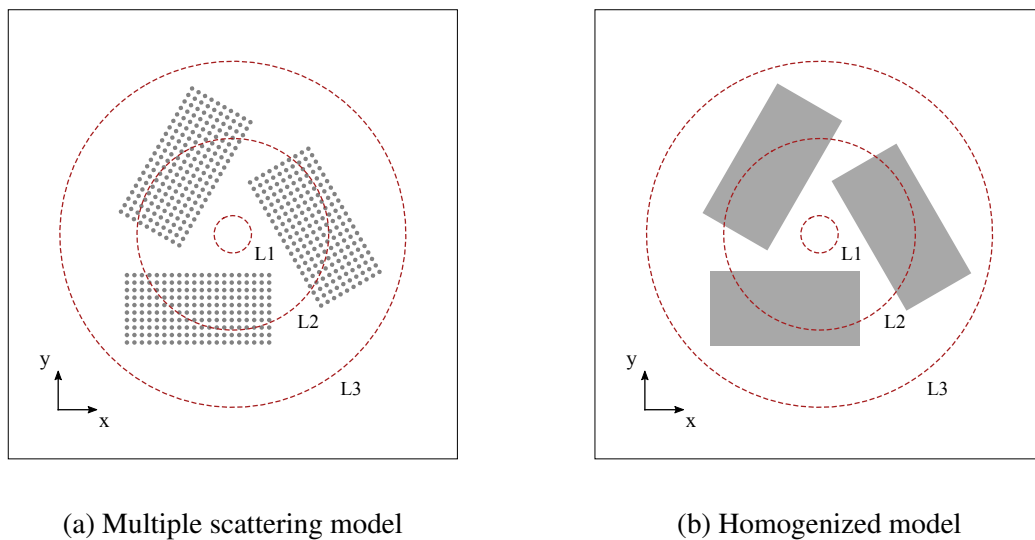
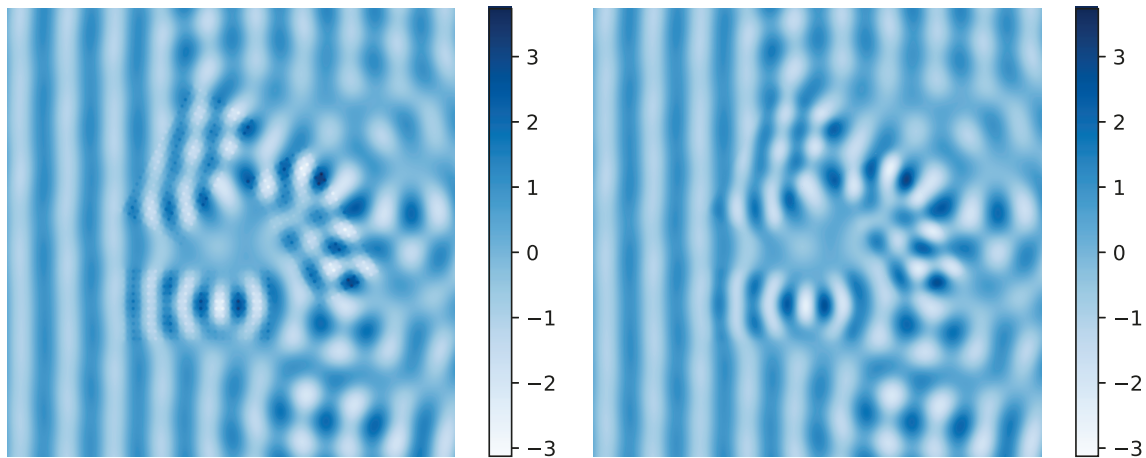


Figure 5.21: Direct numerical simulation models for multiple scattering

The models were solved by using the multiple scattering algorithm and BEM as in previous sections. For solving the homogenized model, the CPU time and memory used are 339s and 0.7443 GB, which are 7.15% and 6.02% of those, 4741 s and 12.36 GB, for solving the multiple scattering model. Figure 5.22 shows the normalized displacement distributions obtained by the two models. Excellent agreement of the general pattern can be observed. The valley of the wave amplitude is formed by the surrounding blocks. In the top region, due to the material difference and angled incident wave, the refracted plane wave can be observed.



(a) Multiple scattering model

(b) Homogenized model

Figure 5.22: Normalized displacement distributions of the two models of multiple scattering

In Figure 5.25 and Figure 5.24, the normalized displacement amplitude $|w|$ and stress amplitude $|\tau_{rz}|$ along the circles marked in Figure 5.21 are plotted in polar coordinates, respectively. It can be observed that, for the positions outside the regions of inhomogeneities, the two models match well, even for the gaps between to regions along L2. For the positions inside, the homogenized mode shows the averaged amplitude of the local perturbations and follows the general trend of the multiple scattering field.

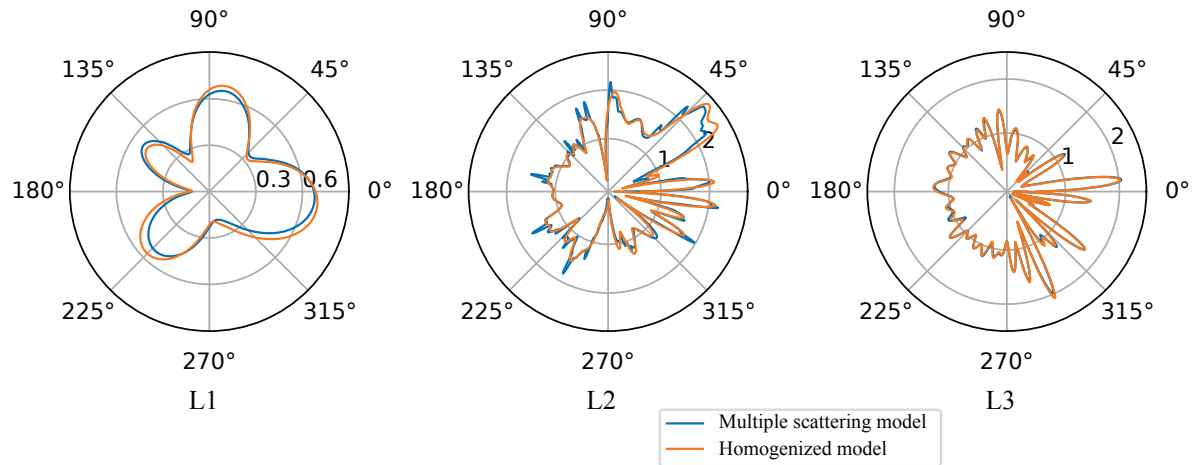


Figure 5.23: Normalized displacement amplitude $|w|$ along the circles

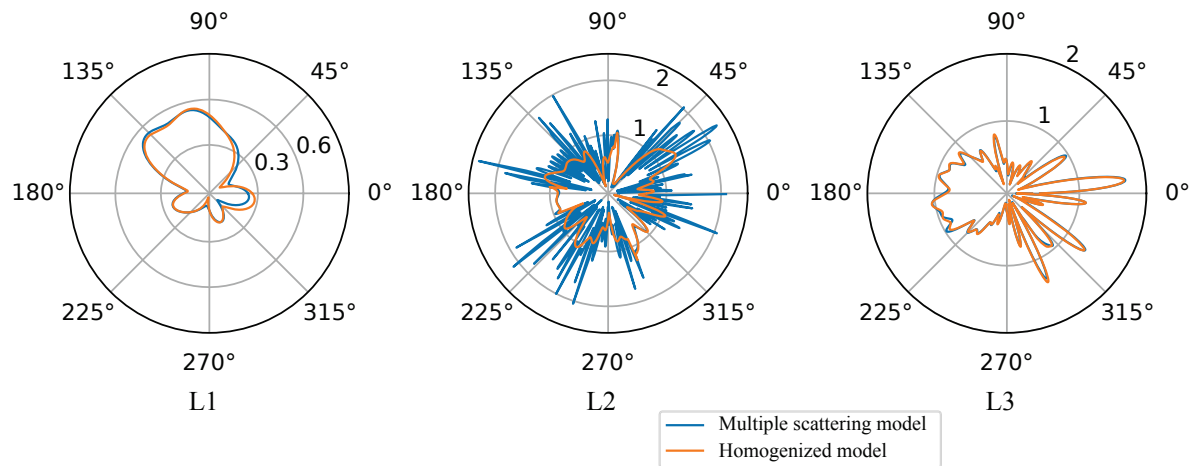


Figure 5.24: Normalized stress amplitude $|\tau_{rz}|$ along the circles

5.6.2 Recovery of the local response

For the damage tolerance design of engineering structures against dynamic failure, it is essential to evaluate the local stress concentration, which is smoothed inherently in the multiscale models. In this section, the method for the recovery of the local response is developed by calculating the local fields based on the known values given by the homogenized model.

By using the eigenfunction expansion in equation 3.3 and the relation of the coefficients in equation (3.5), the relation between the coefficients and the boundary values of resultant wave field along the unit cell boundary can be established. After discretizing the boundary into M segments uniformly and truncating the series at the order of N , the vector of boundary values can be represented by A_n as

$$\{\xi\} = [Z] \{A\} , \quad (5.9)$$

where $\{\xi\}$ is the boundary values of the resultant wave field, which is the superposition of the incident wave and scattered wave, along the unit cell boundary. The element of matrix $[Z]$ is

$$\begin{aligned} [Z]_{(2p-1,n)} &= \left[H_n^{(1)}(k_m r_p) + T_n J_n(k_m r_p) \right] e^{in\varphi_p} \\ [Z]_{(2p,n)} &= \mu_m k_m \left[H_n^{(1)'}(k_m r_p) + T_n J_n'(k_m r_p) \right] e^{in\varphi_p} n_{rp} + \\ &\quad \mu_m(in) \left[H_n^{(1)}(k_m r_p) + T_n J_n(k_m r_p) \right] e^{in\varphi_p} n_{\varphi p} , \end{aligned} \quad (5.10)$$

where $p \in [1, M]$ indicates the p th node, n_r and n_φ are the cosines of the outward normal vector at the node relative to the positive r and φ direction, and the T_n is the relation between A_n and B_n as shown in equation (3.8).

From the solution of the multiple scattering wave field in large scale with BEM, the vector $\{\xi\}$ along the boundary of any unit cell can be obtained. Therefore, the coefficients A_n of that unit cell can be determined as the least squares solution by solving the equation (5.9) with SVD. Then, the local wave fields in that unit cell can be obtained by substituting the coefficients into the series in equation (3.3).

As an example, the unit cell in the 6th row and 11th column of the lower left array in

Figure 5.21 is selected. Its boundary values are extracted from the multiple scattering wave field in large scale as shown in Figure 5.22b. The local response is recovered and compared with the one obtained from direct numerical simulation as shown in Figure 5.22a.

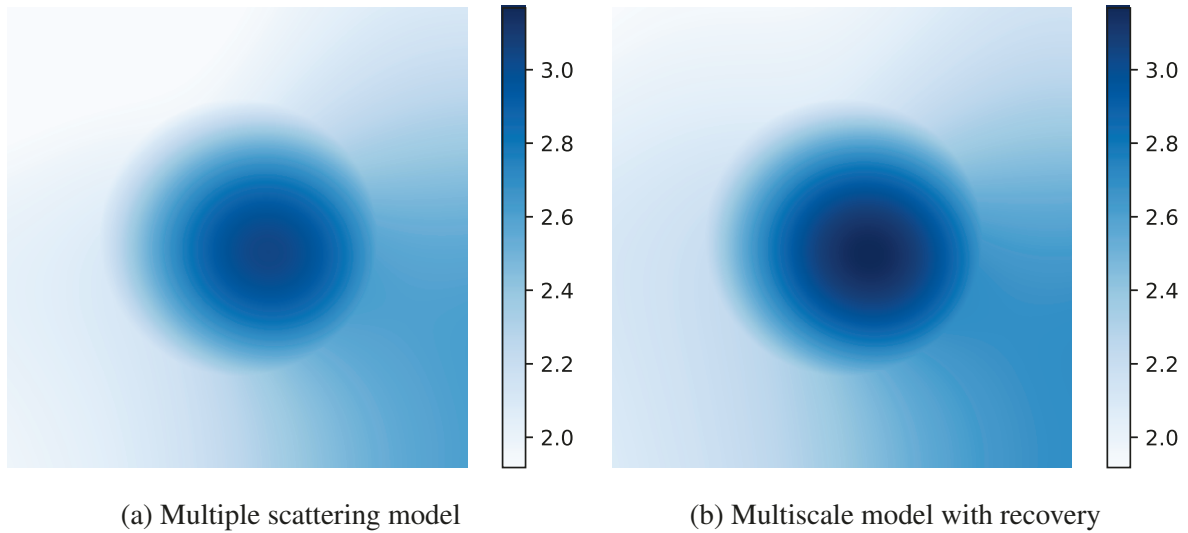


Figure 5.25: Comparison of the recovered local response with the direct numerical simulation.

The comparison of displacement amplitude distributions in the unit cell is shown in Figure 5.25. It can be observed that, comparing with the result of direct numerical simulation, the local response is mostly recovered. Figure 5.26 shows the displacement amplitude along the horizontal center line across the unit cell. The recovered displacement amplitude can follow the trend of the original one with a smaller error comparing with one of the homogenized model.

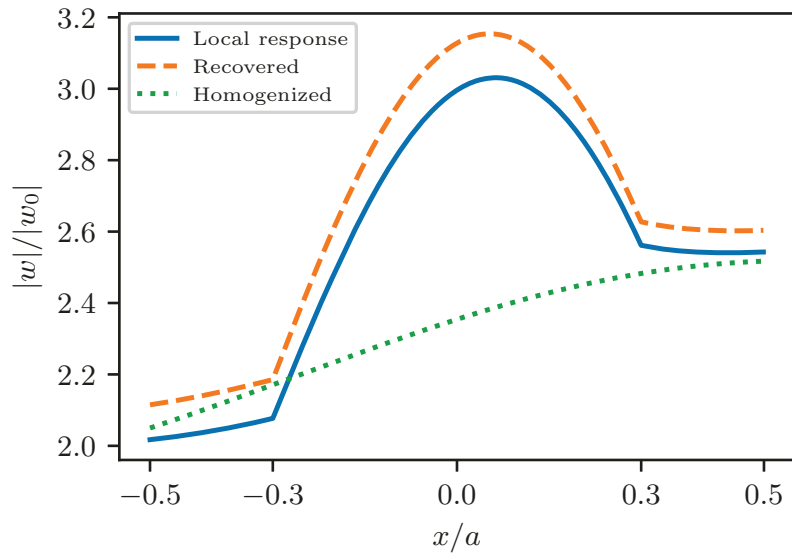


Figure 5.26: Normalized displacement amplitude $|w|$ along the center line.

The stress amplitude $|\tau_{xz}|$ and $|\tau_{yz}|$ are shown in Figure 5.27 and Figure 5.28, respectively. It can be observed that the stress at the interface, where the stress concentration occurs, can be well recovered, while the homogenized model fails to express the detailed distributions.

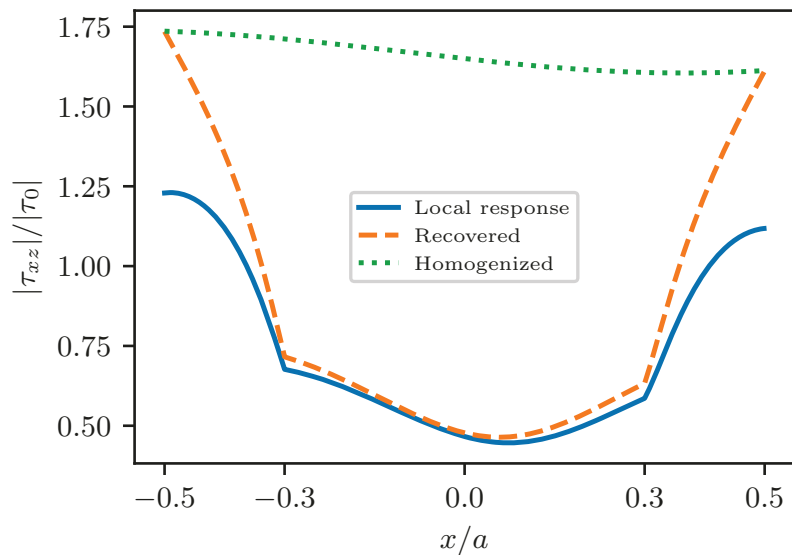


Figure 5.27: Normalized stress amplitude $|\tau_{xz}|$ along the center line.

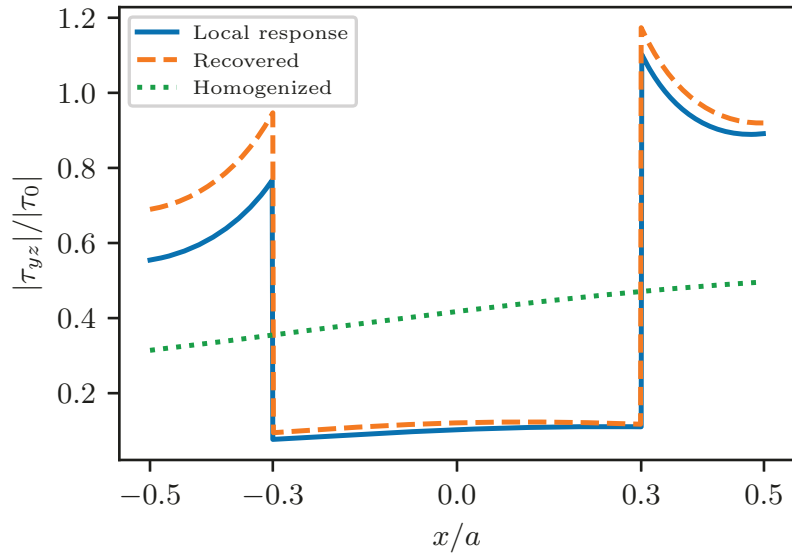


Figure 5.28: Normalized stress amplitude $|\tau_{yz}|$ along the center line.

The amplitudes of displacement and stress along the interface of the circular inhomogeneity are shown in Figure 5.29, Figure 5.30 and Figure 5.31. Although, for the displacement amplitude, the homogenized model follows the trend in general, there are large errors for the stress amplitudes, while the recovered stress show good accordance with the original distributions.

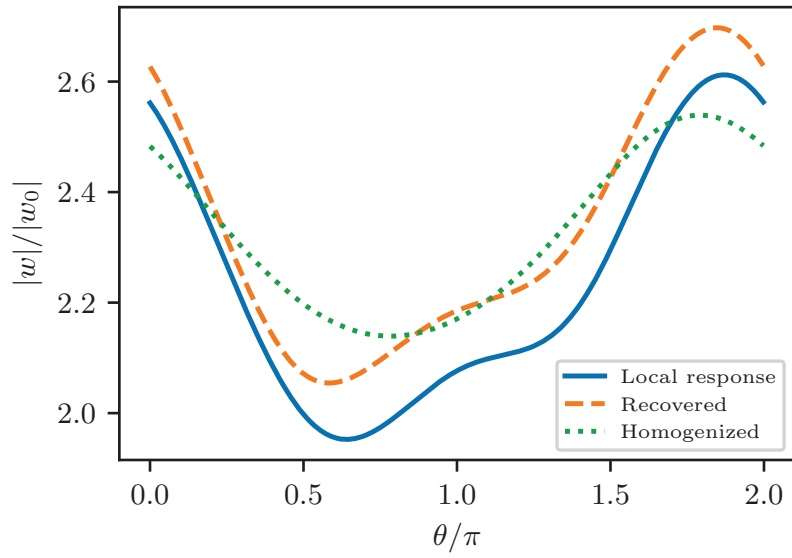


Figure 5.29: Normalized displacement amplitude $|w|$ along the interface.

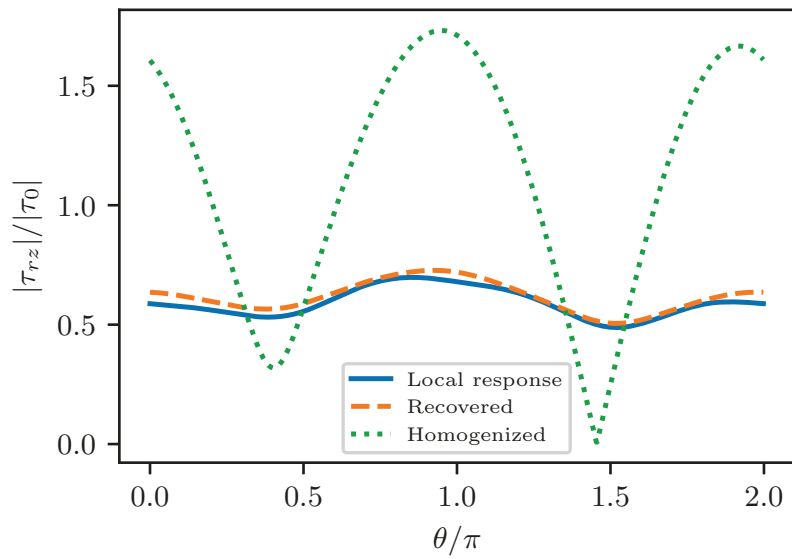


Figure 5.30: Normalized stress amplitude $|\tau_{rz}|$ along the interface.

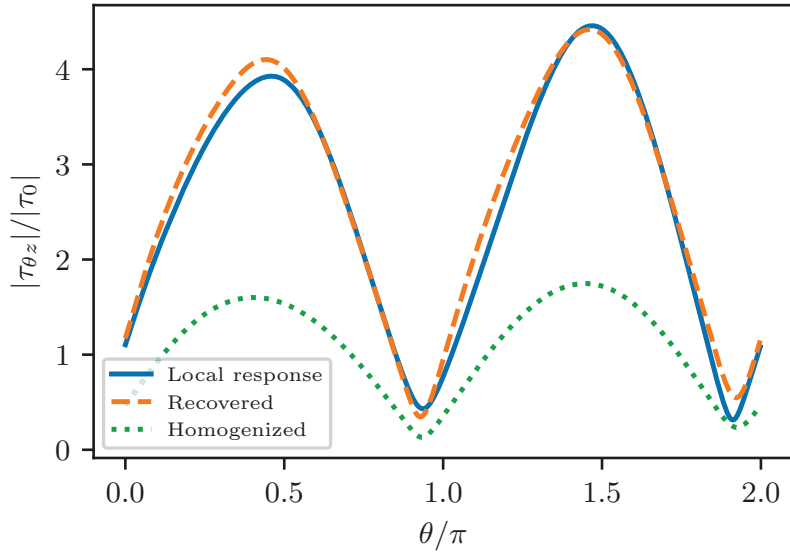


Figure 5.31: Normalized stress amplitude $|\tau_{\theta z}|$ along the interface.

5.7 Conclusion

In this chapter, a computational homogenization method based on the optimization of boundary integral is presented. The boundary values of explicitly solved multiple scattering wave fields or eigenstates of RVEs with PBC are determined as the boundary responses of the RVE. The residue function which indicates the mismatch between the boundary responses of the RVE and the homogenized substitution is first defined as the objective function to be minimized over the complex-valued material properties. For the random materials, the circular RVE with sufficient size is defined inside of the large region of inhomogeneities. The wave field is explicitly solved by using multiple scattering method. For the periodic materials under frequencies in the pass-band, the RVE is defined as the unit cell with PBC, and its eigenstate is obtained by solving the non-linear eigenvalue problem. For the periodic materials under frequencies in the stop-band, the RVE with PBC is substituted by multiple unit cells surrounded by a number of identical

cells for approximating the ambient wave field in infinitely periodic structure. The validity of the homogenization method have been demonstrated by the direct numerical simulations of the original multiple scattering model and the homogenized model. The homogeneous material with the obtained effective material properties is adequate in approximating the heterogeneous material in multiple scattering problem in large scale. The effective properties of the periodic material under different frequencies are computed. The frequencies are ranging from quasi-static limit to the top limit of first stop-band, which shows the applicability of the developed method in a wide range of frequency. The obtained effective properties agree well with the ones obtained in Section 4.2. At last, the multiscale modeling method is summarized. The multiple scattering in large scale can be simulated efficiently with reasonable accuracy, and the local response can be accurately recovered on demand.

Chapter 6: Contributions and future work

6.1 Main contributions

This thesis developed the computational methods for the multiscale modeling of elastic wave propagation in heterogeneous materials. Throughout this project, four major techniques essential to the elastodynamic multiscale modeling have been developed, (i) an efficient method for solving the elastic waves scattered by large number of inhomogeneities; (ii) an efficient method for the determination of eigenstates of periodic unit cells under designated frequency and propagation direction; (iii) two computational homogenization methods based on the domain averaging of the computed wave fields; (iv) a computational homogenization method based on the boundary matching with the use of the boundary values of computed wave fields.

The main contributions of this thesis are summarized as follows.

6.1.1 Efficient method for solving the multiple scattering problem

By using the eigenfunction expansion and discretizing the superposition of scattered wave fields, the scattering mechanism has been simplified to a linear transformation and then the expansion coefficients can be obtained by solving the linear equations. The validity and robustness of the procedure have been demonstrated by verifications and tests under limiting conditions. This method is proved to be capable of simulating the multiple scattering of P/SV/SH waves by a large number of circular inhomogeneities with various properties.

6.1.2 Efficient method for eigenstate determination

An efficient analytical-numerical method has been developed for computing the local response of periodic materials under designated frequency and angle of wave propagation. By the use of eigenfunction expansion, the nonlinear eigenvalue problem is established with the expansion coefficients being the eigenvector, which facilitates the numerical solution of the nonlinearity caused by the arbitrarily specified propagation angle. The accuracy of the method is validated by comparing the obtained dispersion relation and eigenstate with the ones computed by using finite element method.

6.1.3 Homogenization methods based on domain averaging

Based on the domain averaging of the explicitly solved wave fields, two computational homogenization methods for periodic materials have been developed. In the first method, the volume average scheme with considering the effective wave form is employed, in which the effective wave number is determined by the self-consistent method. The convergence of the effective wave number provides a guideline for the assumption of the effect wave form. The second homogenization method is based on the assumption of the effective wave number and kinetic energy equivalence. The homogenization results for both quasi-static and dynamic cases are verified by comparing with the existing results and the direct numerical simulations.

6.1.4 Homogenization method based on boundary matching

A new computational homogenization method has been developed based on matching the boundary response of the RVE. The residue function which indicates the mismatch between the boundary responses of the RVE and the homogenized substitution is defined as the objective function which is to be minimized over the complex-valued material properties. Depending on the different frequencies and materials, different RVEs are modeled for determining the boundary response. The method is applicable to both random materials and periodic materials, and applicable to a wide range of frequency, which includes the first stop-band of the periodic material. The method is verified by the comparison between the direct numerical simulations.

At last, the multiscale modeling method is demonstrated. The multiple scattering in large scale can be simulated efficiently with reasonable accuracy, and the local response can be accurately recovered on demand.

6.2 Future works

Based on the developments achieved in this thesis, attentions will be paid on the following topics in the future.

6.2.1 Extension to in-plane wave problem

Although the in-plane multiple scattering problem is solved in Section 2.5, this thesis is mainly focused on the antiplane shear wave. The developed methods can be expanded to in-plane wave problems, which is more common in practical applications.

For the eigenstate determination method, since the periodic boundary condition still holds, the eigenvalue problem can be derived with the series coefficients being the eigenvector and the Bloch wave number being the eigenvalue. The difference will be at the relation between the coefficients and the boundary values. The dimension of the problem will be doubled because the P wave and SV wave are coupled, two sets of coefficients need to be determined simultaneously by the boundary condition.

For the homogenization methods, if the effective material is assumed to be isotropic, one more modulus will be needed. Therefore, one more assumption will be needed for the energy equivalence method, and two more independent variables need to be adjusted for the boundary matching method.

6.2.2 Different shapes of inhomogeneity

The inhomogeneities considered in this thesis is limited to circular in shape. In practical applications, different inhomogeneities with different shapes may exist. When different shapes are considered, the eigenfunctions will need to be replaced for its single scattering problem, which can be determined analytically or numerically. However, the developed computational framework for solving the multiple scattering problem can still be used with different transfer matrices which represent the mechanical behaviors.

Since the developed homogenization methods are all based on the explicitly solved wave fields, the algorithms are independent to the details of the solution determination procedures. So the homogenization methods can be directly applied to evaluate the effective properties.

6.2.3 Viscoelastic materials

To further extend the applicability of the developed methods of this work, the materials of the matrix and inhomogeneities can be considered to be with viscosity. For harmonic incident waves, the wave number in viscoelastic materials will be complex-valued, which implies that the amplitude of wave decreases and the energy is dissipated as the wave propagating. The method for solving the local wave field can be applied by extending the wave number to complex domain. Since the effect of scattered waves decays, the multiple scattering method can be further accelerated by neglecting the interaction between two inhomogeneities with long distance. After solving the local wave field, the homogenization methods can be applied directly.

6.2.4 Experimental verifications

Experiments can be conducted for verifying the developed methods. The experimental model can be set up for measuring the reflection and transmission of the heterogeneous material. Then the homogenization methods can be validated by comparing the reflection and transmission predicted by the homogenized model with the experimental results.

Bibliography

- Achenbach, J. D. *Wave propagation in elastic solids*. North-Holland Publishing Company, 1973.
- Allaire, G. Homogenization and two-scale convergence. *SIAM Journal on Mathematical Analysis*, 23(6):1482–1518, 1992.
- Antonakakis, T., Craster, R. V., and Guenneau, S. Homogenisation for elastic photonic crystals and dynamic anisotropy. *Journal of the Mechanics and Physics of Solids*, 71:84–96, 2014.
- Arabnejad, S. and Pasini, D. Mechanical properties of lattice materials via asymptotic homogenization and comparison with alternative homogenization methods. *International Journal of Mechanical Sciences*, 77:249–262, 2013.
- Axmann, W. and Kuchment, P. An efficient finite element method for computing spectra of photonic and acoustic band-gap materials: I. scalar case. *Journal of Computational Physics*, 150(2):468–481, 1999.
- Backus, G. E. Long-wave elastic anisotropy produced by horizontal layering. *Journal of Geophysical Research*, 67(11):4427–4440, 1962.
- Benites, R., Aki, K., and Yomogida, K. Multiple-scattering of SH-waves in 2-D media with many cavities. *Pure and Applied Geophysics*, 138(3):353–390, 1992.
- Benites, R. A., Roberts, P. M., Yomogida, K., and Fehler, M. Scattering of elastic waves in 2-D

- composite media .1. theory and test. *Physics of the Earth and Planetary Interiors*, 104(1-3): 161–173, 1997.
- Biwa, S., Yamamoto, S., Kobayashi, F., and Ohno, N. Computational multiple scattering analysis for shear wave propagation in unidirectional composites. *International Journal of Solids and Structures*, 41(2):435–457, 2004.
- Bose, S. K. and Mal, A. K. Elastic-waves in a fiber-reinforced composite. *Journal of the Mechanics and Physics of Solids*, 22(3):217–229, 1974.
- Cai, L. W. and Williams, J. H. Large-scale multiple scattering problems. *Ultrasonics*, 37(7): 453–462, 1999a.
- Cai, L. W. and Williams, J. H. Full-scale simulations of elastic wave scattering in fiber-reinforced composites. *Ultrasonics*, 37(7):463–482, 1999b.
- Carcione, J. M., Picotti, S., Cavallini, F., and Santos, J. E. Numerical test of the Schoenberg-Muir theory. *Geophysics*, 77(2):C27–C35, 2012.
- Casadei, F. and Ruzzene, M. Frequency-domain bridging method for the analysis of wave propagation in damaged structures. *Wave Motion*, 49(6):605–616, 2012.
- Casadei, F., Rimoli, J. J., and Ruzzene, M. A geometric multiscale finite element method for the dynamic analysis of heterogeneous solids. *Computer Methods in Applied Mechanics and Engineering*, 263:56–70, 2013.
- Casadei, F., Rimoli, J. J., and Ruzzene, M. Multiscale finite element analysis of elastic wave scattering from localized defects. *Finite Elements in Analysis and Design*, 88:1–15, 2014.

- Casadei, F., Rimoli, J. J., and Ruzzene, M. Multiscale finite element analysis of wave propagation in periodic solids. *Finite Elements in Analysis and Design*, 108:81–95, 2016.
- Colton, D. and Kress, R. *Integral Equation Methods in Scattering Theory*. Society for Industrial and Applied Mathematics, Philadelphia, PA, 2013.
- Dravinski, M. and Yu, M. C. Scattering of plane harmonic SH waves by multiple inclusions. *Geophysical Journal International*, 186(3):1331–1346, 2011.
- Eshelby, J. D. The determination of the elastic field of an ellipsoidal inclusion, and related problems. *Proceedings of the Royal Society of London. Series A. Mathematical and Physical Sciences*, 241(1226):376–396, 1957.
- Fokin, V., Ambati, M., Sun, C., and Zhang, X. Method for retrieving effective properties of locally resonant acoustic metamaterials. *Physical Review B*, 76(14):144302, 2007.
- Foldy, L. L. The multiple scattering of waves .1. general theory of isotropic scattering by randomly distributed scatterers. *Physical Review*, 67(3-4):107–119, 1945.
- Gao, K., Chung, E. T., Gibson, R. L., Fu, S. B., and Efendiev, Y. A numerical homogenization method for heterogeneous, anisotropic elastic media based on multiscale theory. *Geophysics*, 80(4):D385–D401, 2015a.
- Gao, K., Fu, S. B., Gibson, R. L., Chung, E. T., and Efendiev, Y. Generalized multiscale finite-element method (GMsFEM) for elastic wave propagation in heterogeneous, anisotropic media. *Journal of Computational Physics*, 295:161–188, 2015b.

- Grechka, V. Effective media: A forward modeling view. *GEOPHYSICS*, 68(6):2055–2062, 2003.
- Hashin, Z. Theory of fiber reinforced materials. *NASA CR-1974*, 1972.
- Helbig, K. and Schoenberg, M. Anomalous polarization of elastic waves in transversely isotropic media. *The Journal of the Acoustical Society of America*, 81(5):1235–1245, 1987.
- Hou, T. Y. and Wu, X.-H. A multiscale finite element method for elliptic problems in composite materials and porous media. *Journal of Computational Physics*, 134(1):169–189, 1997.
- Hu, X., Ho, K.-M., Chan, C. T., and Zi, J. Homogenization of acoustic metamaterials of helmholtz resonators in fluid. *Physical Review B*, 77(17):172301, 2008.
- Huang, Z.-G. and Chen, Z.-Y. Acoustic waves in two-dimensional phononic crystals with reticular geometric structures. *Journal of Vibration and Acoustics*, 133(3):031011–031011–6, 2011.
- Hui, T. and Oskay, C. A high order homogenization model for transient dynamics of heterogeneous media including micro-inertia effects. *Computer Methods in Applied Mechanics and Engineering*, 273:181–203, 2014.
- Kadic, M., Milton, G. W., van Hecke, M., and Wegener, M. 3d metamaterials. *Nature Reviews Physics*, 1(3):198–210, 2019.
- Kim, J. Y. Dynamic self-consistent analysis for elastic wave propagation in fiber reinforced composites. *Journal of the Acoustical Society of America*, 100(4):2002–2010, 1996.

- Kim, J. Y. Antiplane shear wave propagation in fiber-reinforced composites. *Journal of the Acoustical Society of America*, 113(5):2442–2445, 2003.
- Kittel, C. *Introduction to Solid State Physics*. Wiley, 2004.
- Kupradze, V. D. *Three-Dimensional Problems of the Mathematical Theory of Elasticity and Thermoelasticity*. North-Holland, 1976.
- Kushwaha, M. S., Halevi, P., Dobrzynski, L., and Djafari-Rouhani, B. Acoustic band structure of periodic elastic composites. *Physical Review Letters*, 71(13):2022–2025, 1993.
- Lax, M. Multiple scattering of waves. *Reviews of Modern Physics*, 23(4):287–310, 1951.
- Lax, M. Multiple scattering of waves .2. the effective field in dense systems. *Physical Review*, 85(4):621–629, 1952.
- Li, F., Wang, Y., and Zhang, C. Boundary element method for bandgap computation of photonic crystals. *Optics Communications*, 285(5):527–532, 2012.
- Liu, Z., Chan, C. T., and Sheng, P. Three-component elastic wave band-gap material. *Physical Review B*, 65(16):165116, 2002.
- Manolis, G. D. and Dineva, P. S. Elastic waves in continuous and discontinuous geological media by boundary integral equation methods: A review. *Soil Dynamics and Earthquake Engineering*, 70:11–29, 2015.
- Mehrmann, V. and Voss, H. Nonlinear eigenvalue problems: a challenge for modern eigenvalue methods. *GAMM-Mitteilungen*, 27(2):121–152, 2004.

- Mei, J., Liu, Z., Shi, J., and Tian, D. Theory for elastic wave scattering by a two-dimensional periodical array of cylinders: An ideal approach for band-structure calculations. *Physical Review B*, 67(24):245107, 2003.
- Mura, T. *Micromechanics of defects in solids*. Martinus Nijhoff, 1987.
- Nemat-Nasser, S., Willis, J. R., Srivastava, A., and Amirkhizi, A. V. Homogenization of periodic elastic composites and locally resonant sonic materials. *Physical Review B*, 83(10):8, 2011.
- Norris, A. N. and Conoir, J. M. Multiple scattering by cylinders immersed in fluid: High order approximations for the effective wavenumbers. *Journal of the Acoustical Society of America*, 129(1):104–113, 2011.
- Oudich, M., Assouar, M. B., and Hou, Z. Propagation of acoustic waves and waveguiding in a two-dimensional locally resonant phononic crystal plate. *Applied Physics Letters*, 97(19):193503, 2010.
- Parnell, W. J. and Abrahams, I. D. Dynamic homogenization in periodic fibre reinforced media. quasi-static limit for SH waves. *Wave Motion*, 43(6):474–498, 2006.
- Parvanova, S. L., Dineva, P. S., and Manolis, G. D. Dynamic behavior of a finite-sized elastic solid with multiple cavities and inclusions using BIEM. *Acta Mechanica*, 224(3):597–618, 2013.
- Parvanova, S. L., Dineva, P. S., Manolis, G. D., and Kochev, P. N. Dynamic response of a solid with multiple inclusions under anti-plane strain conditions by the BEM. *Computers & Structures*, 139:65–83, 2014.

- Parvanova, S. L., Manolis, G. D., and Dineva, P. S. Wave scattering by nanoheterogeneities embedded in an elastic matrix via bem. *Engineering Analysis with Boundary Elements*, 56: 57–69, 2015.
- Qu, J. and Cherkaoui, M. *Fundamentals of micromechanics of solids*. John Wiley & Sons, Inc., 2006. ISBN 9789350245262.
- Rayleigh, J. W. S. B. *On the Light from the Sky: Its Polarization and Colour*. Philosophical Magazine, 1870.
- Rijpsma, G. and Zijl, W. Upscaling of Hooke's law for imperfectly layered rocks. *Mathematical Geology*, 30(8):943–969, 1998.
- Sabina, F. J. and Willis, J. R. A simple self-consistent analysis of wave-propagation in particulate composites. *Wave Motion*, 10(2):127–142, 1988.
- Sabina, F. J., Bravo-Castillero, J., Guinovart-Diaz, R., Rodriguez-Ramos, R., and Valdiviezo-Mijangos, O. C. Overall behavior of two-dimensional periodic composites. *International Journal of Solids and Structures*, 39(2):483–497, 2002.
- Schoenberg, M. and Muir, F. A calculus for finely layered anisotropic media. *GEOPHYSICS*, 54(5):581–589, 1989.
- Sheikhassani, R. and Dravinski, M. Scattering of a plane harmonic SH wave by multiple layered inclusions. *Wave Motion*, 51(3):517–532, 2014.
- Sigalas, M. M. and Economou, E. N. Elastic and acoustic wave band structure. *Journal of Sound and Vibration*, 158(2):377–382, 1992.

- Sigalas, M. M. and Garcia, N. Theoretical study of three dimensional elastic band gaps with the finite-difference time-domain method. *Journal of Applied Physics*, 87(6):3122–3125, 2000.
- Srivastava, A. and Nemat-Nasser, S. Mixed-variational formulation for phononic band-structure calculation of arbitrary unit cells. *Mechanics of Materials*, 74:67–75, 2014.
- Sumiya, T., Biwa, S., and Haiat, G. Computational multiple scattering analysis of elastic waves in unidirectional composites. *Wave Motion*, 50(2):253–270, 2013.
- Tsvankin, I., Gaiser, J., Grechka, V., Baan, M. v. d., and Thomsen, L. Seismic anisotropy in exploration and reservoir characterization: An overview. *GEOPHYSICS*, 75(5):75A15–75A29, 2010.
- Varadan, V. K., Varadan, V. V., and Pao, Y. H. Multiple-scattering of elastic-waves by cylinders of arbitrary cross-section .1. SH-waves. *Journal of the Acoustical Society of America*, 63(5):1310–1319, 1978.
- Veres, I. A., Berer, T., and Matsuda, O. Complex band structures of two dimensional phononic crystals: Analysis by the finite element method. *Journal of Applied Physics*, 114(8):083519, 2013.
- Wang, C. and Wang, X. Modeling and simulation of wave scattering of multiple inhomogeneities in composite media. *Composites Part B: Engineering*, 90:341–350, 2016.
- Wang, X. and Sudak, L. J. Scattering of elastic waves by multiple elastic circular cylinders with imperfect interface. *Waves in Random and Complex Media*, 17(2):159–187, 2007.

- Wang, X. D. and Gan, S. Effective antiplane dynamic properties of fiber-reinforced composites. *Journal of Applied Mechanics-Transactions of the Asme*, 69(5):696–699, 2002.
- Wang, X. D. and Meguid, S. A. Diffraction of SH wave by interacting matrix crack and an inhomogeneity. *Journal of Applied Mechanics-Transactions of the Asme*, 64(3):568–575, 1997.
- Waterman, P. C. New formulation of acoustic scattering. *Journal of the Acoustical Society of America*, 45(6):1417, 1969.
- Willis, J. R. *Dynamics of composites*, book section 5, pages 265–290. Springer-Verlag Wien, New York, 1997.
- Wu, L. Z. Interaction of two circular cylindrical inhomogeneities under anti-plane shear. *Composites Science and Technology*, 60(12-13):2609–2615, 2000.
- Wu, Y., Lai, Y., and Zhang, Z.-Q. Effective medium theory for elastic metamaterials in two dimensions. *Physical Review B*, 76(20):205313, 2007.
- Yang, M., Ma, G., Wu, Y., Yang, Z., and Sheng, P. Homogenization scheme for acoustic metamaterials. *Physical Review B*, 89(6):064309, 2014.
- Yang, R. B. and Mal, A. K. Multiple-scattering of elastic-waves in a fiber-reinforced composite. *Journal of the Mechanics and Physics of Solids*, 42(12):1945–1968, 1994.
- Yang, R. B. and Mal, A. K. Elastic waves in a composite containing inhomogeneous fibers. *International Journal of Engineering Science*, 34(1):67–79, 1996.

Zhang, J., Ye, W., and Yu, T. X. Numerical simulation of effective phase velocity and attenuation of shear elastic wave propagation in unidirectional composite materials. *Ultrasonics*, 53(6):1200–1211, 2013.

Zhen, N., Li, F.-L., Wang, Y.-S., and Zhang, C.-Z. Bandgap calculation for mixed in-plane waves in 2d phononic crystals based on Dirichlet-to-Neumann map. *Acta Mechanica Sinica*, 28(4):1143–1153, 2012.

Zijl, W., Hendriks, M. A. N., and 't Hart, C. M. P. Numerical homogenization of the rigidity tensor in Hooke's law using the node-based finite element method. *Mathematical Geology*, 34(3):291–322, 2002.